Earth-Science Reviews 261 (2025) 105027

Contents lists available at ScienceDirect

Earth-Science Reviews

journal homepage: www.elsevier.com/locate/earscirev

Invited Review

Dispersed organic matter from pre-Devonian marine shales: A review on its composition, origin, evolution, and potential for hydrocarbon prospecting

Qingyong Luo[a,b], Fariborz Goodarzi[c], Ningning Zhong[a,b,*], Nansheng Qiu[a,b,*], Xiaomei Wang[d], Václav Suchý[e], Imran Khan[a,b,f,g], Xiaowei Zheng[a,b], Bei Liu[h], Omid H. Ardakani[i], Ye Zhang[j,k], Dahua Li[j,k], Jin Wu[a,b], Zilong Fang[a,b], Ruitan Shi[a,b], Christian B. Skovsted[l], Hamed Sanei[m], Yaohui Xu[n], Jia Wu[a,b], Wenxin Hu[a,b], Guoqiang Duan[a,b]

[a] State Key Laboratory of Petroleum Resources and Engineering, China University of Petroleum (Beijing), Beijing, China
[b] College of Geoscience, China University of Petroleum, Beijing, China
[c] FG & Partner Ltd, Research Group, 29 Hawkside Mews NW, Calgary, Alberta, Canada
[d] Key Laboratory of Petroleum Geochemistry, Research Institute of Petroleum Exploration and Development, China National Petroleum Corporation, Beijing, China
[e] Nuclear Physics Institute, v. v. i.,Academy of Sciences of the Czech Republic, Na Truhlářce 39/64, 180 86 Prague, Czech Republic
[f] Organic Geochemistry Unit, Key Laboratory of Geoscience Big Data and Deep Resource of Zhejiang Province, School of Earth Sciences, Zhejiang University, Hangzhou, China
[g] Department of Earth Sciences, COMSATS University Islamabad, Abbottabad Campus, Abbottabad, Khyber Pakhtunkhwa, Pakistan
[h] School of Earth Resources, China University of Geosciences, Wuhan, Hubei, China
[i] Natural Resources Canada, Geological Survey of Canada, Calgary, AB, Canada
[j] National Joint Engineering Research Center for Shale Gas Exploration and Development, Chongqing Institute of Geology & Mineral Resources, Chongqing, China
[k] Key Laboratory of Shale Gas Exploration, Ministry of Natural Resources, Chongqing Institute of Geology & Mineral Resources, Chongqing 401120, China
[l] Department of Palaeobiology, Swedish Museum of Natural History, Box 50007, SE-104 05 Stockholm, Sweden
[m] Lithospheric Organic Carbon Group (LOC), Department of Geoscience, Aarhus University, Aarhus, Denmark
[n] Hubei Cooperative Innovation Center of Unconventional Oil and Gas, Yangtze University, Wuhan, China.

ARTICLE INFO

Keywords:
In-source solid bitumen
Graptolite
Vitrinite-like maceral
Thermal maturity
Organic petrology
Maceral
Shale
Pre-Devonian

ABSTRACT

The pre-Devonian shales are important natural archives, preserving extensive information on paleobiology, paleoenvironment, and paleoecology, and also acting as important hydrocarbon source rocks for both unconventional and conventional petroleum systems. In China, however, most of the pre-Devonian shales are post-mature, resulting in a gradual convergence in the chemical composition and structure of organic matter (OM). This convergence complicates OM identification under optical microscope, making it challenging to trace its genesis and evolution due to similar optical characteristics. Additionally, the absence of true vitrinite particles poses an additional challenge in the evaluation of thermal maturity of these shales, a challenge that has persisted for decades. This study compares detailed optical characteristics and genesis of selected OM types, namely, graptolite, vitrinite-like maceral (VLM), solid bitumen (SB) in the pre-Devonian shales to improve identification and differentiation between these macerals. The physicochemical evolution of OM is reviewed based on the naturally and artificially matured samples, with emphasis on the organic petrology and petroleum production in some of the most extensively studied pre-Devonian shales globally. VLM and graptolites exhibit higher reflectance and stronger anisotropy than co-occurring in-source SB, with their reflectance as indicators to evaluate OM maturity in these marine shales. VLM can be distinguished from SB by its elongate and syndepositional occurrence, and from graptolites by the characteristic biological structures of graptolite. The origin of VLM is hypothesized to be a product of early diagenetic anaerobic biodegradation of lamalginite and/or bituminite in the Precambrian shales, although its origin in the Cambrian shales remains unclear. On the other hand, in-source SB is derived from the transformation of liptinites or from the cracking of the residual petroleum, or a combination thereof. Graptolites are associated with high total organic carbon (TOC), S_1, S_2, and hydrogen index (HI) contents, with kerogen predominantly classified as Type II-III, indicating significant hydrocarbon generation potential. Notably, in-source SB plays a significant role in gas generation. In the early mature pre-Devonian shales, OM mainly consists of lamalginite and bituminite; whereas in-source SB becomes the dominant OM in the

* Corresponding authors at: State Key Laboratory of Petroleum Resources and Engineering, China University of Petroleum (Beijing), Beijing, China.
E-mail addresses: nnzhongxp@cup.edu.cn (N. Zhong), qiunsh@cup.edu.cn (N. Qiu).

https://doi.org/10.1016/j.earscirev.2024.105027
Received 7 February 2024; Received in revised form 22 November 2024; Accepted 10 December 2024
Available online 13 December 2024

postmature pre-Devonian shales. Non-granular graptolites are commonly observed in the Ordovician-Silurian Wufeng–Longmaxi shales, contributing significantly to OM. A comparison of naturally and artificially matured samples suggests that low-maturity liptinites transform into SB as thermal maturity increases. This finding is essential for reconstructing the original composition and hydrocarbon potential of these economically significant marine shales.

1. Introduction

The pre-Devonian shales record crucial geochemical, environmental, ecological, and climatic conditions in Earth's history, which likely played a significant role on the evolutionary progress of life (Li et al., 2010; Planavsky et al., 2011; Lyons et al., 2014; Planavsky et al., 2014a; Planavsky et al., 2014b; Zhang et al., 2015; Zhang et al., 2016; Li et al., 2017; Reinhard et al., 2017; Zhang et al., 2019b; Planavsky et al., 2021; Planavsky and Mills, 2021; Wang et al., 2022a; Fakhraee et al., 2023). Additionally, these marine shales are significant hydrocarbon source rocks globally (Goodarzi, 1984; Goodarzi, 1985a; Bertrand and Heroux, 1987; Bertrand, 1990; Lüning et al., 2000; Zou et al., 2010; Zou et al., 2012; Dai et al., 2014; Dai et al., 2016; Luo et al., 2016b; Zou et al., 2016; Hayton et al., 2017; Luo et al., 2017b; Luo et al., 2018; Luo et al., 2020). In particular, the Lower Paleozoic shales serve as primary hydrocarbon source rocks for both unconventional and conventional petroleum systems in regions such as China, Arabia, and North Africa (Lüning et al., 2000; Zou et al., 2010; Zou et al., 2012; Dai et al., 2014; Dai et al., 2016; Zhu et al., 2016; Zou et al., 2016; Zhu et al., 2018; Zhu et al., 2020; Zhu et al., 2021). The recent significant breakthrough in shale gas exploration in the Cambrian Qiongzhusi and the Ordovician-Silurian Wufeng–Longmaxi formations in China has spurred research into the organic petrology of the Lower Paleozoic shales in recent decades (Luo et al., 2017b; Luo et al., 2018; Luo et al., 2019; Wang et al., 2019; Luo et al., 2020; Wang et al., 2020; Luo et al., 2021; Teng et al., 2022; Luo et al., 2023; Wu et al., 2023a; Wu et al., 2023b).

Studies have shown that dispersed organic matter (OM) in these pre-Devonian shales exhibit variable composition. For example, the maceral compositions in the Paleoproterozoic Barney Creek and Mesoproterozoic Velkerri black shales from Australia are mainly composed of lamalginite, solid bitumen (SB), mineral-bituminous groundmass, and thucholite (Crick et al., 1988; Crick, 1992), and the Mesoproterozoic Hongshuizhuang and Xiamaling shales from northern China primarily contain lamalginite, bituminite (or its equivalents: 'amorphous OM', 'sapropelinite', 'amorphinite', etc.), SB, mineral-bituminous groundmass, and thucholite (Luo et al., 2014; Luo et al., 2021; Wu et al., 2022). The Cambrian-Ordovician Alum shales in Scandinavia mainly consist of alginite, SB, vitrinite-like maceral (VLM), zooclasts, and bituminite (Petersen et al., 2013; Sanei et al., 2014; Luo et al., 2018; Luo et al., 2021; Zheng et al., 2021a; Zheng et al., 2023b), and the Upper Ordovician black shales from Quebec, Canada are mainly composed of SB, alginite, and zooclasts (Haeri-Ardakani et al., 2015; Lavoie et al., 2016). In China, the pre-Devonian shales, largely distributed in the Sichuan, Tarim, and Ordos basins, are generally postmature due to intense tectonic-thermal evolution (Xiao et al., 2000; Luo et al., 2016b; Luo et al., 2017b; Luo et al., 2018; Wang et al., 2019; Luo et al., 2020; Wang et al., 2020; Luo et al., 2021; Li et al., 2022). Their OM composition is simple, dominated by in-source SB (Luo et al., 2018; Wang et al., 2019; Luo et al., 2020; Wang et al., 2020; Luo et al., 2021; Luo et al., 2023). Consequently, fully understanding their original OM compositions and thermal evolutionary processes remains challenging, which limits the evaluation of their hydrocarbon generation potential (Luo et al., 2018; Wang et al., 2019; Luo et al., 2020; Luo et al., 2021; Teng et al., 2022; Luo et al., 2023). To simulate the natural thermal evolution of OM in the pre-Devonian shales, low-maturity shales have been subjected to artificial maturation experiments to observe the physicochemical transformation of various OM as thermal maturity increases (Hackley and Lewan, 2018; Luo et al., 2018; Luo et al., 2021; Song et al., 2023; Zheng et al., 2023a; Arysanto et al., 2024).

Vitrinite reflectance is a classic and reliable thermal maturity indicator; however, vitrinite is generally absent in the pre-Devonian rocks (Stach et al., 1982; Taylor et al., 1998; Suárez-Ruiz et al., 2012). As a result, the evaluating thermal maturity in these sediments has posed a challenge for many years. To overcome this, alternative parameters, such as T_{max} (the temperature at the maximum hydrocarbon generation rate during pyrolysis), molecular biomarkers, and the reflectance of VLM, zooclasts, and SB are widely used (Clausen and Teichmüller, 1982; Goodarzi, 1984; Goodarzi, 1985a; Goodarzi, 1985b; Goodarzi and Norford, 1985; Bertrand and Heroux, 1987; Goodarzi and Higgins, 1987; Goodarzi and Norford, 1987; Goodarzi and Norford, 1989; Bertrand, 1990; Goodarzi et al., 1992a; Goodarzi et al., 1992b; Goodarzi et al., 1992c; Bertrand, 1993; Landis and Castaño, 1995; Xiao et al., 1996; Xiao et al., 1997; Xiao et al., 2000; Bertrand et al., 2003; Petersen et al., 2013; Sanei et al., 2014; Luo et al., 2018; Mastalerz et al., 2018; Wang et al., 2019; Luo et al., 2020; Sanei, 2020; Wang et al., 2020; Luo et al., 2021; Luo et al., 2023). However, these alternative thermal maturity indications have their limitations. For example, biomarker ratios can be influenced by factors other than thermal maturity, such as biological sources and depositional conditions, leading to uncertainty in their geochemical significance (Peters et al., 2005). Similarly, T_{max} can also be influenced by several factors beyond the paleotemperature, including high clay content, organic sulfur, S_1, uranium, kerogen type, and extensive weathering (Yang and Horsfield, 2020). VLM is widespread in the pre-Devonian shales; however, its origin remains a subject of ongoing debate. Moreover, distinguishing VLM from other organic fragments may be problematic, complicating the application of its reflectance as thermal maturity indicators (Buchardt and Lewan, 1990; Xiao et al., 1997; Xiao et al., 2000; Schmidt et al., 2015; Luo et al., 2021; Wu et al., 2023a; Wu et al., 2023b). The Lower Paleozoic shales contain abundant zooclasts, including graptolites, scolecodonts, and chitinozoans, and their reflectance characteristics have been studied for decades. Among these, graptolite reflectance is considered particularly useful for evaluating OM maturity due to its abundance and its optical properties similar to the vitrinite (Goodarzi, 1984; Goodarzi and Norford, 1985; Goodarzi and Norford, 1987; Goodarzi et al., 1992c; Petersen et al., 2013; Luo et al., 2020). On the other hand, the use of SB reflectance (BR_o) as thermal maturity index is still contentious, given the different mechanism of formation, including deasphalting, biodegradation, and thermal cracking; SB in the shales and reservoirs especially displays extremely distinct optical characteristics (Hwang et al., 1998; Mastalerz et al., 2018; Hackley et al., 2020b; Luo et al., 2021).

The hydrocarbon generation potential of graptolite and SB has attracted significant attention due to the successful shale gas exploration in the Lower Cambrian and graptolite-bearing shales in recent years. Recent studies suggest that mature graptolite concentrate exhibits high TOC, S_1, S_2, and HI, which indicates good hydrocarbon generation potential (İnan et al., 2016; Wang et al., 2017a), comparable to kerogen type II-III (Bustin et al., 1989; Hoffknecht, 1991; Luo et al., 2020). SB is a major OM constituent in mature to postmature pre-Devonian marine shales, such as those found in the Chinese marine shales, the Ordovician Utica, Upper Devonian-Lower Carboniferous Woodford and Bakken, Devonian Marcellus, Duvernay, and Barnett shales from North America and so on (Petersen et al., 2013; Haeri-Ardakani et al., 2015; Hackley and Cardott, 2016; Liu et al., 2017; Hackley et al., 2018; Luo et al., 2018; Mastalerz et al., 2018; Wang et al., 2019; Luo et al., 2020; Luo et al., 2021). However, SB has not been fully quantified to date in terms of the hydrocarbon generation potential relative to associated kerogen macerals (Mastalerz et al., 2018).

In China, the misidentification of organic macerals due to inexperience, and complex optical and morphological properties of graptolites, chitinozoans, VLM, and SB in the post-mature pre-Devonian shales is a common issue (Xiao et al., 2000; Luo et al., 2016b; Luo et al., 2017b; Luo et al., 2018; Wang et al., 2019; Luo et al., 2020; Wang et al., 2020; Luo et al., 2021; Li et al., 2022). For example, graptolite in the Wufeng–Longmaxi formations may be mistaken for VLM or SB, while in the Lower Cambrian shales, VLM is often misidentified as graptolite or SB (Luo et al., 2018; Luo et al., 2020; Luo et al., 2021; Luo et al., 2023). Consequently, the wrong conversion equation to calculate equivalent vitrinite reflectance ($EqVR_o$) based on their misidentified maceral is commonly used, which in turn, results in inaccurate conclusions pertaining to the thermal maturity of the source rock. Lastly, erroneous identification of macerals further complicates the assessment of the hydrocarbon potential of source rocks.

This paper provides a detailed reevaluation of the optical properties of selected maceral, including graptolite, VLM, and SB found in the pre-Devonian shales to help improve identification and distinction between these macerals. The detailed result of the reanalysis will be presented together with the results of a simulated thermal maturation study to demonstrate the physicochemical transformation and the overall hydrocarbon generation potential of these macerals.

2. Sampling and methods

The pre-Devonian shales were collected from drill cores and outcrops from various locations around the world. These include samples from the Mesoproterozoic Hongshuizhuang and Xiamaling formations from northern China, the Neoproterozoic Datangpo, Doushantuo, and Dengying formations, the Lower Cambrian shales and Wufeng–Longmaxi formations from Sichuan Basin, China, the Lower Cambrian Yurtus Formation from the Tarim Basin, China, the Ulalik/Pingliang formations from the Ordos Basin, China, the Salt Range Formation from Pakistan, and the Alum shales of Northern Europe.

Two graptolite-bearing Alum shales from Sweden with $EqVR_o$ of 0.58 and 0.87 %, respectively, were selected for the separation of graptolite fragments for better understanding the hydrocarbon generation potential of graptolites. The shales were immersed in a 10 % hydrochloric acid solution for over 12 h to dissolve calcium minerals until the particle size was reduced to less than 3 mm. The samples were then subjected to a three-stage sequential acid digestion using hydrofluoric acid totaling 15 days, with the acid being replaced every five days, to remove silicate minerals. After acid treatment, the samples were thoroughly rinsed with deionized water to remove all the residual acid. The samples were then sequentially sieved through a series of sieves with mesh sizes of 3 mm, 180 μm, 45 μm, and 15 μm to separate OM. Graptolite fragments were manually separated by flotation using a flat-bottomed petri dish, with individual fragments being meticulously selected under the stereoscopic microscope. These graptolite fragments were then dried and weighed for subsequent analysis and ground to a particle size of 0.15 mm using an agate mortar.

The hydrocarbon generation potential of the isolated graptolite fragments was analyzed using the Wildcat Technologies' HAWK Pyrolysis instrument, which measured the S_1, S_2, T_{max}, and TOC values (Espitalié et al., 1977). The instrument was initially purged for 3 min, followed by a 3-min hold at 300 °C, and then heated to 600 °C at a rate of 25 °C/min.

For organic petrological observation, the pre-Devonian shales were cut either perpendicular or parallel to bedding and polished following ISO (2009) standard. These samples were examined using a Leica DM4500P microscope under reflected white and incident blue light using a 50 × oil immersion objective for detailed organic petrological analysis.

3. Optical characteristics of OM

OM in the pre-Devonian shales typically consists of algae-derived liptinite macerals (e.g., alginites, bituminite, and mineral-bituminous groundmass), VLM, graptolite, SB, and thucholite (Goodarzi, 1984; Goodarzi, 1985a; Goodarzi, 1985b; Bertrand and Heroux, 1987; Crick et al., 1988; Buchardt and Lewan, 1990; Crick, 1992; Goodarzi et al., 1992c; Bertrand, 1993; Gentzis and Goodarzi, 1993; Bustin and Guo, 1999; Xiao et al., 2000; Bertrand and Malo, 2012; Luo et al., 2014; Lavoie et al., 2016; Luo et al., 2016b; Luo et al., 2017a; Ardakani et al., 2018; Luo et al., 2018; Luo et al., 2020; Luo et al., 2021; Zheng et al., 2021b; Wu et al., 2022; Luo et al., 2023; Wu et al., 2023a; Wu et al., 2023b). The optical characteristics and genesis of the algae-derived liptinite macerals in the pre-Devonian shales are comparable to those found in the post-Devonian shales, which have been extensively described in detail by Pickel et al. (2017), Hackley et al. (2018), and references therein. This paper will focus specifically on the optical characteristics and genesis of VLM, graptolite, SB, and thucholite, offering a detailed discussion on their significance in the pre-Devonian shales.

3.1. Vitrinite-like maceral (VLM)

Primary indigenous VLM has been widely recognized in the pre-Devonian shales for more than 40 years and has been described as exhibiting optical characteristics similar to vitrinite. VLM has been identified in formations such as the Mesoproterozoic Hongshuizhuang and Xiamaling formations of the Yanshan Basin, the Lower Cambrian Niutitang Formation and the Wufeng–Longmaxi shales of the Sichuan Basin, the Lower Cambrian Yurtus Formation of the Tarim Basin, and the Alum shale of North Europe (Figs. 1 and 2) (Kisch, 1980; Van Gijzel, 1981; Thomsen et al., 1983; Buchardt and Lewan, 1990; Xiao et al., 2000; Petersen et al., 2013; Luo et al., 2014; Sanei et al., 2014; Luo et al., 2020; Luo et al., 2021; Yao et al., 2021; Zheng et al., 2021a; Zheng et al., 2021b; Teng et al., 2022; Wu et al., 2022; Luo et al., 2023; Wu et al., 2023a; Wu et al., 2023b). However, despite extensive research, there is still no consensus on its origin, and it is often difficult to distinguish from other OM types, such as graptolite and SB. Consequently, VLM is not recognized as an official maceral by the International Committee for Coal and Organic Petrology (ICCP) and is excluded from the dispersed OM classification (Gonçalves et al., 2024). Under the optical microscope, VLM displays an irregularly ellipsoidal or elongated shape in sections perpendicular to bedding, aligning parallel to bedding plane (Figs. 1, 2, and Table 1). In sections parallel to bedding, VLM exhibits irregular blocky morphology. In the mature shales, VLM shows no to brown fluorescence under fluorescent light and appears gray under white light (Figs. 1 and 2) (Luo et al., 2021; Wu et al., 2023a; Wu et al., 2023b). In the postmature shales, VLM's surface brightness increases with thermal maturity (Figs. 1, 3, 4, and Table 1) (Wu et al., 2023a). In the lower mature shales, VLM exhibits weak anisotropy with increased anisotropy corresponding to higher maturity (Figs. 1, 3, 4, and Table 1). This observation is consistent with a positive correlation between VLM bireflectance and maximum reflectance ($VLMR_{max}$) (Luo et al., 2021; Wu et al., 2023a). Under polarized white light, VLM exhibits optical extinction phenomena with stage rotation, showing two diametrically opposite maximum reflectances and two diametrically opposite minimum reflectances in anisotropic VLM (Wu et al., 2023a). Notably, these optical extinction characteristics of VLM closely resemble those of graptolites, as discussed below. Graptolites can be fragmented into small pieces, which may obscure clear biological structures (Fig. 5f), complicating the differentiation between VLM and graptolites. This finding is consistent with the previous research results that VLM in the graptolite-bearing shales has been regarded to be the graptolite fragments (Petersen et al., 2013; Teng et al., 2022), as discussed in section 4.1. However, there is strong evidence that graptolite is not the source of VLM in the Precambrian–Lower Cambrian shales based on two reasons:

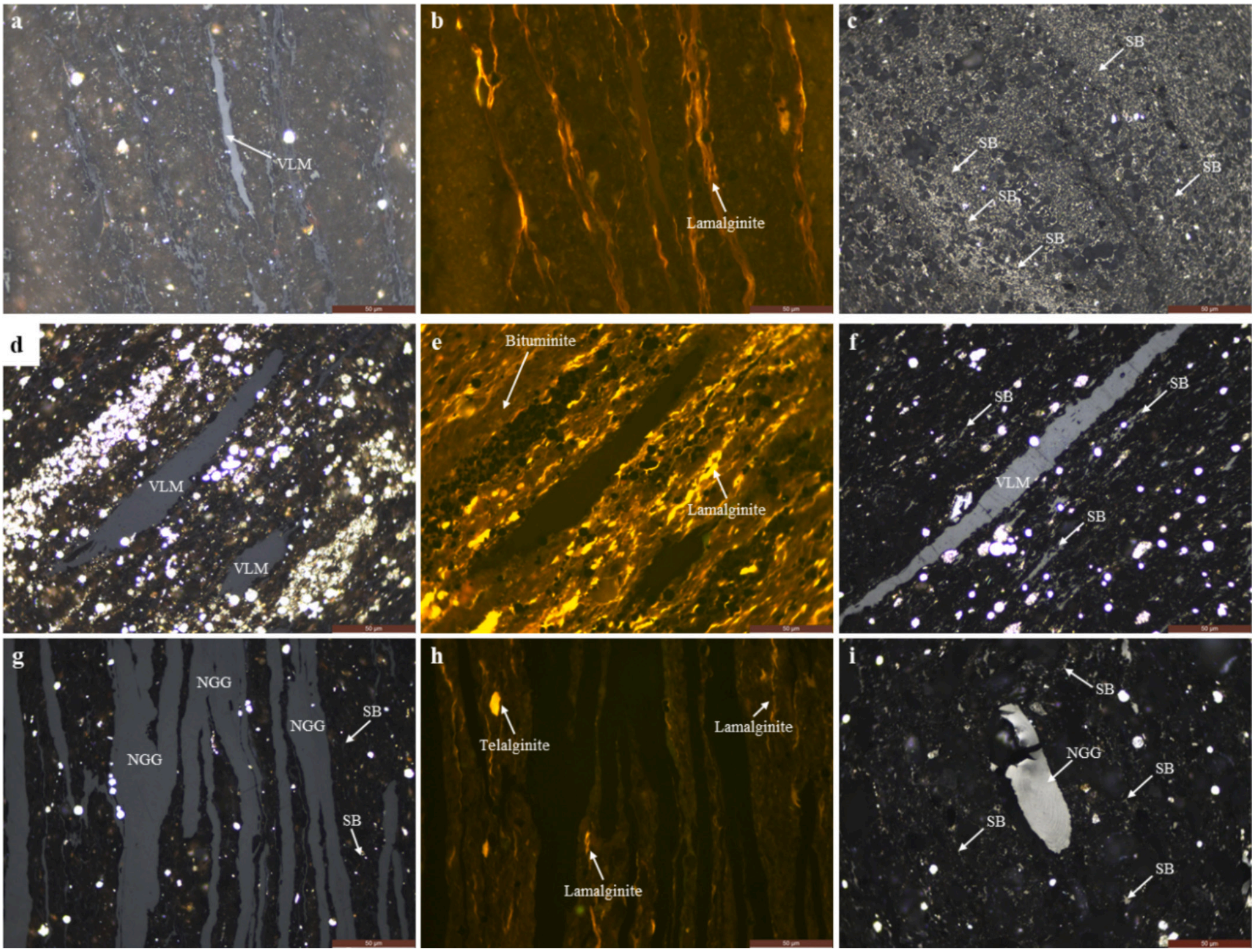

Fig. 1. Typical maceral photos in the low-maturity and postmature shales. a, VLM and lamalginite in the low-maturity Mesoproterozoic Xiamaling shale, reflected light. b, VLM and lamalginite in the Mesoproterozoic Xiamaling shale, same field as a, fluorescent light. c, In-source SB in the postmature Neoproterozoic Datangpo shale, reflected light. d, VLM, bituminite, and lamalginite in the low-maturity Cambrian Alum shale, reflected light. e, VLM, bituminite, and lamalginite in the Cambrian Alum shale, same field as d, fluorescent light. f, VLM and SB in the postmature Cambrian Alum shale, reflected light. g, non-granular graptolite (NGG) and SB in the low-maturity Ordovician Alum shale, reflected light. h, NGG and alginite in the low-maturity Ordovician Alum shale, same field as g, fluorescent light. i, NGG with fusellar layers and SB in the postmature Wufeng–Longmaxi shale, polarized white light.

(1) No graptolite fossils have been observed in these Precambrian–Lower Cambrian hand specimens; (2) VLM lacks the characteristic periderm structures seen in graptolites (Fig. 1a-f), whereas graptolite typically display distinct biological structures, such as fusellar layers, common canal, or theca (Figs. 1g, 2i, and k) (Goodarzi and Norford, 1985; Goodarzi and Norford, 1987; Luo et al., 2018; Luo et al., 2020). Based on the differing morphological characteristics and temporal manifestation, the isolated elongate OM exhibiting optical characteristics similar to vitrinite and lacking distinct biological characteristics of graptolite periderm can be classified based on their age and paleontological context. Specifically, these fragments are classified as VLM in the Precambrian–Cambrian shales and graptolite fragments for the Ordovician–Silurian graptolite-bearing shales, respectively.

3.2. Graptolite periderm

Graptolites are widely distributed in the Paleozoic sediments globally, including the Lower Silurian hot shales of North Africa and Arabia (Lüning et al., 2000; Lüning et al., 2003; İnan et al., 2016), the Alum shale, Słowińska, Piaśnica, Kaporye, and Türisalu formations, and the Silurian rocks of the Barrandian area from Europe (Suchý et al., 2015; Zheng et al., 2021a; Zheng et al., 2021b; Zheng et al., 2022; Zheng et al., 2023b), the Upper Ordovician-Middle Devonian sediments from Arctic Canada (Riediger et al., 1989; Link et al., 1990; Goodarzi et al., 1992c; Gentzis et al., 1996), and the Pingliang and Wufeng–Longmaxi formations from China (Luo et al., 2016b; Luo et al., 2017b; Luo et al., 2018; Wang et al., 2019; Luo et al., 2020). It is generally accepted that OM in the Lower Paleozoic shales is largely derived from marine primary producers. However, optical microscopy and scanning electron microscopy (SEM) observations reveal that graptolite periderms contribute variably to total dispersed OM, with percentages of 20 %– 93 % in the Wufeng–Longmaxi Formations (Luo et al., 2016b). In some samples, the high contribution of graptolite may be attributed to the sampling location within graptolite enrichment zones. Chitinozoans have also been found to contribute significantly to OM composition in the Ordovician Utica shales (Ardakani et al., 2018). These studies provide additional evidences that zooclasts, such as graptolites and chitinozoans, make an important contribution to total OM within specific geological period and depositional environment (Luo et al., 2016b; Ardakani et al., 2018; Luo et al., 2020).

Petrographically, graptolites exhibit two distinct surface morphology, i.e., granular (GG) and non-granular (NGG), when

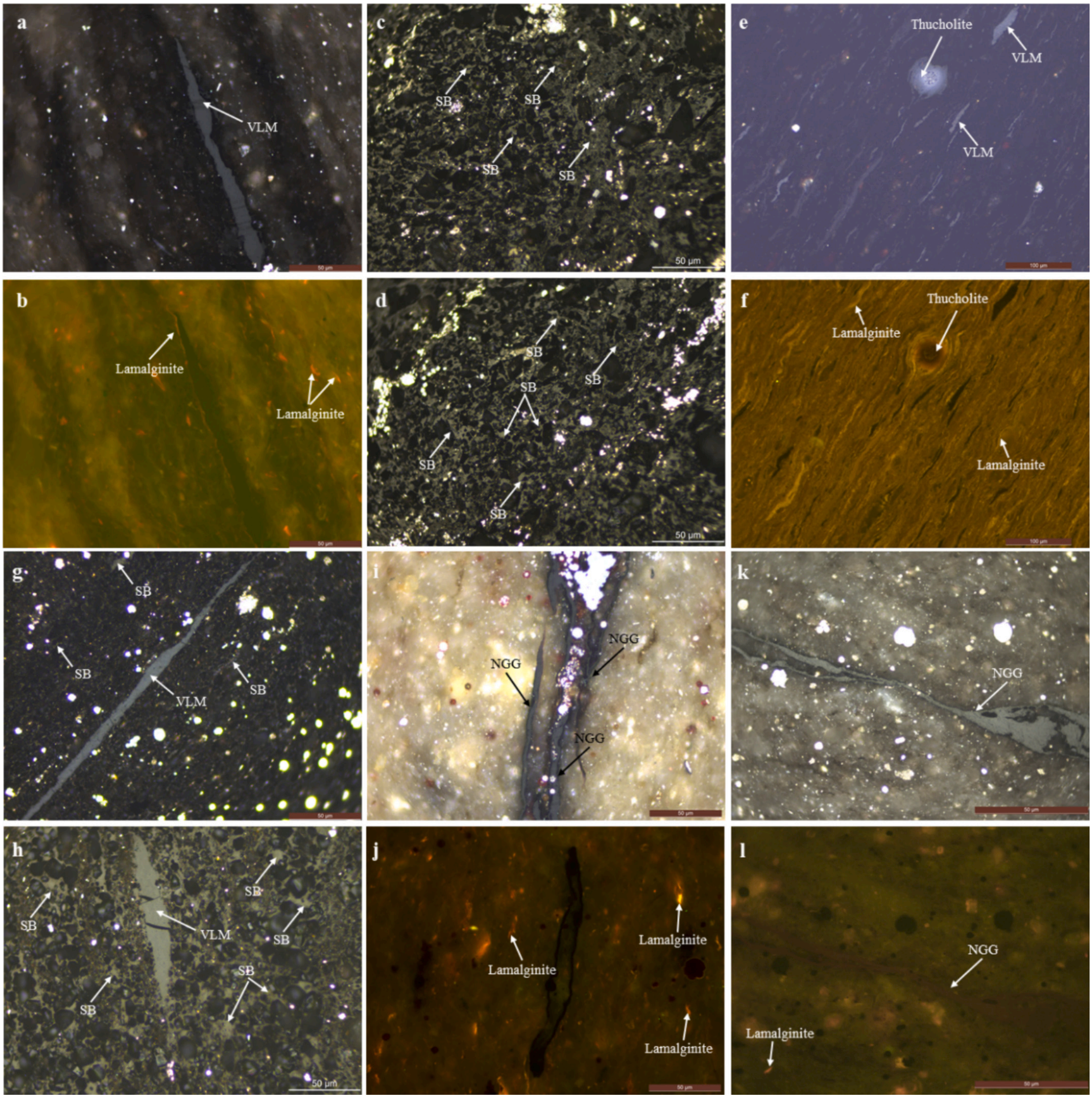

Fig. 2. Typical maceral photos in the pre-Devonian shales. a, VLM and lamalginite in the low-maturity Mesoproterozoic Hongshuizhuang shale, reflected light. b, VLM and lamalginite in the low-maturity Mesoproterozoic Hongshuizhuang shale, reflected light, same field as a, fluorescent light. c, SB in the postmature Neoproterozoic Doushantuo shale, reflected light. d, SB in the postmature Neoproterozoic Doushantuo shale, reflected light. e, VLM, thucholite, and lamalginite in the low-maturity Neoproterozoic-Cambrian Salt Range shale, reflected light. f, VLM, thucholite, and lamalginite in the low-maturity Neoproterozoic-Cambrian Salt Range shale, reflected light. Same field as e, fluorescent light. g, VLM and SB in the Cambrian Yurtus shale, reflected light. h, VLM and SB in the Cambrian Yurtus shale, reflected light. i, NGG in the low-maturity Ordovician Pingliang shale, reflected light. j, NGG and lamalginite in the low-maturity Ordovician Pingliang shale, fluorescent light. k, NGG and lamalginite in the low-maturity Ordovician Ulalik shale, reflected light. l, NGG and lamalginite in the low-maturity Ordovician Ulalik shale, same field as k, fluorescent light.

observed under reflected white light microscopy (Goodarzi, 1984; Goodarzi, 1985a; Goodarzi and Norford, 1985; Goodarzi and Norford, 1987; Bustin et al., 1989; Goodarzi and Norford, 1989; Riediger et al., 1989; Bertrand, 1990; Link et al., 1990; Goodarzi et al., 1992c; Petersen et al., 2013; Hackley and Cardott, 2016; İnan et al., 2016; Luo et al., 2016b; Luo et al., 2017b; Luo et al., 2018; Synnott et al., 2018; Wang et al., 2019; Luo et al., 2020). Graptolite fragments are segmented and exhibit distinctive microstructures under a microscope, including common canal, fusellar layers, thecae, cortical tissue and granularity, which aid in distinguishing them from other macerals (Goodarzi, 1984; Goodarzi, 1985a; Petersen et al., 2013; Luo et al., 2016b; Luo et al., 2018; Luo et al., 2020). GG generally exhibits soft texture with fine-grained or reticular structure, whereas NGG is brittle and hard, featuring a smooth surface (Goodarzi, 1984; Goodarzi, 1985a; Luo et al.,

Table 1
Comparison of structural and optical characteristics between NGG, in-source SB, and VLM in the sediments (Luo et al., 2020; Luo et al., 2021; Luo et al., 2023). The anisotropy and random reflectance of NGG and VLM were compared with that of co-occurring in-source SB in the postmature samples.

Maceral	NGG	in-source SB	VLM
Age	Mainly at Ordovician–Silurian	Any age	Precambrian–Cambrian
Hand specimen	Obvious macroscopic graptolites	Generally difficult to be observed	Unobservable
Occurrence	Complex biological structures with fusellar layers, common canal or theca, elongate, parallel to bedding	Small size, filled in pores and cracks, or dispersed in clay minerals or occasionally parallel to bedding	Elongate, irregular lenses, parallel to bedding
Surface feature	Smooth, homogenous	Less homogeneous	Smooth, homogenous
Mineral inclusion	Sometimes with pyrite grains	Generally without mineral inclusions	Occasionally with mineral grains
Anisotropy	Stronger	Weaker	Stronger
Random reflectance	Higher	Lower	Higher
Origin	Original OM	Secondary OM	Original OM

2018; Luo et al., 2020). The surface texture of graptolites (NGG vs. GG) appears to correlate with surrounding lithology: NGG is typically found in shale matrices, while GG is more commonly associated with carbonate matrices (Goodarzi and Norford, 1985; Goodarzi and Norford, 1987; Petersen et al., 2013).

The microstructure of graptolites is best observed under polarized white light, where it shows sharp contrast in microstructure as the objective stage is rotated (Goodarzi and Norford, 1989; Luo et al., 2020). At low maturity, both GG and NGG display minimal differences in reflectance. However, as maturity increases, NGG exhibits much stronger anisotropy and higher reflectance compare to GG (Goodarzi, 1984; Goodarzi, 1985a; Goodarzi and Norford, 1985; Goodarzi et al., 1992c; Luo et al., 2018; Luo et al., 2020). NGG is more abundant than GG in the Lower Paleozoic shales, which is consistent with the shaly matrix of these formations (Goodarzi, 1984; Luo et al., 2016b; Wang et al., 2019; Luo et al., 2020; Zheng et al., 2021a; Zheng et al., 2022). When observed under polarized white light, NGG shows optical extinction twice as the stage is rotated, revealing two diametrically opposed graptolite minimum reflectances (GR_{omin}) and two diametrically opposed graptolite maximum reflectances (GR_{omax}) (Malinconico, 1992; Malinconico, 1993; Luo et al., 2016b; Luo et al., 2018; Luo et al., 2020). This phenomenon is less pronounced in GG, which is consistent with its weaker anisotropy (Luo et al., 2020). Given its abundance and distinct characteristics, this paper will primarily focus on NGG. NGG has an elongated shape in sections perpendicular to bedding, while fusellar layers are more easily observed in sections parallel to bedding (Fig. 1i and Table 1). In the low-maturity shales, NGG exhibits a weaker anisotropy compared to the postmature shales (Figs. 1, 5 and Table 1), aligning with the positive relationship between GR_{omax} and bireflectance (Luo et al., 2017b; Luo et al., 2020). NGG can be further categorized into two types: blocky-shaped and lath-shaped. The blocky-shaped has lower bireflectance and maximum reflectance than the lath-shaped type (Riediger et al., 1989).

3.3. *In-source solid bitumen*

The terms bitumen and SB carry different meanings across scientific disciplines. For example, organic geochemists define bitumen as OM that is soluble in organic solvents such as toluene, dichloromethane, trichloromethane, or carbon disulfides (Durand, 1980; Killops and Killops, 2013). In contrast, organic petrographers refer to SB as a secondary maceral, formed from kerogen (Sanei et al., 2015; Hackley and Cardott, 2016; Mastalerz et al., 2018; Sanei, 2020; Luo et al., 2021; Liu et al., 2022). SB is further classified into pre-oil and post-oil SB, based on the timing of its formation relative to oil generation (Mastalerz et al., 2018; Liu et al., 2019a), whereby mature SB can be partially dissolved in organic solvents (Curiale, 1986; Hackley and Cardott, 2016; Mastalerz et al., 2018). When BR_o exceeds 1.5 %, SB is referred to as pyrobitumen (Mastalerz et al., 2018). Pyrobitumen is insoluble in organic solvent, making it difficult to distinguish from kerogen using organic geochemical methods (Mastalerz et al., 2018). However, SB/pyrobitumen is easily distinguishable from kerogen under an optical microscope. SB/pyrobitumen typically exhibits pore or fracture-filing characteristics, whereas kerogen macerals retain their original morphology. SB has been categorized into various types based on reflectance, intensity of fluorescence, solubility, fusibility, and hydrogen/carbon atomic ratio (Abraham, 1918; Hunt et al., 1954; Abraham, 1960; Jacob, 1989; Mastalerz et al., 2018). While these classifications are still in use (Cardott, 1991; Golubev et al., 2008; Shalaby et al., 2012), they lack genetic implications and have limited applicability in shale oil and gas exploration and development.

Differentiating SB from bituminite in the immature-low mature shales can be challenging (Hackley et al., 2018). Bituminite typically contains fine mineral inclusions (detrital and/or early diagenetic) and exhibits a slightly lower reflectance (< 0.30 %) compared to SB (Fig. 1) (Hackley et al., 2018; Liu et al., 2020; Teng et al., 2021). SB was once liquid with high viscosity and mobility in the oil window, so it generally exhibits pore- and fracture-filling characteristics (Figs. 1, 2, 3, 4, 5, and Table 1) (Mastalerz et al., 2018; Liu et al., 2019a). Some studies have described SB as “OM cements” due to its infilling void spaces (Camp, 2019). This pore- and fracture-filling nature helps distinguish SB from kerogen macerals under a microscope, as SB conforms to the shape of the voids it occupies (Figs. 1, 2, 3, 4, 5, and Table 1) (Hackley and Cardott, 2016; Hackley and Lewan, 2018; Hackley et al., 2018; Luo et al., 2018; Mastalerz et al., 2018; Hackley et al., 2020a; Luo et al., 2020; Luo et al., 2021). However, SB is often mistaken as other macerals for various reasons, including sample type and researcher experience. For examples, Mastalerz et al. (2018) found that in kerogen concentrates from mudstone samples, SB was often mistaken for amorphous OM, even though SB as dominant OM in whole rock samples. Similarly, in the Yanchang Formation of the Ordos Basin, sapropelinite, amorphous kerogen, and amorphinite identified in earlier studies were later reclassified as SB, leading to incorrect descriptions of kerogen type (Hackley et al., 2017b). In the Wufeng–Longmaxi Formations, graptolites were occasionally mistaken for SB, resulting in inaccurate equivalent vitrinite reflectance (EqVRo) calculations due to the use of a conversion equation for the wrong maceral (Luo et al., 2016b; Luo et al., 2018). Although SB usually does not exhibit fluorescence, some newly formed SB in early mature source rocks can show weak brownish fluorescence, especially pre-oil bitumen (Mastalerz et al., 2018). In the postmature shales, SB appears dispersed and has a less smooth surface (Figs. 1, 2, 3, 4, 5, and Table 1) (Petersen et al., 2013; Haeri-Ardakani et al., 2015; Hackley and Cardott, 2016; Liu et al., 2017; Luo et al., 2018; Mastalerz et al., 2018; Wang et al., 2019; Luo et al., 2020; Luo et al., 2021). In the gas-bearing shales, SB tends to form networks within the rock matrix (Cardott et al., 2015; Luo et al., 2018; Misch et al., 2019; Luo et al., 2021). SB typical has lower reflectance and anisotropy than co-occurring graptolites and VLM (Figs. 6, 7 and Table 1) (Luo et al., 2018; Luo et al., 2021). In some cases, subrounded to rounded OM that fills pores may be mistaken as SB when viewed under non-polarized light (Fig. 6a). However, under polarized light, fusellar layers observed in these OM fragments can help identify them as NGG (Fig. 6b). Thus, the combination of polarized and non-polarized light is essential for accurately distinguishing between OM types (Luo et al., 2018; Luo et al., 2020). In some mature to postmature marine shales, in-source SB is the

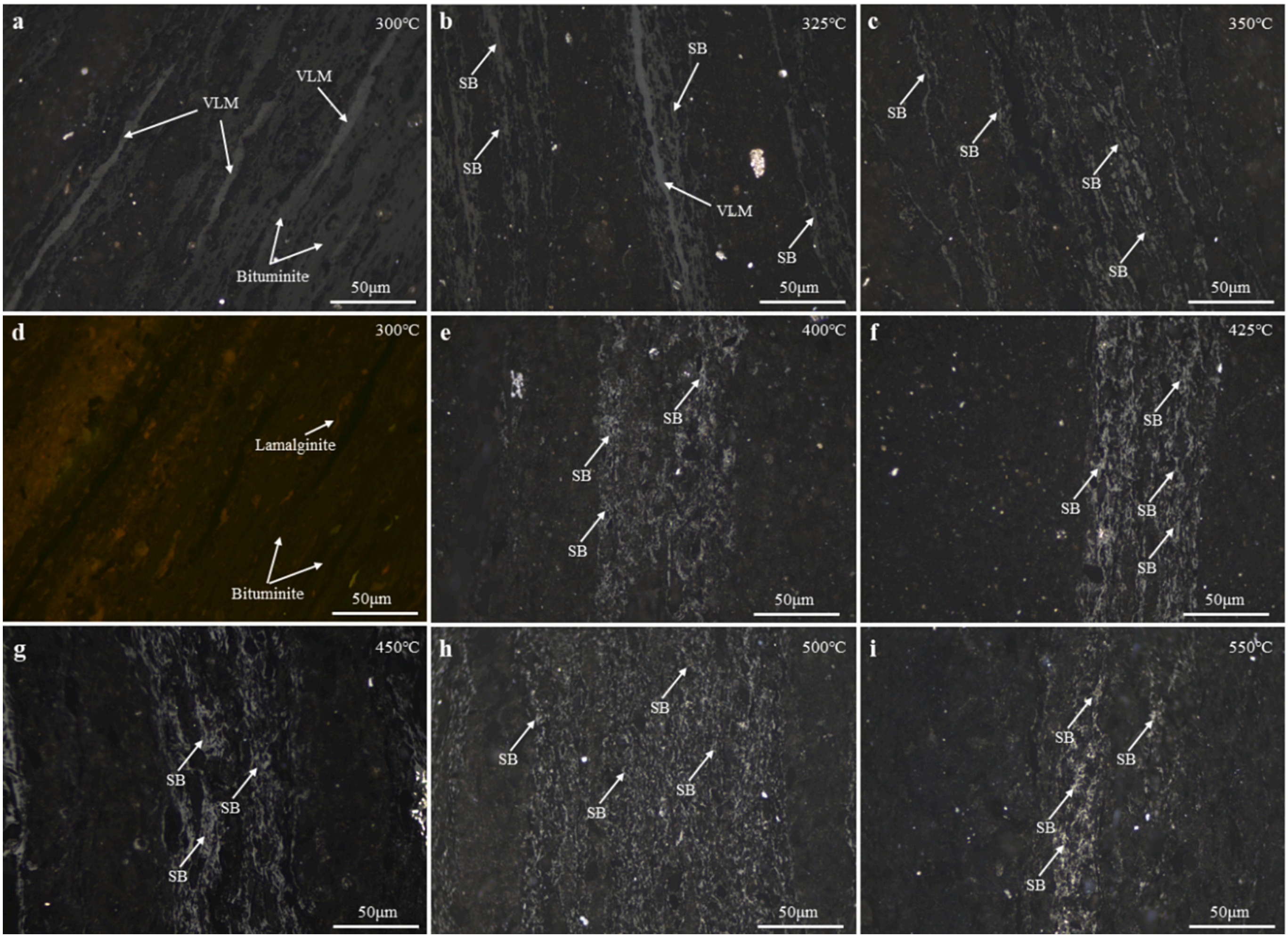

Fig. 3. Maceral evolution in the Mesoproterozoic Xiamaling artificially-matured shales. a, VLM and bituminite, 300 °C, 3 days, reflected light. b, VLM and SB, 325 °C, 3 days, reflected light. c, SB, 350 °C, 3 days, reflected light. d, VLM and bituminite, 300 °C, 3 days, same field as a, fluorescent light. e, SB, 400 °C, 3 days, reflected light. f, SB, 425 °C, 3 days, reflected light. g, SB, 450 °C, 3 days, reflected light. h, SB, 500 °C, 3 days, reflected light. i, SB, 550 °C, 3 days, reflected light.

predominant OM component. This is particularly true for pre-Devonian postmature marine shales in China, where OM content can reach up to 100 % SB, as well as in formations such as the Ordovician Utica, Upper Devonian–Lower Carboniferous Woodford, Bakken, Devonian Marcellus, Duvernay, and Barnett shales in North America (Petersen et al., 2013; Haeri-Ardakani et al., 2015; Hackley and Cardott, 2016; Liu et al., 2017; Luo et al., 2018; Mastalerz et al., 2018; Wang et al., 2019; Luo et al., 2020; Luo et al., 2021).

3.4. Thucholite

Thucholite in shales typically exhibits an irregular, sub-rounded or rounded shape with a diameter of 10 to 50 μm. Thucholite is composed of radioelement-bearing mineral particles, such as uranium (U) and thorium (Th), in addition to bitumen (Fig. 2e and f) (Crick et al., 1988; Rasmussen et al., 1989; Crick, 1992; Rasmussen et al., 1993; Luo et al., 2014). The overall shape of thucholite resembles a spherical eye (Fig. 2e and f), which can be easily confused with telalginite (Crick et al., 1988; Rasmussen et al., 1989; Crick, 1992; Rasmussen et al., 1993; Luo et al., 2014). In addition, OM in thucholite often forms a halo surrounding the radioactive mineral particles (Fig. 2e and f). The inner portion of thucholite generally exhibits higher reflectance and weaker fluorescence compared to its outer rim, suggesting that the outer perimeter underwent weaker polymerization than the inner rim (Fig. 2e and f) (Crick et al., 1988; Rasmussen et al., 1989; Crick, 1992; Rasmussen et al., 1993; Luo et al., 2014; Khan et al., 2020). The radioactive mineral particles are primarily xenotime, zircon, and monazite (Rasmussen et al., 1989; Rasmussen et al., 1993; England et al., 2001; Luo et al., 2014). These mineral particles are typically less than 10 μm in diameter and are believed to originate mainly from terrigenous clastic sources (Rasmussen et al., 1989; Rasmussen et al., 1993; England et al., 2001; Luo et al., 2014; Khan et al., 2020).

4. The genesis of typical maceral in the pre-Devonian shales

4.1. Vitrinite-like maceral

VLM, also referred to as protobitumen or marine vitrinite, is of an uncertain origin (Alpern, 1980; Zhong and Qin, 1995; Xiao et al., 1997; Luo et al., 2014; Khan et al., 2020; Yao et al., 2021). Protobitumen, which is elongated and parallel to bedding, is considered as a syndepositional, primary, and autochthonous maceral with optical characteristics similar to vitrinite (Alpern, 1980; Luo et al., 2014; Khan et al., 2020; Yao et al., 2021). Therefore, protobitumen is classified as part of VLM, although its genesis is specifically linked to the biodegradation of algae (Alpern, 1980; Luo et al., 2014; Khan et al., 2020). In this paper, we use the term VLM instead of protobitumen or marine vitrinite.

Despite their distinct origins and characteristics, VLM is often mistaken for graptolite periderm fragments or SB (Petersen et al., 2013; Hackley et al., 2018; Schmidt et al., 2019). VLM and graptolites display a

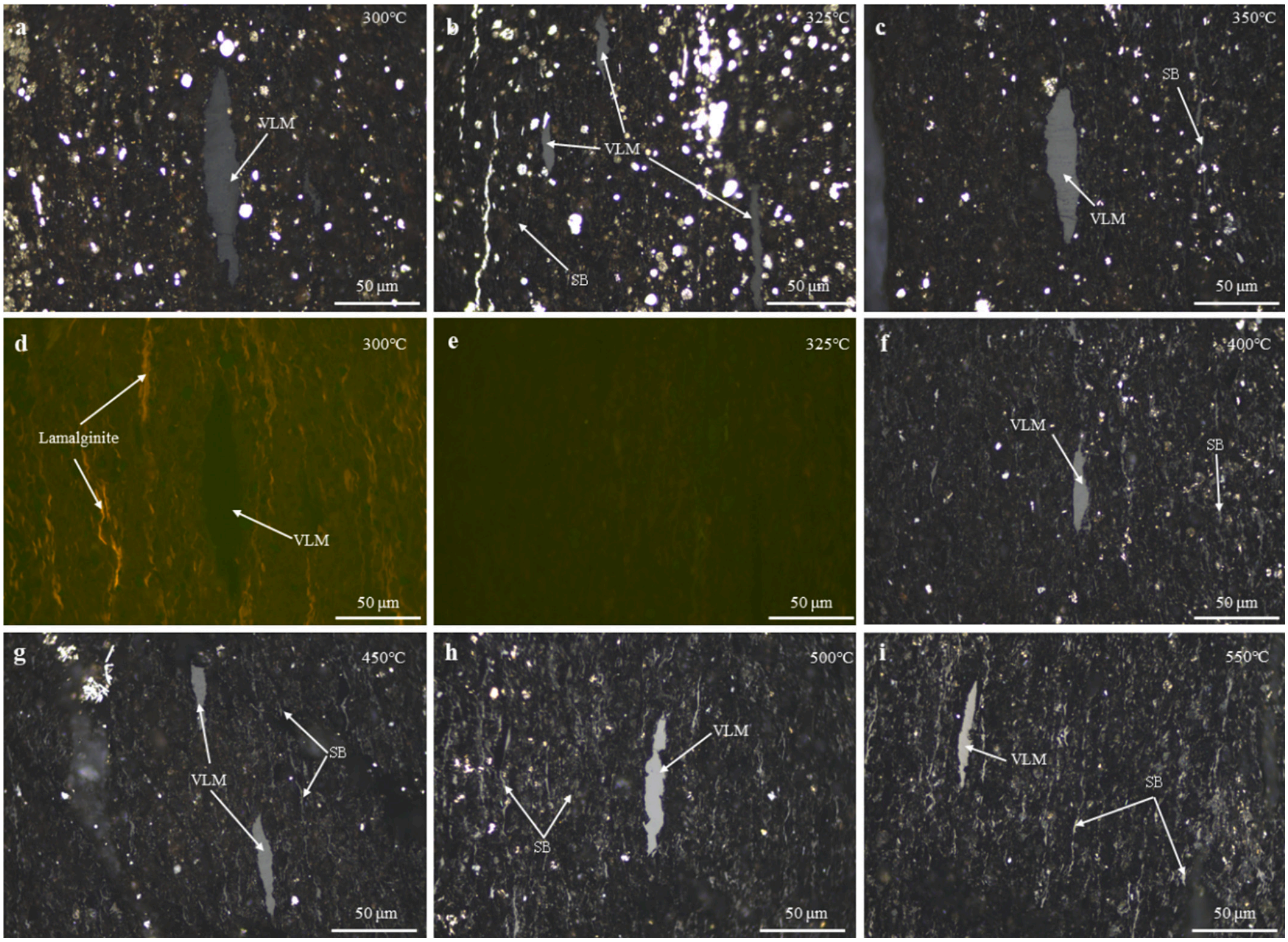

Fig. 4. Maceral evolution in the Cambrian Alum artificially-matured shales. a, VLM, 300 °C, 3 days, reflected light. b, VLM and SB, 325 °C, 3 days, reflected light. c, VLM and SB, 350 °C, 3 days, reflected light. d, VLM and lamalginite, 300 °C, 3 days, same field as a, fluorescent light. e, VLM and SB, 325 °C, 3 days, same field as b, fluorescent light. f, VLM and SB, 400 °C, 3 days, reflected light. g, VLM and SB, 450 °C, 3 days, reflected light. h, VLM and SB, 500 °C, 3 days, reflected light. i, VLM and SB, 550 °C, 3 days, reflected light.

stronger anisotropy than co-occurring in-source SB (Fig. 7) (Luo et al., 2017b; Luo et al., 2018; Luo et al., 2020; Wu et al., 2023a). Morphologically, VLM appears as irregularly elongated or ellipsoidal shape, and lacks the complex biological structures seen in graptolites, such as fusellar layers, common canal or theca (Figs. 1, 2, 3, 4, and Table 1). In contrast, in-source SB has a less homogeneous surface and lower reflectance than co-occurring VLM and graptolites. SB primarily fills pores and cracks, is dispersed within clay minerals, or occasionally aligns parallel to bedding (Figs. 1, 2, 3, 4, 5 and Table 1).

The origin of VLM has been heavily debated. Buchardt and Lewan (1990) proposed that VLM originates from the gelification of polysaccharides (such as chitin) from various organic sources. Xiao et al. (2000) examined the organic petrological characteristics of VLM in the Tarim Basin and suggested that VLM is a syndepositional maceral, primarily formed from the gelification of algae. Petersen et al. (2013) found that the reflectance distribution of VLM is similar to graptolite reflectance, interpreting VLM as previously unrecognized fragments of graptolites. Schmidt et al. (2019) documented that VLM random reflectance ($VLMR_o$) follows a similar trend to BR_o with increasing thermal maturity, and proposed that VLM may actually be SB. Khan et al. (2020) argued that VLM (referred to as protobitumen) forms through selective biodegradation of the hydrogen-rich components in OM by methanogens or sulfate-reducing bacteria under anaerobic conditions at the sediment-water interface during early diagenesis. Teng et al. (2022) speculated that VLM in the Wufeng–Longmaxi shales is a syndepositional maceral derived from graptolite fragments and acritarchs. Luo et al. (2021) conducted simulated experiments on immature Mesoproterozoic Xiamaling shales, finding that VLM was detectable at 300–325 °C but disappeared at 350–550 °C (Fig. 3). However, in the artificially matured Alum shales, VLM was consistently observed after heating at 300–550 °C (Fig. 4), aligning with observations in the naturally matured Cambrian Alum and Niutitang shales (Fig. 1) (Luo et al., 2021). The variable behaviours of VLM in these shales suggests differences in their origin and genetic mechanisms (Figs. 3 and 4) (Luo et al., 2021).

Large accumulations of SB have been widely observed in the low-maturity shales from North America (Hackley et al., 2018; Hackley et al., 2020a). VLM in the Precambrian–Cambrian shales, such as the Xiamaling and Alum shales, may represent large accumulations of SB with better polishing, distinct from in-source SB within the matrix (Hackley et al., 2018; Hackley et al., 2020a). However, this explanation for the origin of VLM in these shales is unlikely due to several key observations: (1) in the Xiamaling shales, VLM is surrounded by bituminite (Fig. 3a), suggesting its indigenous and syndepositional property. This encirclement suggests that VLM was deposited alongside other OM rather than forming as secondary SB; (2) in-source SB exhibits a strong capacity for gas generation during the postmature stage, as discussed in Section 8.2. If VLM was simply large accumulations of SB in the

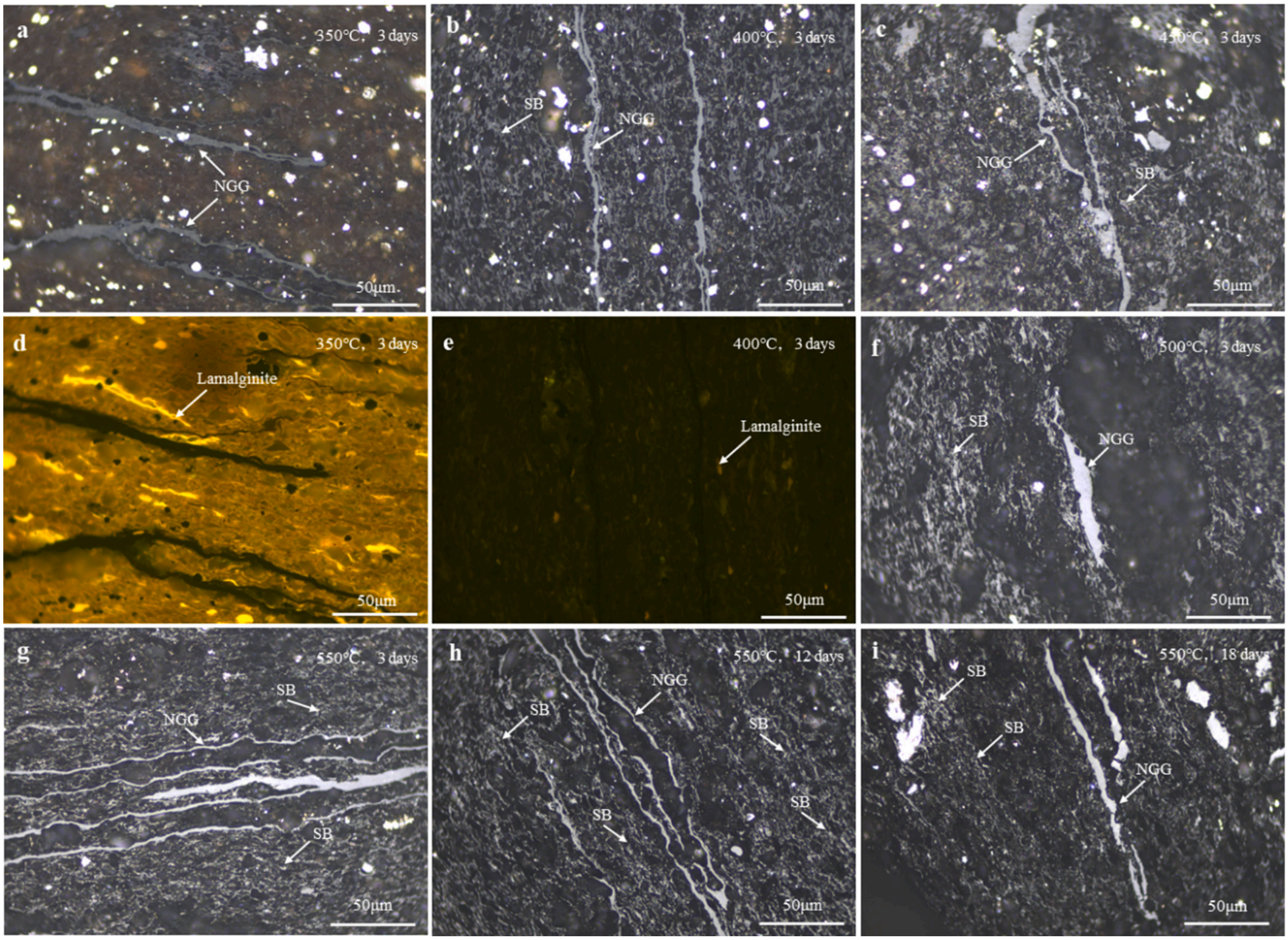

Fig. 5. Maceral evolution in the Ordovician Alum artificially-matured shales. a, NGG and lamalginite, 350 °C, 3 days, reflected light. b, NGG and SB, 400 °C, 3 days, reflected light. c, NGG and SB, 450 °C, 3 days, reflected light. d, NGG and lamalginite, 350 °C, 3 days, same field as a, fluorescent light. e, NGG and lamalginite, 400 °C, 3 days, same field as b, fluorescent light. f, NGG and SB, 500 °C, 3 days, reflected light. g, NGG and SB, 550 °C, 3 days, reflected light. h, NGG and SB, 550 °C, 12 days, reflected light. i, NGG and SB, 550 °C, 18 days, reflected light.

Cambrian shales, we would expect its mass to decrease significantly due to hydrocarbon generation as thermal maturity increases. However, VLM persists in the both natural and laboratory-matured Cambrian shales, implying its refractory nature (Figs. 1 and 4); (3) VLM in the Cambrian postmature shales shows much stronger anisotropy than co-occurring in-source SB (Fig. 7c and d). This anisotropy is a distinguishing feature between the two macerals, further supporting that VLM is not simply SB but a distinct maceral.

Previous study on the Precambrian natural and artificial shales suggested that VLM in the Precambrian shales is associated with bacterial degradation processes of bituminite or lamalginite, such as methanogens or sulphate-reducing bacteria activity under anoxic conditions (Khan et al., 2020; Luo et al., 2021; Yao et al., 2021). These biodegradation processes occur in the depositional water column, or during early diagenesis, selectively degrading the hydrogen-rich components of OM. The detection of 25-norhopane compounds and unresolved compound mixtures (UCM) in the Precambrian shales, such as those from the Hongshuizhuang, Xiamaling, and Salt Range formations, further confirms that OM in these shales has undergone extensive biodegradation (Luo et al., 2014; Luo et al., 2015; Khan et al., 2020).

VLM in the Cambrian natural and artificially matured samples is tightly compacted by surrounding minerals, indicating its resistance to decomposition and degradation. For example, Luo et al. (2021) proposed that VLM in the Cambrian shales may originate from reproductive cells of green algae and cyanobacteria, known as akinete cells, which exhibit spherical, oval, or elongated oval shapes (Figs. 1 and 2) (Fay, 1983; Luo et al., 2021). Akinete cells have thick walls and are surrounded by a multilayered extracellular envelope composed of mucilaginous sheaths, glycogen, and dense fibers (Braune, 1980; Nichols et al., 1980; Herdman, 1988; Stasiuk, 1993; Perez et al., 2016; Perez et al., 2018). These cells are typically connected by cell walls, forming beaded or elongated shapes, and they exhibit strong tolerance to extreme environmental conditions.

4.2. *Graptolite periderm*

GG and NGG are thought to originate from different parts of the graptolite (Goodarzi, 1984). GG likely derived from the common canal, while NGG is probably associated with the graptolite wall, which contains parallel layers (Goodarzi, 1984). Luo et al. (2018) conducted an artificial maturation experiment on a graptolite-bearing shale from Estonia. The original shale sample, which is mature with a graptolite random reflectance (GR_o) of 0.65 %, exhibits a granular texture in its graptolites. However, after heating the sample at 400 °C for three days, NGG became the dominant organic component, and GG was barely observed in the artificially matured sample, which had a GR_o of 1.24 %. Based on this experiment, this suggests that GG can be transformed into NGG through heating (Luo et al., 2018).

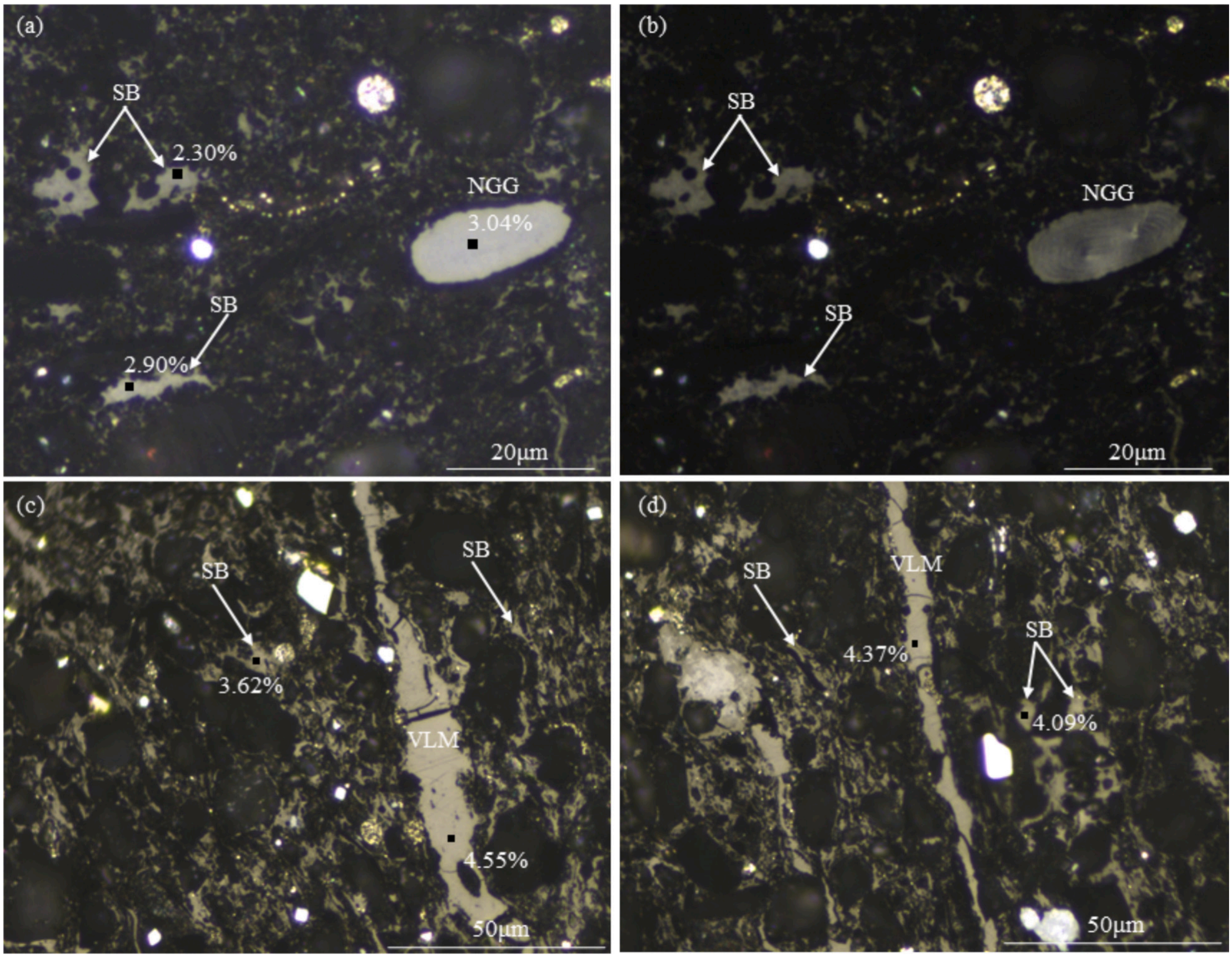

Fig. 6. The reflectance comparison between NGG, VLM, and co-occurring SB. a, NGG displays a higher reflectance than SB in the Wufeng-Longmaxi Formation, reflected light. b, same field as a, polarized light. c, VLM displays a higher reflectance than SB in the Niutitang Formation, reflected light. d, VLM displays a higher reflectance than SB in the Niutitang Formation, reflected light. Fig. a and b is cited from Luo et al. (2019).

4.3. In-source solid bitumen (SB)

Several processes have been proposed to explain the formation of reservoir SB, including thermal cracking (Stasiuk, 1997; Hu et al., 2010), gas deasphalting (Hwang et al., 1998), biodegradation (George et al., 1994), thermochemical sulfate reduction (TSR) (Machel et al., 1995; Stasiuk, 1997; Machel, 2001; Hu et al., 2010), oil mixing (Hwang et al., 1998), and clay minerals adsorption (Czarnecka and Gillott, 1980; Dean and McAtee, 1986; Dubey and Waxman, 1991; Pernyeszi et al., 1998). Identifying a specific mechanism for SB formation, especially for the postmature SB, is difficult, as multiple mechanisms usually contribute (Rogers et al., 1974; Stasiuk, 1997; Gao et al., 2018; Mastalerz et al., 2018). The widespread occurrence SB in the dolomites from the Sinian Dengying and Cambrian Longwangmiao formations, Sichuan Basin is thought to be related to hydrothermal activity and TSR based on a comprehensive geochemical and petrographic analysis (Gao et al., 2018; Zhang et al., 2019a). However, the permeability and porosity of many reservoirs are usually much higher than those in shales, making it difficult for processes (i.e., hydrothermal activity and TSR) to occur in less permeable shales. Thus, the formation of in-source SB differs from that of reservoir SB (Luo et al., 2021). The optical properties of SB in the Cambrian postmature shales (in-source SB) are compared with those of the Sinian-Cambrian postmature reservoir dolomites (reservoir SB), revealing that in-source SB has much lower anisotropy than reservoir SB (Luo et al., 2021). This difference may arise from their respective origins: reservoir SB and in-source SB are derived from the thermal cracking of expelled petroleum and retained petroleum, respectively (Goodarzi et al., 1993; Stasiuk, 1997; Luo et al., 2018; Mastalerz et al., 2018). Because of geo-chromatographic effects, the retained petroleum generally contains more polar hydrocarbons than the expelled petroleum (Tissot and Welte, 1984; Jubb et al., 2019), significantly affecting the optical characteristics of SB (Carr and Williamson, 1990; Stasiuk, 1997; Hackley and SanFilipo, 2016; Hackley et al., 2020b; Luo et al., 2021). Saturates and aromatics are more effective than NSO-enriched oil to generate anisotropic SB (Stasiuk, 1997).

The pre-Devonian marine shales are generally rich in OM, with Type II kerogen, indicating a high oil-generative potential (Luo et al., 2018; Luo et al., 2020; Luo et al., 2021). In-source SB in these shales is thought to form from the secondary cracking of residual petroleum, in-situ thermal transformation of oil-prone OM, or a combination of both (Luo et al., 2018; Mastalerz et al., 2018; Luo et al., 2020; Sanei, 2020; Luo et al., 2021; Liu et al., 2022). The thermal conversion of algae-derived kerogen, such as alginite and bituminite, into in-source SB has been widely observed in both natural and artificial shale samples (Figs. 3, 4, and 5) (Luo et al., 2018; Mastalerz et al., 2018; Luo et al., 2021; Liu et al., 2022). In the marine shales from North America and China with a VR_o range of 0.9–5.0 %, OM is primarily composed of in-source SB, as algae-derived OM has been largely transformed into hydrocarbons and/or SB (Hackley and Cardott, 2016; Luo et al., 2018; Mastalerz et al., 2018; Luo et al., 2020; Luo et al., 2021).

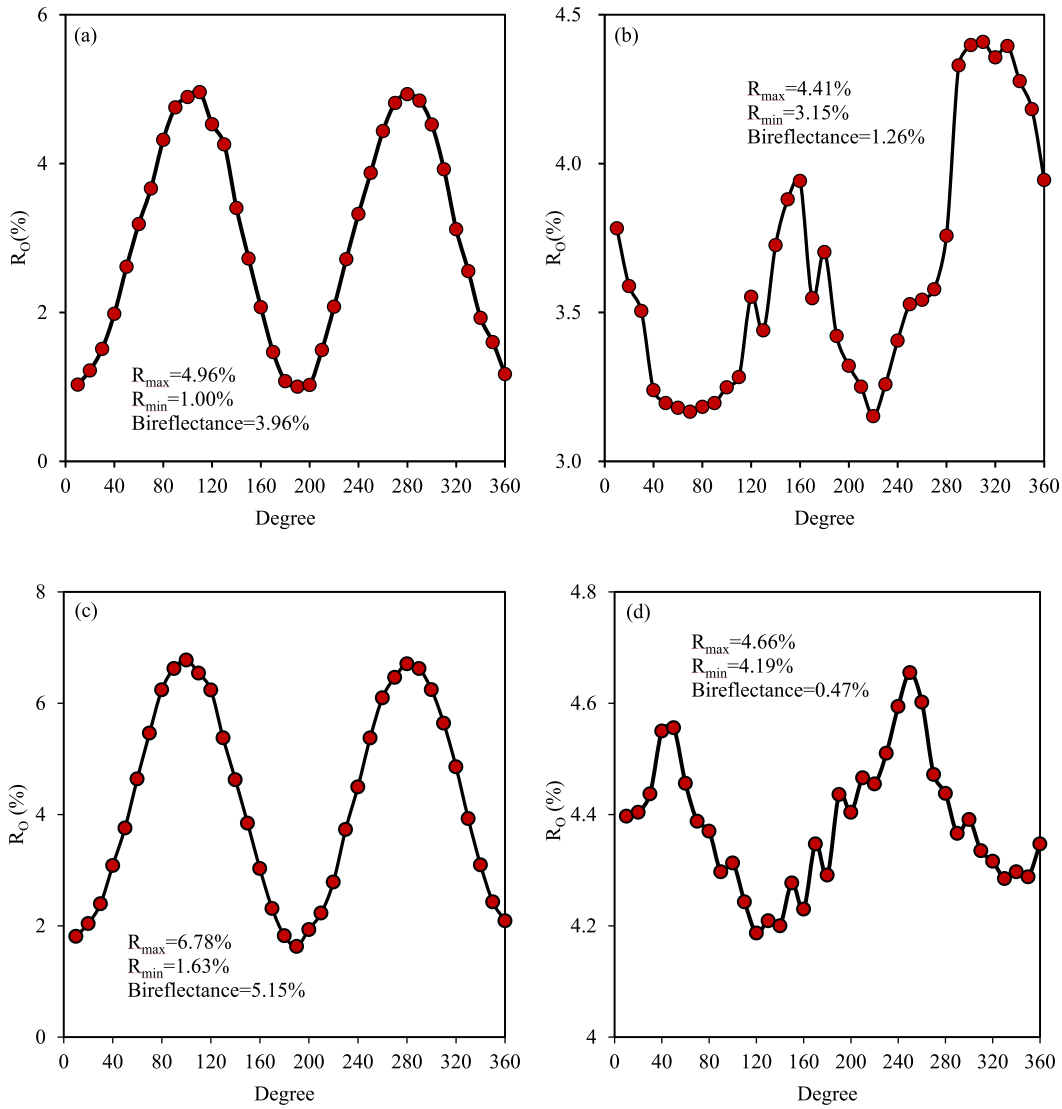

Fig. 7. The bireflectance comparison between NGG, VLM, and co-occurring SB. a, NGG displays strong anisotropy as indicated by its bireflectance of 3.96 % in the Wufeng-Longmaxi Formation. b, SB displays lower anisotropy as indicated by its bireflectance of 1.26 % compared with co-occurring GG in a. c, VLM displays strong anisotropy as indicated by its bireflectance of 5.15 % in the Niutitang Formation. d, SB displays lower anisotropy as indicated by its bireflectance of 0.47 % compared with co-occurring VLM in c.

4.4. Thucholite

Thucholite was first identified in carbonaceous material containing radioactive elements (Ellsworth, 1928). It is commonly found in sandstone and conglomerate reservoirs, where it forms through the polymerization of bitumen induced by the ionizing radiation emitted from radioactive elements in mineral particles (Crick et al., 1988; Rasmussen et al., 1989; Crick, 1992; Rasmussen et al., 1993; Luo et al., 2014). Thucholite was also detected in the shales from formations such as Barney Creek, Hongshuizhuang, Xiamaling, Salt Range, and Alum formations (Fig. 2e and f) (Crick et al., 1988; Luo et al., 2014; Khan et al., 2020; Zheng et al., 2021b; Luo et al., 2023). However, its formation in shales differs from that in sandstone and conglomerate reservoirs due to the low permeability and porosity of shales. In shales, radioactive mineral particles, likely derived from the source area through strong chemical weathering, were transported and deposited onto algal mats. The ionizing radiation from these radioactive particles then polymerized the alginites (Luo et al., 2014; Khan et al., 2020). Reflectance distribution and optical analysis of thucholite indicate that the radioactive heat does not significantly affect the overall thermal maturity of the rock unit (Luo et al., 2014).

5. Thermal maturity indicators for the pre-Devonian shales

5.1. Vitrinite-like maceral reflectance

Thermal simulation experiments conducted by Luo et al. (2021) demonstrate that VLM is highly sensitive to temperature, with its reflectance ($VLMR_o$) increasing as temperature rises. In the Lower Cambrian marine shales, $VLMR_o$ can effectively characterize OM maturity due to its synsedimentary primary characteristics and distinct optical properties (Buchardt and Lewan, 1990; Xiao et al., 2000; Schmidt et al., 2019; Luo et al., 2021). Xiao et al. (2000) reported that $VLMR_o$ could be used to evaluate thermal maturity and identified three stages in the thermal evolution of VLM. At each stage, linear relationships between $VLMR_o$ and $EqVR_o$ were established based on both artificially and naturally matured shales (Xiao et al., 2000): $EqVR_o = 1.26 \times VLMR_o + 0.21$ for $VLMR_o < 0.75$ %; $EqVR_o = 0.28 \times VLMR_o + 1.03$ for $VLMR_o$ between 0.75 % and 1.50 %; $EqVR_o = 0.81 \times VLMR_o + 0.18$ for $VLMR_o > 1.50$ %. Wu et al. (2023b) confirmed that VLM has a similar chemical structure with vitrinite, based on its Raman spectral characteristics, further validating the use of $VLMR_o$ as a reliable thermal maturity indicator. Luo et al. (2021) established a conversion equation between $VLMR_o$ in sections perpendicular to bedding and $EqVR_o$ based on thermal simulation experiments, $EqVR_o = 1.07 \times VLMR_o - 0.18$. Additionally, Wu et al. (2023a) found that $VLMR_{max}$ has a good positive correlation with $VLMR_o$, and obtained an equivalent conversion formula between $VLMR_{max}$ and $EqVR_o$, wherein $EqVR_o = 0.67 \times VLMR_{max} + 0.32$.

5.2. Graptolite reflectance

Graptolite reflectance, which increases with burial depth, has proven to be a useful proxy for evaluating thermal maturity in the pre-Devonian shales. However, the relationship between graptolite reflectance and $EqVR_o$ remains a topic of debate (Teichmüller, 1978; Crowther, 1981; Goodarzi, 1984; Goodarzi and Norford, 1987; Goodarzi and Norford, 1989; Riediger et al., 1989; Link et al., 1990; Cole, 1994; Gentzis et al., 1996; Petersen et al., 2013; Luo et al., 2017b; Luo et al., 2018; Luo et al., 2020). The postmature graptolites display a strong anisotropy, so $GR_{o\text{-}max}$ has traditionally been used to determine thermal maturity (Teichmüller, 1978; Crowther, 1981; Goodarzi, 1984; Goodarzi and Norford, 1987; Goodarzi and Norford, 1989; Riediger et al., 1989; Link et al., 1990; Gentzis et al., 1996; Petersen et al., 2013; Luo et al., 2017b). Recent research has shown that the measurement process for GR_o is simpler, more accurate, and provides more practical values, with a much lower standard deviation compared to GR_{omax}. This suggests that GR_o could be reliably used to evaluate thermal maturity instead of GR_{omax} (Luo et al., 2018; Wang et al., 2019; Luo et al., 2020; Song et al., 2023). Raman spectral analysis of both natural and artificially matured samples further supports the use of GR_o as a thermal maturity indicator. The chemical structure of graptolite periderm responds to thermal evolution in a manner similar to that of vitrinite, reinforcing the validity of GR_o as a maturity parameter. Additionally, the separation between the G and D peaks in the Raman spectra of graptolite periderm has been proposed as an effective thermal maturity parameter in the graptolite-bearing shales (Hao et al., 2019; Wang et al., 2019; Luo et al., 2020).

GR_o is generally considered to be close to $EqVR_o$ (Table 2 and Fig. 8a) (Bustin et al., 1989; Bertrand, 1990). Cole (1994) found that the relationship between GR_o and $EqVR_o$ varied based on redox conditions, with $EqVR_o$ is equivalent to 80 % and 65 % of GR_o deposited under reducing and oxygenated environments, respectively (Table 2 and Fig. 8a). Petersen et al. (2013) identified a bimodal distribution in graptolite reflectance and established a relationship between the "lower values" group of GR_o and $EqVR_o$ through T_{max} conversion (Table 2 and Fig. 8a). Synnott et al. (2018) observed a linear correlation between GR_o and T_{max}, with GR_o being typically higher than $EqVR_o$ (Table 2 and Fig. 8a). However, Synnott et al. (2018) also pointed out that the differences in the slope of the plot between GR_o and T_{max} could be attributed to the differential evolution of GR_o in variable graptolite species, or to inaccurate T_{max} in the postmature shales due to low S_2. Based on artificial maturation experiments on graptolite-bearing shales and coals, GR_o was close to vitrinite reflectance at the same thermal maturity, and their relationship was as follows: $EqVR_o = 0.99 \times GR_o + 0.08$ (Table 2 and Fig. 8a) (Bustin et al., 1989; Bertrand, 1990; Luo et al., 2018; Luo et al., 2020). However, an anomalous decrease in the slope of GR_o was first reported in the artificially matured graptolite-rich samples using hydrous gold tube pyrolysis. This anomaly was attributed to suppressed GR_o in the postmature stage, likely due to the presence of nanoporosities (Zheng et al., 2022). This suggests that a thermal maturity correction may be required for transforming GR_o into $EqVR_o$ in the postmature samples (Zheng et al., 2022).

5.3. In-source solid bitumen reflectance

BR_o increases with thermal maturity and serves as an alternative

Table 2
Empirical equations used to calculate $EqVR_o$ from GR_o or GR_{omax}.

Equations	References	Formation	GR_o data range
$Log_{10} GR_o = -0.04 + 1.10 \times Log_{10} EqVR_o$	(Bertrand, 1990)	upper Gaspe Limestone Group and Chaleurs Group, Canada	0.50–3.0 %
$EqVR_o = 0.8 \times GR_o$ (anoxic) $EqVR_o = 0.65 \times GR_o$ (oxic)	(Cole, 1994)	Silurian Qusaiba Shale, Saudi Arabia	0.62–2.05 %
$EqVR_o = 0.882 \times GR_o - 0.366$	(Zhong and Qin, 1995)	Cambrian-Ordovician, China	1.80–4.90 %
$EqVR_o = 0.73 \times GR_o + 0.16$	(Petersen et al., 2013)	Alum shale, Scandinavia	0.47–2.14 %
$EqVR_o = 0.785 \times GR_o + 0.05$	(Colţoi et al., 2016)	Silurian intervals, Romania	No data
$EqVR_o = 0.232 + 0.499 \times GR_o$	(Synnott et al., 2018)	Cape Phillips Formation, Canada	0.59–1.02 %
$EqVR_o = 1.055 \times GR_o - 0.053$ $EqVR_o = 0.546 \times GR_{omax} + 0.35$	(Luo et al., 2018)	Wufeng–Longmaxi formations	0.65–4.03 %
$EqVRo = 0.97 \times GR_o - 0.2$ (2.19 % < GR_o < 3.5 %) $EqVRo = 0.22 \times GR_o + 2.55$($GR_o$ > 3.5 %)	(Wang et al., 2019)	Wufeng–Longmaxi formations	1.21–4.91 %
$EqVR_o = 0.99 \times GR_o + 0.08$ $EqVR_o = 0.515 \times GR_{omax} + 0.506$	(Luo et al., 2020)	Data were collected from references	0.43–4.62 %

maturity indicator in sedimentary rocks (mostly shales and carbonate rocks) when vitrinite is absent, especially in the pre-Devonian rocks where SB is a prominent component (Jacob, 1989; Landis and Castaño, 1995; Schoenherr et al., 2007; Hackley and Cardott, 2016; Luo et al., 2018; Mastalerz et al., 2018; Liu et al., 2019a; Schmidt et al., 2019; Luo et al., 2020; Luo et al., 2021; Luo et al., 2023; Hackley et al., 2024). Numerous empirical equations have been proposed to calculate $EqVR_o$ from BR_o (Table 3 and Fig. 8b). However, these equations are often derived from data specific to particular rock types or sedimentary basins, making their general application across different terranes questionable. In theory, each formation should have its own equation to calculate $EqVR_o$. Despite these limitations, the empirical equations from Jacob (1989), Landis and Castaño (1995), and Schoenherr et al. (2007) are still widely used. It is important to note that the equation in Schoenherr et al. (2007) was based on the datasets from the other two studies.

Several factors influence BR_o, such as lithology, SB type, optical characteristics of SB, pore development in SB, and the original kerogen composition. The correlations between BR_o and vitrinite reflectance vary across different lithologies (e.g., limestone, shale, sandstone) (Bertrand, 1990; Bertrand, 1993; Bertrand and Malo, 2001). Pre-oil SB has lower reflectance than post-oil SB and should be excluded from BR_o measurements (Liu et al., 2019a). SB can show diverse optical characteristics, affecting the reliability of BR_o as a maturity indicator. For example, Landis and Castaño (1995) studied the reflectance of anisotropic, granular, and homogenous SB, suggesting that only homogenous SB is recommended for reflectance measurement. Secondary organic pores, which form in SB due to hydrocarbon generation during thermal maturation, can lower reflectance values by adsorbing light (Loucks et al., 2009; Schieber, 2010; Curtis et al., 2012; Loucks et al., 2012; Cardott et al., 2015; Liu et al., 2017; Camp, 2019; Liu et al., 2022). Granular SB with nanopores exhibits lower reflectance than SB with smooth surfaces (Sanei et al., 2015). Moreover, SB in marine shales can be mistaken for vitrinite, leading to incorrect thermal maturity assessments (Wei et al., 2016; Hackley and Lewan, 2018; Hackley et al., 2020a; Goodarzi et al., 2022). Recent studies have focused on

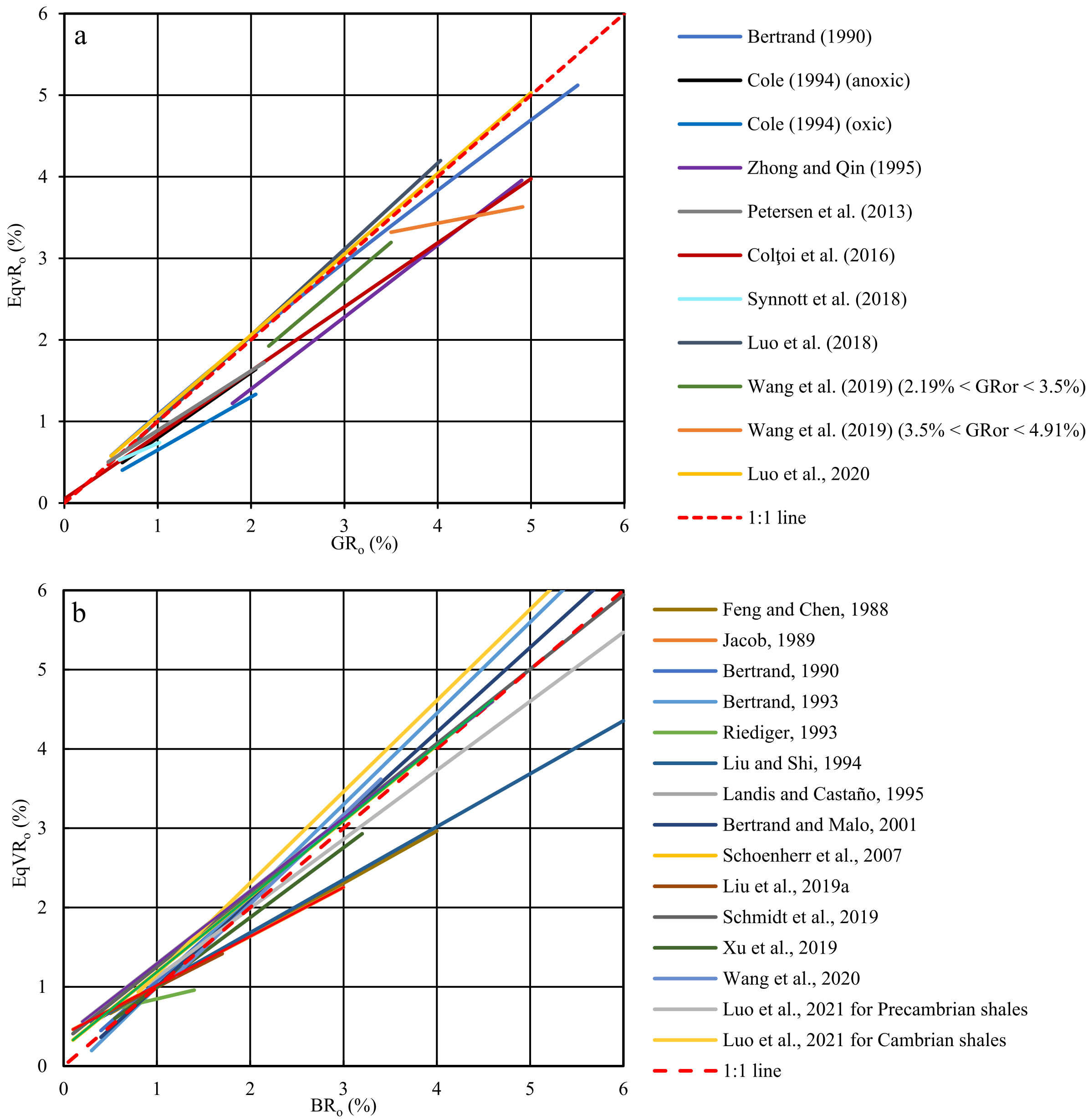

Fig. 8. a, Empirical equations between EqVR$_o$ and GR$_o$. b, Empirical equations between EqVR$_o$ and BR$_o$.

comparing BR$_o$ in reservoirs and associated source rocks buried at comparable depths, revealing significant differences. For example, in a single well from the Sichuan basin, reservoir SB in a Sinian Dengying dolomite reservoir at a depth of 5033 m has a reflectance of 4.58 %, which is notably higher than BR$_o$ of ~3.39 % from a Lower Cambrian Qiongzhusi black shale at 4976 m depth (Table 4). A similar pattern was observed in a single well from the Tarim basin, where BR$_o$ in six black shales from the Yurtus Formation (depth 5835–5854 m) ranges from 2.05 to 2.29 %, which is lower than BR$_o$ of 3.2 % in the Upper Sinian dolomite reservoir at a depth of 5869 m (Table 4). Comparable findings have also emerged from boreholes in North America. In the R. Ricker #1 well from the Midland Basin, BR$_o$ values has been measured in 16 samples of the Wolfcamp Formation at a depth of 2410.15–2443.22 m. BR$_o$ falls into the range of 0.55–0.73 %, averaging 0.68 %, in 12 siliceous and calcareous mudrocks, whereas BR$_o$ spans from 0.69 to 0.86 %, averaging 0.77 %, in 4 fine-grained carbonates (Table 4) (Hackley et al., 2020b). Similarly, in the Williston Basin of North Dakota, BR$_o$ is 0.38 % in organic-rich mudstone (~3264.25 m deep) and 0.55 % in carbonate beds from the Ordovician Stonewall Formation (~3264.22 m deep) (Table 4) (Jubb et al., 2019). The differences in reflectance can be due to the higher aromatic contents in the expelled petroleum, with more aromatics resulting in a higher reflectance for reservoir SB compared to in-source SB (Carr and Williamson, 1990). A recent study showed that BR$_o$ in the Alum shales increased at a slower rate than that in the Mesoproterozoic Xiamaling shales, likely due to differences in kerogen composition (Luo et al., 2021). For this reason, this paper focuses exclusively on in-source SB, hereinafter referred to simply as SB. In the pre-Devonian naturally or artificially matured samples, BR$_o$ shows a strong positive linear correlation with both GR$_o$ and VLMR$_o$, with correlation coefficients (R^2) of 0.88 or 0.98, respectively (Luo et al., 2018; Wang et al., 2019; Luo et al., 2020; Luo et al., 2021). BR$_o$ is generally lower than co-occurring GR$_o$ and VLMR$_o$ in the samples (Fig. 6 and Table 1) (Luo et al., 2018; Wang et al., 2019; Luo et al., 2020; Luo et al., 2021; Song et al., 2023). Hackley et al. (2024) recently found that BR$_o$ measured prior to extraction correlates strongly with T_{max}, suggesting that BR$_o$ can serve as a direct proxy for thermal maturity in the Paleozoic marine shales. The results of thermal simulation experiments have demonstrated that SB is sensitive to temperature, with its reflectance

Table 3
Empirical equations used to calculate $EqVR_o$ from BR_o.

Equation	References	Sample information	BR_o (%) range
$EqVR_o = 0.6569 \times BR_o + 0.3364$	(Feng and Chen, 1988)	SB in the reservoirs or source rocks	~0.5–4.0
$EqVR_o = 0.618 \times BR_o + 0.4$	(Jacob, 1989)	Migrabitumen	~0.1–3.0
$EqVR_o = (BR_o + 0.03)/0.96$	(Bertrand, 1990)	Kerogen from various lithologies	~0.4–2.0
$EqVR_o = (BR_o - 0.13)/0.87$	(Bertrand, 1993)		~0.3–6.0
$EqVR_o = 0.618 \times BR_o + 0.4$	(Riediger, 1993)	Migrabitumen	~0.1–0.52
$EqVR_o = 0.277 \times BR_o + 0.57$		Kerogen from the Lower Jurassic sulfur-rich source rocks	~0.52–1.4
$EqVR_o = 0.668 \times BR_o + 0.346$	(Liu and Shi, 1994)	SB in the carbonates	~0.3–6.0
$EqVR_o = (BR_o + 0.41)/1.09$	(Landis and Castaño, 1995)	SB in the reservoirs or source rocks	~0.2–4.6
$EqVR_o = (BR_o - 0.059)/0.936$	(Bertrand and Malo, 2001)	Kerogen from Siluro-Devonian rocks	~0.4–6.5
$EqVR_o = (BR_o + 0.2443)/1.0495$	(Schoenherr et al., 2007)	Data were collected from references	~0.1–4.6
$EqVR_o = 0.5992 \times BR_o + 0.3987$	(Liu et al., 2019a)	SB in the New Albany Shale	~0.35–1.71
$EqVR_o = 0.938 \times BR_o + 0.3145$	(Schmidt et al., 2019)	Data were collected from references	~0.1–6.0
$EqVR_o = 0.8798 \times BR_o + 0.1145$	(Xu et al., 2019)	SB in the Mesoproterozoic Hongshuizhuang shales	~0.58–3.18
$EqVR_o = 1.125 \times BR_o - 0.2062$	(Wang et al., 2020)	SB in the Silurian shales	~1.21–3.37
$EqVRo = 0.87 \times BRo + 0.25$	(Luo et al., 2021)	SB in the Mesoproterozoic Xiamaling shales	~0.76–4.82
$EqVRo = 1.15 \times BRo + 0.01$		SB in the Cambrian shales	~0.79–3.89

increases as temperature rises (Luo et al., 2018; Wang et al., 2019; Xu et al., 2019; Luo et al., 2020; Luo et al., 2021). Thus, increasing BR_o serves as a reliable indicator of OM maturity and thermal evolution in shales (Table 3) (Luo et al., 2018; Wang et al., 2019; Xu et al., 2019; Luo et al., 2020; Luo et al., 2021; Hackley et al., 2024).

6. The maceral composition of the pre-Devonian shales and its implications

OM serves as the primary source for most petroleum, and both the generation potential and the properties of resulting petroleum are highly dependent on maceral composition (Tissot et al., 1974; Tissot and Welte, 1984). This section reviews the maceral composition of some globally well-studied Paleoproterozoic to Silurian shales, providing insights into their petroleum production, and in some cases, their production potential.

6.1. Australia

6.1.1. The Paleoproterozoic Barney Creek Formation, McArthur Basin

The petrographic examination of the Paleoproterozoic Barney Creek shales reveals that lamalginite is the dominant maceral, oriented parallel to bedding and surrounding mineral grains. This oil-prone liptinite maceral constitutes more than 2 % of OM dispersed in the rock, with local concentrations exceeding 10 %. However, bioclasts are absent, and SB is predominantly observed as fine granules dispersed within the mineral matrix, believed to be the residual product of hydrocarbon generated from lamalginite (Crick et al., 1988; Ranasinghe and Crosdale, 2022). These organic-rich shales in the greater McArthur Basin have the potential to generate both conventional and unconventional oil and gas. As one of the oldest active hydrocarbon systems globally, the Paleoproterozoic Barney Creek shale is organic-rich (TOC up to 7 %), contains oil-prone kerogen, and represents an important hydrocarbon-bearing system with ongoing exploration activities (Jarrett et al., 2019). The substantial OM content highlights the potential for hydrocarbon generation, positioning the McArthur Basin as a key area of interest for current and future exploration (Jarrett et al., 2019). Consequently, it holds significant economic value as a potential target for petroleum exploration (Munson et al., 2020).

6.1.2. The Mesoproterozoic Velkerri Formation, McArthur Basin

OM in the Mesoproterozoic Velkerri black shales primarily originated from prokaryotes, likely cyanobacteria (Summons et al., 1994; Demoulin et al., 2019), which thrived in the suboxic to anoxic environments (Faiz et al., 2022). Petrographic studies identified various types of organoclasts, including alginite, bituminite, SB, and thucholite. Some alginites display akineted cell-heterocyst type structures, suggesting the remnants of cyanobacteria (Stasiuk et al., 2014). Bituminite, observed only at low maturities, often contains mineral inclusions and mixes with other OM (Faiz et al., 2022). In these shales, SB exhibits reflectance values comparable to co-existing alginite, but at higher maturities, the polished surfaces of larger SB grains are irregularly shaped, with significant reflectance anisotropy and mottled textures (Faiz et al., 2022). The Velkerri Formation, located within the Beetaloo Sub-basin, is notable for its high TOC content, reaching up to 10 %. Since the initial discovery of live hydrocarbons in 1985, exploration of the Velkerri Formation has focused on assessing its oil and gas reserves (Cox et al., 2022). The formation also garners substantial interest as an unconventional gas play (Close et al., 2017; Revie and MacDonald, 2017), with estimated gas-in-place reserves of approximately 3.34×10^{12} m^3 (Munson, 2014; Revie and MacDonald, 2017).

6.2. China

6.2.1. The Mesoproterozoic Hongshuizhuang Formation, North China

The Hongshuizhuang shales were primarily deposited in shallow shelf under low-energy, anoxic environments (Luo et al., 2014; Luo et al., 2016a). These organic-rich shales have a thickness ranging from 35 to 48 m, with TOC contents between 0.41 and 8.00 %, averaging 3.56 % (Luo et al., 2013; Luo et al., 2014). The OM composition is dominated by lamalginite, bituminite, VLM and rare thucholite (Fig. 2). On the

Table 4
Comparison of in-source SB (shale and mudstone) and reservoir SB (carbonate and dolomite) reflectance in the sediments at close depth from the same well.

Basin	Formation	Depth (m)	Lithology	BR_o (%)	Source
Sichuan basin	Qiongzhusi	4976	Shale	3.39	This study
	Dengying	5033	Dolomite	4.58	
Tarim basin	Yurtus	5835–5854	Shale	2.05–2.29	
	Qigebulake	5869	Dolomite	3.20	
Midland basin	Wolfcamp	2410.15–2443.22	Siliceous and calcareous mudstones	0.55–0.73 (Avg. 0.68)	(Hackley et al., 2020b)
			Carbonate	0.69–0.86 (Avg. 0.77)	
Williston basin	Stonewall	3264.25	Mudstones	0.38	(Jubb et al., 2019)
		3264.22	Carbonate	0.55	

other hand, VLM comprises less than 10 % of OM and has a reflectance of 0.68–0.78 % (Luo et al., 2014; Luo et al., 2016a; Ma et al., 2017; Luo et al., 2023). The oil saturation index (OSI) of the Hongshuizhuang shales ranges from 50 to 135 mg/g, with an average of 85 mg/g (Li et al., 2023). Core samples from the JQ1 well revealed abundant oil shows (Luo et al., 2016a), and the estimated oil reserves in the Jibei Depression of the Yanshan Basin could reach up to 1×10^{19} tons (Li et al., 2023). These findings indicate that the Hongshuizhuang Formation has a significant exploration potential for shale oil.

6.2.2. The Mesoproterozoic Xiamaling Formation, North China

The Xiamaling Formation is considered as low-maturity source rocks, primarily deposited in an anoxic environment, and contains abundant black shales with well–preserved OM (Zhang et al., 2015; Zhang et al., 2016; Wang et al., 2017b; Wang et al., 2018; Zhang et al., 2019b; Luo et al., 2021; Wu et al., 2022). This formation ranges from 0 to 450 m in thickness, with TOC of 0.50–16.70 %, averaging 1.67 % (Liu et al., 2019b). In the Xiamaling shales from Xiahuayuan, Hebei Province, $VLMR_o$ falls in the range of 0.43–0.68 % (Luo et al., 2021; Wu et al., 2022; Luo et al., 2023). The OM composition is similar to that of the Hongshuizhuang Formation, with lamalginite and bituminite being the primary components, VLM comprising less than 10 %, and occasional thucholite (Fig. 1) (Luo et al., 2021; Wu et al., 2022). The $EqVR_o$ values, calculated from BR_o, range between 1.3 and 2.0 % in the Jingxi sag and Mihuai uplift. The black shales in these regions, with a thickness of 100–250 m, show potential as favorable exploration targets for shale gas (Liu et al., 2019b; Zhang et al., 2022).

6.2.3. The Neoproterozoic Datangpo Formation, Sichuan Basin

The Datangpo Formation was deposited in a relatively restricted sedimentary basin with limited communication with the open ocean, as indicated by the reconstruction of paleogeography and paleobathymetry (Li et al., 2012). The thickness of the shales ranges from 16 to 180 m. Their TOC varies between 0 and 8.50 %, and minerals are dominated by clays and quartz with a percentage of 57–68 % and 5–22 %, respectively (Li et al., 2012; Cheng et al., 2018; Ye et al., 2018). BR_o within the Datangpo Formation ranges from 3.19 to 3.80 %, with the maceral composition primarily consisting of SB (Fig. 1c) (Luo et al., 2023). The Datangpo Formation is well-known for its manganese ores (Yu et al., 2016; Ma et al., 2019). However, shale gas exploration in the Datangpo Formation has yet to show significant progress.

6.2.4. The Neoproterozoic Doushantuo Formation, Sichuan Basin

The Doushantuo Formation consists primarily of marine shales and carbonates, preserving a compelling record of multicellular fossil life and acritarchs, which are considered as evidence of some of Earth's earliest macroscopic animals (Xiao et al., 1998; Xiao et al., 2004; Yin et al., 2007; Cohen et al., 2009). This formation is divided into four units, with the second unit deposited in dysoxic-anoxic environments. The second unit contains organic-rich shales with thickness ranging from 50 to 115 m (Li et al., 2004; Yong et al., 2012; Cheng et al., 2013; Xu and Guo, 2015; Zhang et al., 2022). The shales have TOC ranging from 0.2 to 4.1 %, and their $EqVR_o$, calculated from BR_o, is 1.80–2.20 %, indicating gas-window maturity (Peng et al., 2017; Zhang et al., 2022). The maceral composition is similar to that of the Datangpo shales, with SB being the only form of OM present (Fig. 2c and d) (Luo et al., 2023). The mineral composition of the Doushantuo Formation is characterized by a high percentage of brittle minerals, ranging from 19.6 and 80.0 %, with an average of 52.3 % (Peng et al., 2017). In Hubei province, the formation has demonstrated significant shale gas potential, with gas contents in wells, such as Eyangye 1, Zidi 1, and Zidi 2, ranging from 0.12 to 4.8 m^3/t. In 2018, Well Eyangye 2 produced 5.5×10^4 m^3/d shale gas after fracturing (Wang et al., 2017c; Li et al., 2019; Zhang et al., 2022). These findings indicate that the Doushantuo Formation holds considerable potential for shale gas production, which is the oldest known shale gas play in the world.

6.2.5. The lower Cambrian shales, Sichuan Basin

The organic-rich Lower Cambrian shales were primarily deposited under euxinic environments, as indicated by Mo, U, and V enrichment, Fe speciation, and Mo isotopic composition (Feng et al., 2014; Cheng et al., 2016). Their maceral composition is dominated by SB, which accounts for more than 95 % of the dispersed OM. The distribution, occurrence, optical characteristics, and genesis of SB in the Lower Cambrian shales are comparable with those observed in the postmature Precambrian Datangpo and Doushantuo samples (Luo et al., 2020; Luo et al., 2021; Luo et al., 2023). However, unlike in the postmature Precambrian samples, VLM is still observed in the postmature Cambrian samples. VLM exhibits a smooth, grayish-white to white surface under reflected light, with similar morphology to that in the low-maturity stage, but displays strong anisotropy (Fig. 1f) (Luo et al., 2021; Wu et al., 2023a; Wu et al., 2023b). In the Cambrian shales from the Sichuan Basin and surrounding region, $VLMR_o$ ranges between 2.24 and 5.49 % (Luo et al., 2023). Shale gas exploration in the Cambrian Qiongzhusi Formation has recently made significant progress. To highlight this, in 2022, the JS103HF exploration well, deployed by SINOPEC Southwest Petroleum Bureau in the Sichuan Basin, achieved high and stable production, with a daily output of 25.86×10^4 m^3 of natural gas and an estimated reserve of 387.8×10^9 m^3 (Jin et al., 2024; Zou et al., 2024). This marks the first major breakthrough in shale gas exploration in the Cambrian Qiongzhusi Formation in China. In 2023, a PetroChina Southwest Oilfield Company deployed shale gas well Zi 201 in Neijiang, Sichuan, achieving a stable daily gas production of 73.88×10^4 m^3 (Zou et al., 2024).

6.2.6. The Wufeng–Longmaxi Formations, Sichuan Basin

During Early–Middle Ordovician period, the sedimentary environments on the Yangtze Platform changed from an open ocean to an anoxic, low-energy environment because of intense tectonic compression. This environmental shift led to the widespread deposition of the Wufeng–Longmaxi black graptolitic shales (Chen et al., 2000; Chen et al., 2004; Chen et al., 2005; Zhang et al., 2009; Mu et al., 2011). These shales are characterized by high TOC contents, ranging from 0.51 to 25.73 %, with an average of 2.59 %. Their significantly large thickness (30–130 m), high maturity, abundant organic pores and strong gas generation intensity make them the most successful exploration targets for shale gas in China (Zou et al., 2011; Dai et al., 2014; Zou et al., 2015; Dai et al., 2016; Luo et al., 2016b; Ma et al., 2016; Zou et al., 2016; Luo et al., 2017b; Luo et al., 2018; Luo et al., 2020). The OM composition of the Wufeng-Longmaxi Formation primarily consists of graptolites and SB. The graptolite periderm is predominantly NGG, though GG is occasionally observed (Fig. 1) (Luo et al., 2016b; Luo et al., 2017a; Luo et al., 2018; Luo et al., 2020). GR_o is in the range of 1.08 to 5.48 % and their $EqVR_o$ is between 1.17 and 4.93 %, indicating that these shales are predominantly in postmature stage (Luo et al., 2018; Luo et al., 2019; Luo et al., 2020). A major breakthrough in shale gas exploration occurred in these graptolite-bearing shales in 2014 in Fuling, Chongqing, with an estimated geological resource of 100×10^9 m^3 (Dai et al., 2014; Dai et al., 2016).

6.2.7. The lower Cambrian Yurtus shales, Tarim Basin

In the Tarim Basin, the Yurtus Formation has been confirmed to contain excellent source rocks, particularly through recent discoveries (Zhu et al., 2016; Zhu et al., 2018; Wu et al., 2021b). These shales were primarily deposited under sustained euxinic conditions, as supported by molybdenum isotope and iron speciation data (Zhu et al., 2021). TOC in the Yurtus Formation mostly ranges from 2 to 6 %, with a maximum up to 17 % (Zhu et al., 2016; Zhu et al., 2018; Wu et al., 2021b). The shales have thicknesses ranging from 10 to 25 m, and seismic data indicate that these organic-rich shales cover an area of approximately 260,000 km^2 (Zhu et al., 2016; Zhu et al., 2018). $VLMR_o$ in the Yurtus shale ranges from 0.85 to 1.61 % in the Shiairike section from the Tarim Basin, with most still in the mature stage (Luo et al., 2023). The maceral composition is dominated by SB, which accounts for more than 90 % of the dispersed OM, followed by algae-derived OM and VLM (Fig. 2g and h) (Luo et al., 2023). These shales have been identified as the source rocks for heavy oil, light oil, condensate, and gas in the Tarim Basin (Cai et al., 2015; Huang et al., 2016; Zhu et al., 2016; Zhu et al., 2018).

6.2.8. The Ulalik Formation, Ordos Basin

The Ordovician Ulalik Formation features graptolite-bearing black shales deposited in the dysoxic-anoxic restricted environments, making them an important target for shale gas exploration in the Ordos Basin (Fu et al., 2021a; Zhang et al., 2023). The thickness of the black shales ranges from 25 to 115 m, with a burial depth of 4000–4900 m. TOC content varies from 0.05 to 4.55 %, mostly remaining below 1.5 %, which is significantly lower than that of the Wufeng–Longmaxi formations (Wu et al., 2021a; Xi et al., 2021). The OM in the Ulalik Formation is mainly composed of lamalginite, graptolites, and rare SB (Fig. 2k and l), with GR_o ranging from 0.45 to 1.68 %, indicating an immature to postmature stage (Wu et al., 2021a; Li et al., 2022). These shales exhibit good gas generation potential, with gas contents ranging from 0.94 to 2.21 m^3/t (Xi et al., 2023). Notably, six industrial oil and gas wells have been successfully completed in the Ulalik Formation in the western area of the Ordos basin, with a daily gas production rate per well ranging from 4.24×10^4 to 26.48×10^4 m^3. This success highlights the Ulalik marine shales' capacity of self-generation and self-storage capacity of hydrocarbons, marking a significant breakthrough in shale gas exploration in northern China, particularly in the marine shales with low TOC content (He, 2003; Zhang et al., 2013; Fu et al., 2021a; Fu et al., 2021b; Wu et al., 2021a; Xi et al., 2021; Xi et al., 2023).

6.3. The Salt Range Formation from Pakistan

The Neoproterozoic–Lower Cambrian Salt Range Formation is one of the most important source rocks in the Upper Indus Basin and Punjab Platform of north Pakistan (Khan et al., 2020). Its deposition occurred in a restricted marine basin along the western passive margin of the Indian Plate (Khan et al., 2020). Notably, a world-class Neoproterozoic–Lower Cambrian petroleum system has already been reported from the Bikaner–Nagaur Basin (NW India) and Huqf Basin (southern Oman), both located near the Indian Plate on the northern margin of the Gondwana (McKerrow et al., 1992; Riaz et al., 2003; Jamil and Sheikh, 2012; Khan et al., 2020; Mandal et al., 2022). Similar to other Neoproterozoic–Lower Cambrian sequences in the Gondwana assembly, the Salt Range Formation exhibits a typical evaporitic sequence, consisting of gypsum, marl, and halite, with high-grade oil shales intercalated towards the top (Meng et al., 2021). These oil shales contain TOC contents up to 46 %, consisting of bituminite, alginites, VLM, and thucholite as the key macerals (Fig. 2e and f), with $VLMR_o$ between 0.2 and 0.4 %, indicating an early oil window maturity (Khan et al., 2020). Some oil seepage in the Upper Indus Basin is believed to have originated from these Salt Range oil shales (Ahmad and Alam, 2007). The Salt Range Formation is recognized as a proven hydrocarbon source rock in the Baghiwala-A well (Punjab Platform, Pakistan) and Karampur-01 well (Bikaner-Nagaur Basin, India) (Peters et al., 1995; Craig et al., 2018; Yasin et al., 2022). However, challenges in developing these oil shales as unconventional hydrocarbon prospects include limited thickness and lateral facies variations (Khan et al., 2020).

6.4. The Alum shales of Northern Europe

The Alum Shale Formation, spanning from the middle Cambrian to the Lower Ordovician, was deposited during a marine transgression on the Baltica paleocontinent (Nielsen and Schovsbo, 2006; Schovsbo et al., 2016). Anoxic conditions and high paleoproductivity contributed to the deposition of organic-rich shales and fossiliferous bituminous limestones, primarily derived from algae, bacteria, and marine fauna (Petersen et al., 2013; Sanei et al., 2014). After deposition, sediments underwent varying burial, resulting in a wide range of thicknesses (20 to 180 m), burial depths (up to over 3 km), and thermal maturities (from immature to late gas generation) (Schovsbo et al., 2016). As the thickest and richest shales in onshore northern Europe (Pool et al., 2012), the Cambrian–Ordovician Alum shale Formation is referred to as the Słowińska Formation and the Piaśnica Formation in NE Poland, the Kaporye Formation in Russia, and the Türisalu Formation in Estonia (Nielsen and Schovsbo, 2006).

The OM in the Cambrian-Ordovician Alum shale includes alginite, bituminite, SB, and thucholite, with graptolite periderm being a significant component in the Ordovician Alum samples (Figs. 1, 4, and 5) (Petersen et al., 2013; Sanei et al., 2014; Luo et al., 2018; Luo et al., 2020; Luo et al., 2021; Zheng et al., 2021a; Luo et al., 2023; Zheng et al., 2023b). In the postmature samples, SB is abundant and dispersed (Figs. 1, 4, and 5), displaying complex distribution patterns that reflect different stages of oil generation (Sanei, 2020). $EqVR_o$ data, converted from GR_o and BR_o, reveals different maturity levels of the Alum shale in North Europe, comprising immature to early mature ($EqVR_o$ from 0.39 to 0.74 %), mature ($EqVR_o$ from 0.83 to 0.98 %), and postmature ($EqVR_o$ from 1.42 to 2.5 %). However, the wide range of BR_o in samples from well DBH15/73 (from 0.53 to 1.44 %) may be due to the intrusion of Carboniferous-Permian dolerite (Zheng et al., 2023b).

The first shale gas exploration borehole, Vendsyssel-1, was drilled in 2015 in Denmark, targeting the Alum shale Formation following an evaluation program conducted by Geological Survey of Denmark and Greenland. Hydrocarbon generation models based on data from the Terne-1 borehole suggest that petroleum was likely generated during the Silurian (Gautier et al., 2013), however, in most areas, the oil thermally cracked into dry gas. Subsidence continued in the Terne-1 well area through the Permian-Triassic, with significant reburial occurring from the Cretaceous to early Paleogene. Despite this, limited data and modeling uncertainty leave the hydrocarbon resources in the region uncertain. Shell's exploration in Skåne region of the southern Sweden between 2008 and 2010 revealed that the Alum shales at a depth of 700–800 m lacked economically viable gas potential due to low gas saturation and high leakage risk, despite having thickness up to 90 m, TOC up to 15 % and $EqVR_o$ up to 2 %. Gas loss in this region was likely caused by uplift-related reductions in reservoir pressure and compromised integrity due to faulting and fracturing. Additionally, shallowly buried (< 150 m) gas-bearing, immature to low-maturity Alum shales in south-central Sweden were found to contain a mix of thermogenic and biogenic gas (Pool et al., 2012; Schovsbo et al., 2014; Luo et al., 2020).

6.5. The Neoproterozoic to Silurian shales in the Barrandian Unit, Czech Republic

The dark Neoproterozoic shales and siltstones form the basement of the Barrandian Unit, an exotic terrane tectonically amalgamated within the high-grade crystalline complexes of the Bohemian Massif, and contain a complex assemblage of highly postmature organic fragments. At least four types of highly postmature OM have been identified: (1) very small (<10 mm), spine-shaped fragments of uncertain affinity (R_{max} = 2.5–7.0 %), (2) larger (10–30 mm), optically isotropic fragments similar to "transitional matter" (R_{max} = 5.0–8.9 %), (3) pyrobitumen–like fragments (R_{max} = 5.5–11 %), and (4) "optical graphite" (R_{max} = 9–15.5 %) (Diessel and Offler, 1975; Diessel et al., 1978; Suchý et al., 2007). Distinguishing between these types of OM, which frequently coexist in the same samples, has proven difficult, particularly in the postmature samples. As a result, the optical reflectance values are typically expressed as the average R_{max} values of all four types of OM present in individual samples, which ranges between 3.1 and 7.7 % across the area (Suchý et al., 2007).

The Lower Paleozoic marine sediments, 1.2–5.1 km thick, overlie the Neoproterozoic basement with an angular discordance, exhibiting a substantially lower degree of thermal maturity. In the Ordovician clayey sediments, the dispersed OM is primarily composed of chitinozoan tests, droplet-like particles of SB, rare algae remains, and graphite to semi-graphite particles, probably of detrital origin (Malán, 1980; Suchý et al., 2015). The reflectance values of the chitinozoan, which range between 1.38 and 3.03 %, point to the wet gas/condensate to dry gas zone of OM maturation. Although the mean TOC values are generally low, some Ordovician sediments contain sufficient TOC (~0.8–2.3 %) to be considered as potential hydrocarbon source rocks (Volk, 2000).

The overlying Lower Silurian Liteň Formation, with thickness of up to 300 m, was deposited during a major marine transgression and contains elevated amounts of OM, with a mean TOC content of 2.06 %. OM consists of abundant debris of graptolites, chitinozoan tests, and SB particles that form discrete, droplet-like bodies embedded in the sediment matrix, along with minor anthracite fragments (Suchý et al., 2002). The Upper Silurian bituminous limestones and shales in the Kopanina and Přídolí formations with a combined thickness of 330 m contain TOC values of up to 3.3 %, representing the best proven source rocks in the basin (Rozkošný et al., 1994; Volk et al., 2000). In addition to abundant zooclasts, these sediments also contain VLM, with reflectance values of 0.93–1.38 %, implying a mature to postmature stage concerning the generation of liquid hydrocarbons (Suchý and Rozkošný, 1996). However, in the western part of the basin, graptolite reflectance values ranging between 0.8 and 1.5 %, along with the local occurrence of liquid petroleum staining in rock fractures and fossil voids, indicate that the Silurian rocks remain within the oil window (Suchý et al., 2002). Multiple generations of fracture-bound solid and semi-solid bitumen, along with the geochemical composition of hydrocarbon inclusions hosted in vein minerals, provide evidence of repeated episodes of ancient petroleum migration expelled from several Lower Paleozoic source rocks (Volk et al., 2000). Although oil-stained cores were retrieved from some test holes, no commercial hydrocarbon accumulations have been discovered in the basin, likely due to the absence of true carrier and reservoir beds (Suchý et al., 2015). Since 2010, the shale gas potential of the Silurian graptolitic shales has been explored, but further exploration activities were stopped due to a growing environmental concern.

6.6. North America

6.6.1. The Upper Ordovician Yeomen Formation, Canada

The Upper Ordovician carbonates of the Yeomen Formation contain organic-rich mudstone intervals known as kukersite, with TOC ranging from 0.74 to 35 %, averaging 9.07 %; these kukersite intervals represent an excellent source rock in the Williston Basin (Osadetz et al., 1992; Stasiuk and Osadetz, 1993; Chen et al., 2019). The Yeoman Formation underwent variable dolomitized, and the burrow-mottled bioclastic carbonates were deposited during a widespread transgression that created a major epeiric sea, covering much of the North American craton (Norford et al., 1994; Pope and Steffen, 2003). OM in this organic-rich interval is predominantly *Gloeocapsomorpha prisca* (*G. prisca*) alginite, SB, with minor amounts of filamentous alginite and acritarchs.

6.6.2. The Cape Phillips Formation, Canada

The Cape Phillips Formation was deposited at the shelf margin of the Canadian Arctic Islands, retreating southwards to form a deep-water embayment during the latest Ordovician. This embayment accumulated a large volume of graptolitic mudrocks, carbonates, microbial and coral-microbial buildups until the Middle Silurian (De Freitas et al., 1999). The shale units of the Cape Phillips Formation are composed of Type II kerogen, with TOC ranging from 0.23 to 6.83 % and HI ranging from 290 to 498 mg/g (Stasiuk and Fowler, 1994; Dewing and Obermajer, 2009; Synnott et al., 2018). The Cape Phillips shales contain AOM, SB, zooclasts, acritarchs, and alginite (Stasiuk and Fowler, 1994; Dewing and Obermajer, 2009; Synnott et al., 2018). Due to the abundance of graptolites and chitinozoans, this organic-rich shale has been the subject of several studies to establish an equivalent thermal maturity indicator (Goodarzi et al., 1992c; Synnott et al., 2018).

6.6.3. The Trenton Group and Blue Mountain Formation, Canada

The Ordovician organic-rich calcareous mudstones of the Trenton Group and Blue Mountain Formation are significant conventional hydrocarbon source rocks in southwestern Ontario (Obermajer et al., 1999). The Trenton Group represents the upper part of a widespread carbonate platform developed during the Middle–Late Ordovician across a vast area of the North American craton (Johnson et al., 1992). The organic-rich Ordovician intervals in southern Ontario contain Type II kerogen, predominantly marine OM consisting of bituminite, SB, zooclasts, acritarchs, and *G. prisca* alginite (Obermajer et al., 1999). TOC and HI values range from 0.07 to 11.26 % and from 37 to 678 mg/g, respectively (Obermajer et al., 1999). The chitinozoan reflectance values, BR_o, and GR_o range from 0.74 to 1.12 %, 0.67 to 0.81 %, and 0.65 to 1.15 %, respectively (Obermajer et al., 1996; Obermajer et al., 1999).

6.6.4. The Upper Ordovician Utica Shale, North America

The Upper Ordovician deep-marine clastic sediments of the Utica shale (50 to 300 m thick) overlie the shallow marine carbonates of the Cambrian–Ordovician St. Lawrence platform. The deposition of the Utica shale coincided with the collapse of the carbonate shelf in the early Late Ordovician within a poorly oxygenated setting, followed by the deposition of Taconian flysch (Lorraine Group) and molasse (Lavoie, 1994; Lavoie, 2008). The thickness and depth of the Utica shale progressively increase from northwest to southeast, and it is remobilized and imbricated within thrust stacks beneath the Appalachian Humber Zone (Lavoie, 2008). TOC contents in the Utica Shale range from 0.08 to 2.25 %, with an average of 1.20 %, while HI values range from 9 to 191 mg/g (Chen et al., 2014; Haeri-Ardakani et al., 2015; Lavoie et al., 2016). The primary OM constituents include SB and zooclasts, such as chitinozoan and graptolite. The kerogen is predominantly marine-derived, as indicated by the presence of chitinozoan and *prasinophyte* algae, such as *Tasmanites* (Haeri-Ardakani et al., 2015; Ardakani et al., 2018). The $EqVR_o$ of the Utica shale in southern Quebec, calculated from BR_o and chitinozoan reflectance, ranges from 1.02 to 2.34 %, suggesting a transition from peak oil window to dry gas zone (Haeri-Ardakani et al., 2015). The Utica shale of the Appalachian Basin is a self-sourced reservoir and a major shale oil and gas play in North America, extending from northeastern U.S. to southern Quebec, Canada. It was estimated to contain 940×10^6 barrels of oil, 1.08×10^{12} m^3 of gas, and 208×10^6 barrels of natural gas liquids (Kirschbaum et al., 2012).

6.6.5. The Upper Ordovician Maquoketa Shale, Illinois Basin, USA

The Maquoketa shale of the Illinois Basin is time-equivalent to the Utica shale of the Appalachian Basin. These shales have TOC contents of <0.1 to 3.26 % (Guthrie and Pratt, 1994; Strapoc et al., 2010), with localized values reaching as high as 8.68 % in certain areas of the Illinois Basin (Guthrie, 1996). The $EqVR_o$ of the Maquoketa shale ranges from 0.65 to 0.88 %, calculated from T_{max} or $VLMR_o$, indicating oil-window maturity (Akar et al., 2015). The kerogen type in the Maquoketa shale is a mixture of Type II, III, and IV kerogen, with HI and OI ranging from 55 to 1042 mg/g and from 9 to 294 mg/g, respectively (Guthrie and Pratt, 1994; Guthrie, 1996; Akar et al., 2015). The significant variations of HI and OI is likely due to the heterogeneous reworking of OM. Furthermore, OM in the Maquoketa shale consists of bituminite, liptodetrinite, VLM, and SB (Akar et al., 2015; Teng et al., 2020). Graptolites have also been observed in the Maquoketa shale (Berry and Marshall, 1971; Guthrie and Pratt, 1994). Despite the low gas content (0.3–0.6 m^3/t in Pike County, Indiana) due to its relatively low TOC content (Strapoc et al., 2010), the Maquoketa shale could serve as a seal for geological sequestration of CO_2 in the Illinois Basin (Medina et al., 2020).

6.7. The Silurian Qusaiba shale in the Middle East

The Lower Silurian Qusaiba shales were deposited in anoxic environments due to a global sea transgression, serving as the primary organic-rich source rocks in Central and Eastern Arabia, which are notable for their "hot shale" characteristics at the base, with a thickness of 3–75 m and TOC averaging 5 % (Mahmoud et al., 1992; Cole, 1994; İnan et al., 2016; Abouelresh, 2017; Cheshire et al., 2017; Ertug et al., 2019; Abouelresh et al., 2020; AlQuraishi et al., 2020; AlGhamdi et al., 2023). In the immature samples, HI values range between 350 and 600 mg/g, reflecting their oil-prone potential (İnan et al., 2016; Abouelresh, 2017). The kerogen in these hot shales is mainly composed of Type II OM, including alginite, graptolite periderms, chitinozoan, acritarch, and liptodetrinite (Cole, 1994; Cole et al., 1994; İnan et al., 2016; Cheshire et al., 2017; Hayton and Jaeger, 2017). The thermal maturity of the Qusaiba shale in Saudi Arabia varies from mature to postmature, as indicated by graptolite reflectance, thermal alteration index, and various spectroscopic and geochemical parameters (İnan et al., 2016; Cheshire et al., 2017; Ertug et al., 2019). Owing to their variable thermal maturity, these hot shales have been recognized for their potential to produce shale oil and shale gas with significant gas reserves discovered in southeastern Saudi Arabia (Mahmoud et al., 1992; Cole, 1994; Cole et al., 1994; İnan et al., 2016; Stewart et al., 2016; Abouelresh, 2017; Cheshire et al., 2017; Abouelresh et al., 2020; AlQuraishi et al., 2020; AlGhamdi et al., 2023).

7. OM evolution in the pre-Devonian shales with increasing maturity

7.1. Maceral composition in the pre-Devonian low-maturity shales

The best available Precambrian low-maturity shales primarily originate from the Hongshuizhuang and Xiamaling formations in northern China, the Salt Range Formation in Pakistan, and the Paleoproterozoic Barney Creek and Mesoproterozoic Velkerri formations in Australia. These shales predominantly consist of lamalginite, bituminite, and mineral-bituminous groundmass, with VLM making up less than 10 % of the composition, along with occasional thucholite (Figs. 1 and 2) (Crick et al., 1988; Crick, 1992; Luo et al., 2014; Khan et al., 2020; Luo et al., 2021; Wu et al., 2022; Luo et al., 2023).

The best available Cambrian mature shales in China are found in the Yurtus Formation within the Tarim Basin. Here, OM is dominated by SB, which constitutes over 90 % of OM, with minor amount of VLM and alginite-derived OM (Fig. 2) (Luo et al., 2023). In contrast, OM in the low-maturity Alum shale from Öland, Sweden is comparable to that in the Hongshuizhuang and Xiamaling formations in northern China, with lamalginite, bituminite, and mineral-bituminous groundmass being the most abundant macerals, followed by VLM (Fig. 1) (Luo et al., 2021; Luo et al., 2023; Wu et al., 2023a; Wu et al., 2023b).

Low-maturity graptolite-bearing shales, although rare in China, have been identified in the Pingliang Formation in Gansu Province (China). This formation features argillaceous dolomites containing low-maturity graptolite periderm, with TOC between 0.24 and 0.83 %, and GR_o of 0.48 %. OM in this formation primarily comprises lamalginite and graptolite periderm (Fig. 2) (Luo et al., 2018). In contrast, low-maturity graptolites are more commonly found in the organic-rich Ordovician Alum shales from northern Europe, which exhibit diverse maceral assemblages, including lamalginite, bituminite, graptolite periderm, with lesser amounts of chitinozoan (Fig. 1) (Petersen et al., 2013; Sanei et al., 2014; Luo et al., 2018; Zheng et al., 2021a; Zheng et al., 2021b).

7.2. Maceral composition in the pre-Devonian postmature shales

The Precambrian postmature shales are mainly from the Datangpo and Doushantuo formations in south China, where maceral compositions are characterized exclusively by the presence of SB (Figs. 1 and 2) (Luo et al., 2023). Similarly, the postmature Cambrian shales have been found in the Niutitang, Qiongzhusi, Shuijingtuo, and Lujiaping formations from the Yangtze area, the Yurtus Formation in the Tarim Basin, and the Cambrian Alum shales in the Bornholm area of Denmark. The maceral composition of these Cambrian shales, like their Precambrian counterparts, is also predominantly SB (Figs. 1 and 2) (Petersen et al., 2013; Luo et al., 2021; Luo et al., 2023). In the postmature graptolite-bearing samples, OM primarily consists of graptolite periderms, with NGG being the most common form, though rare GG is present, along with SB (Fig. 1) (Petersen et al., 2013; Luo et al., 2016b; Luo et al., 2020; Zheng et al., 2021a; Zheng et al., 2021b; Zheng et al., 2022).

7.3. OM evolution in the artificially-matured pre-Devonian shales

The low-maturity Mesoproterozoic Xiamaling shales, Cambrian Alum shales, and Ordovician graptolite-bearing Alum shales were selected for the thermal simulation experiments to investigate OM evolution, with detailed results provided by Luo et al. (2018, 2021). For example, $VLMR_o$ of the original SD-XHY-6 sample from the Mesoproterozoic Xiamaling Formation in northern China is 0.54 % (Luo et al., 2021). After heating at 300 °C for 3 days, $VLMR_o$ increased to 0.70 %, with OM comprising SB, bituminite, VLM, and lamalginite (Fig. 3). The fluorescence of lamalginite decreased, mainly appearing as a deep yellow color, while abundant SB appeared in the sample (Fig. 3) (Luo et al., 2021). Upon heating to 325 °C for 3 days, $VLMR_o$ increased to 1.09 %, with OM dominated by SB, with minimal VLM present, and no fluorescent OM was observed (Fig. 3) (Luo et al., 2021). At temperature of 350 °C and above, no lamalginite or VLM were observed in the sample, and only very fine, dispersed SB was present (Fig. 3) (Luo et al., 2021), a pattern consistent with the observation by Song et al. (2023) on the Xiamaling shales pyrolysis residues. In addition, BR_o increased progressively with higher temperature: 1.42 % (350 °C, 3 days), 2.10 % (400 °C, 3 days), 2.59 % (425 °C, 3 days), 2.78 % (450 °C, 3 days), 3.59 % (500 °C, 3 days), and 4.68 % (550 °C, 3 days) (Luo et al., 2021). A similar variation in maceral composition and reflectance was observed in another Xiamaling artificially-matured sample, as reported in Luo et al. (2021). These artificial maturation experiments of the low-maturity Xiamaling shales demonstrate that the maceral composition in the original shales is dominated by the lamalginite, bituminite, and VLM, which was gradually converted to SB with heating (Fig. 3) (Luo et al., 2021). The maceral composition of the artificially postmature samples closely resembles that of the Neoproterozoic Datangpo and Doushantuo naturally postmature shales (Figs. 1, 2, and 3) (Luo et al., 2021).

$VLMR_o$ of the original Cambrian Alum shale sample SD-O-1 from Sweden is 0.50 %, and its OM is dominated by algae-derived OM and VLM (Luo et al., 2021). After heating at 300 °C for 3 days, $VLMR_o$ rose to 0.80 %, though the maceral composition remained largely unchanged, with lamalginite, bituminite, and VLM still prevalent (Fig. 4) (Luo et al., 2021). Upon further heating to 325 °C for 3 days, $VLMR_o$ increased to 1.20 %, SB became the predominant maceral, and VLM was still detected. After heating at 350 °C for 3 days, $VLMR_o$ reached 1.67 %, and no liptinite was observed (Fig. 4) (Luo et al., 2021). As the temperature increased, both $VLMR_o$ and VLM anisotropy gradually increased, showing optical characteristics similar to those in the natural Cambrian postmature samples. SB became the dominant maceral, making up over 90 % of OM, followed by VLM (Fig. 4) (Luo et al., 2021). These experiments indicate that the original macerals in the low-maturity Alum shale, mainly lamalginite and bituminite, were progressively transformed into SB, similar to the maceral composition of the Cambrian postmature natural shales from China and Denmark (Figs. 1 and 4) (Luo et al., 2021).

The graptolite random reflectance of the original Ordovician Alum shale from Sweden is 0.80 %, with OM assemblage mainly consisting of liptinite, SB, and graptolite (Luo et al., 2018). After heating at 350 °C for 3 days, GR_o displayed no significant variation, and OM composition remained largely unchanged (Fig. 5). However, upon heating to 400 °C for 3 days, GR_o increased to 1.04 %, with the maceral composition shifting to predominantly NGG and SB, with liptinite disappearing

(Fig. 5). As temperature and time increased, GR_o gradually rose, and OM became dominated by NGG and SB (Fig. 5) (Luo et al., 2018). Similar to the Swedish shale, GR_o of the Estonian shale also increased gradually with increasing temperature and time, and SB gradually became the predominant maceral in the artificially-matured shales (Luo et al., 2018). These observations are consistent with the observation by Song et al. (2023) on the pyrolysis residues of the Ordovician Alum shale. Graptolites exhibit a unique original morphological characteristics and a stronger resistance to thermal degradation compared to other types of OM, similar to observations on graptolites from the Boas River Formation in Canada (Reyes et al., 2018). Overall, OM in these graptolite-bearing shales changes from the initial lamalginite, bituminite, mineral-bituminous groundmass, and GG/NGG to SB and NGG with increasing temperature and time (Figs. 1, 2, and 5) (Luo et al., 2018; Song et al., 2023). The maceral composition of the artificially-matured graptolite-bearing samples closely resembles that of the postmature Wufeng–Longmaxi natural shales (Figs. 1 and 5) (Luo et al., 2018).

Similar OM evolution was also observed in the post-Silurian shales. For example, Valentine et al. (2021) conducted hydrous pyrolysis on organic-rich immature New Albany shale (0.25 % BR_o) from the Illinois Basin, and observed that SB became the predominant OM in the pyrolysis residues, forming a significant SB network. *Tasmanites* developed a gray reflecting surface similar to SB, progressively converting into hydrocarbons as thermal maturity increased during artificial hydrous pyrolysis (Hackley et al., 2017a). In the Eocene Green River oil shale, oil-prone OM converted into newly formed SB in the solid residues after pyrolysis, and bituminite directly converted into SB in situ (Hackley and Lewan, 2018; Hackley et al., 2022), which resembles observations made in the Xiamaling solid residues (Luo et al., 2021). In all cases, BR_o in shales increases with rising temperature and time (Hackley and Lewan, 2018; Valentine et al., 2021; Hackley et al., 2022), consistent with findings in the pre-Devonian shales discussed above. Further hydrous pyrolysis experiments conducted by Zheng et al. (2023a) and Arysanto et al. (2024) on the Mississippian Woodford shale and Lower Toarcian Posidonia shale, respectively, revealed similar OM transformations. Liptinites showed a significant decrease in fluorescence and volume as temperature increased from 280 to 340 °C, indicating hydrocarbon generation, while alginites began bituminizing at the particle margins. However, SB was not present in these artificial samples due to the relatively low temperature (Zheng et al., 2023a; Arysanto et al., 2024). These findings illustrate the gradual transformation of liptinite to hydrocarbon and SB with increasing thermal maturity.

8. The hydrocarbon generation potential of graptolites and in-source SB

8.1. Graptolites

The hydrocarbon generation potential of graptolite periderm has gained substantial attention due to the breakthrough in shale gas exploration in the graptolite-bearing shales. Several scholars have focused on separating graptolite from shales for organic geochemical analyses (İnan et al., 2016; Wang et al., 2017a). İnan et al. (2016) observed that immature graptolites exhibit HI value of 200 mg/g and OI value of 30 mg/g (Table 5). Similarly, Wang et al. (2017a) analyzed two Wufeng–Longmaxi shales with $EqVR_o$ of 1.1 %, finding that graptolites had TOC contents of 42.93 and 71.34 %, HI values of 74 and 85 mg/g, S_1 values of 6.55 and 15.18 mg/g, and S_2 values of 31.71 and 60.36 mg/g, respectively (Table 5). These HI values, though higher than those of the whole rock samples, are notably lower than those of the immature graptolites (Table 5) (İnan et al., 2016; Wang et al., 2017a). In this study, graptolites were separated from the Swedish graptolite-bearing Alum shale with an $EqVR_o$ of 0.58 %. The graptolites belong to the *Graptoloidea* and are characterized into three main groups: ① *Diplograptidae* dominated by *Normalograptidae* and *Neodiplograptidae*, hereinafter referred to as *Diplograptidae* (Fig. 9a); ② *Monograptus* (*Stimulograptus*), hereinafter referred to as *Stimulograptus* (Fig. 9b); ③ *Monograptus* (*Rastrites*), hereinafter referred to as *Rastrites* (Fig. 9c). TOC contents of *Diplograptidae*, *Stimulograptus*, and *Rastrites* are high, ranging from 67.71 to 72.00 %, with S_1, S_2, and HI values being >20 mg/g, 177–205 mg/g, and 247–302 mg/g, respectively (Table 5). Notably, *Diplograptidae* had relatively higher HI value than that of *Stimulograptus* and *Rastrites*, and all were higher than previously reported values (Wang et al., 2017a), likely due to the lower thermal maturity of the samples in this study (Table 5). For graptolites isolated from Alum shale with an $EqVR_o$ of 0.87 %, TOC, S_1, S_2, and HI values are 66.14 %, 6.21 mg/g, 150.92 mg/g, and 228 mg/g, respectively (Fig. 9d and Table 5). The HI vs. T_{max} plot in Fig. 10 indicates the kerogen types of the graptolite periderms are primarily II-III. Moreover, weak brown fluorescence in the graptolite periderm of the Chinese Ulalik and Czech Liteň mature shales (Figs. 1 and 2), corroborating with findings by Hoffknecht (1991) and Wang et al. (2019), supports the idea that graptolite periderm has some hydrocarbon generation potential (Luo et al., 2020). Further evidence of hydrocarbon potential was provided by pyrolysis-gas chromatography analyses on isolated graptolites, which revealed CH_4 yields of 23.61 mg/g and 12.35 mg/g, respectively (Wang et al., 2017a). Wang et al. (2022b) applied atomic force microscopy-based infrared spectroscopy (AFM-IR) to a Lower Paleozoic graptolite-bearing shale from the Baltic Basin (Lithuania) with a thermal maturity of 0.80 %, and found that graptolites exhibited a homogeneous molecular composition, with A-factor values ranging from 0.40 to 0.46. Results from Raman spectroscopy, AFM-IR, infrared spectroscopy, and electron probe analyses confirmed that the chemical structure and elemental composition of graptolite OM were similar to those of vitrinite (Hao et al., 1990; Morga and Kamińska, 2018; Wang et al., 2019; Luo et al., 2020). These findings collectively demonstrate that graptolites can serve as effective indicators of thermal maturity and potential sources of hydrocarbons in the pre-Devonian shales.

8.2. In-source SB

The hydrocarbon general potential of SB is crucial in evaluating its oil- or gas-prone properties within shales, particularly in the context of shale gas and oil exploration (Mastalerz et al., 2018). Gai et al. (2018)

Table 5
Organic geochemical data of isolated graptolites and whole rock.

Sample ID	Sample type	Formation	$EqVR_o$ (%)	S_1 (mg/g)	S_2 (mg/g)	T_{max} (°C)	TOC (%)	HI (mg/g)	OI (mg/g)	Source
MB-2	Shale	O_3w	1.10	0.54	1.77	455	3.04	58	8	(Wang et al., 2017a)
MB-3	Shale	S_1l		0.69	2.88	458	3.88	74	5	
MB-2	Graptolite	O_3w		6.55	31.71	464	42.93	74	43	
MB-3	Graptolite	S_1l		15.18	60.36	456	71.34	85	2	
K1	Graptolite	S_1	/	/	/	/	/	200	30	(İnan et al., 2016)
Dalarna-1	*Diplograptidae*	S_1	0.58	23.29	205.01	421	67.71	302	16	This study
	Rastrites			21.70	177.07	424	71.43	247	17	
	Stimulograptus			20.39	179.45	423	72.00	249	28	
AS-DD-LG	Diplograptidae	O_1	0.87	6.21	150.92	426	66.14	228	11	

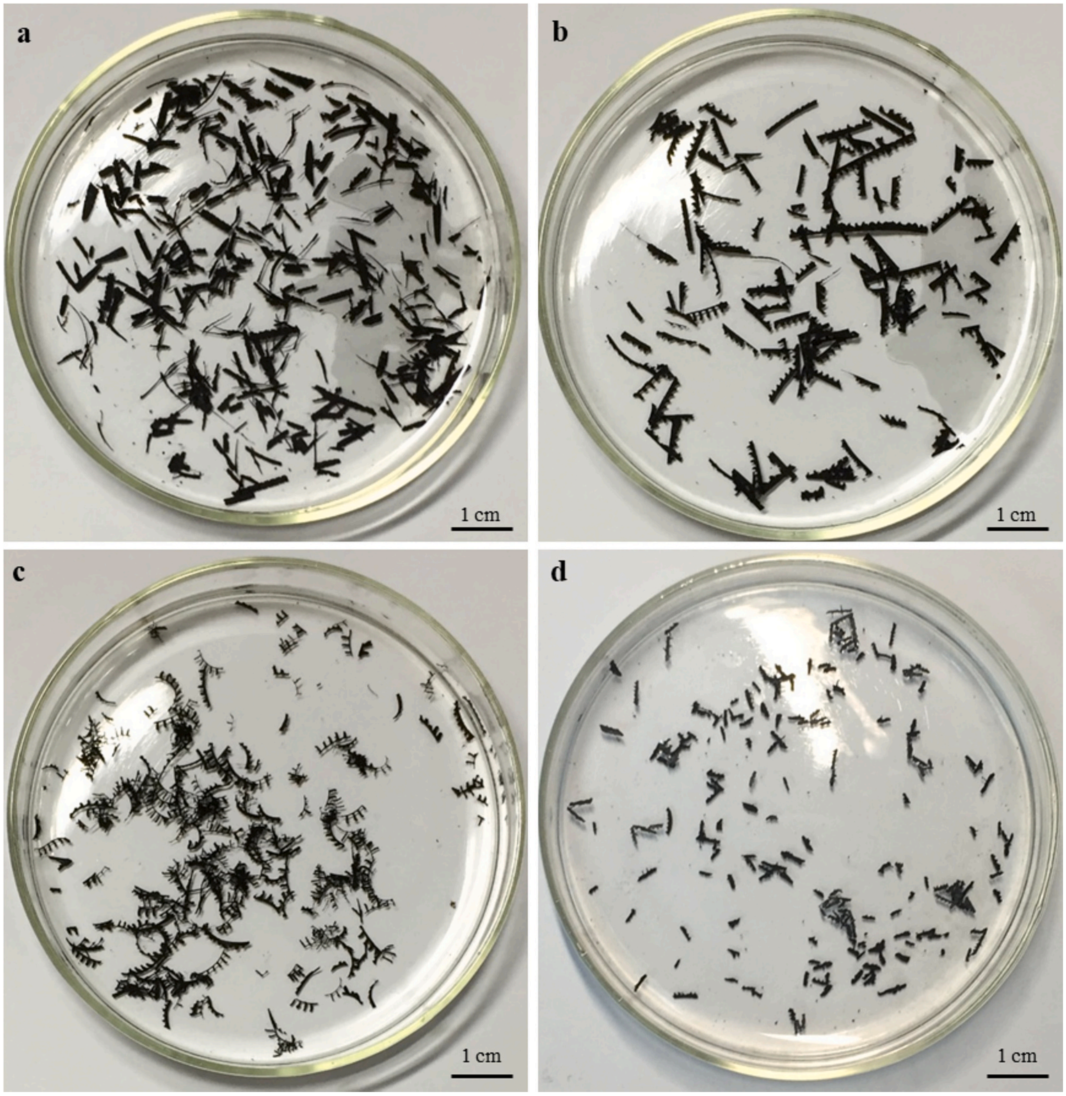

Fig. 9. Isolated graptolites from the Alum shale, Sweden. a, *Diplograptidae*. b, *Stimulograptus*. c *Rastrites*. d, unsorted graptolite.

conducted sealed gold tube pyrolysis to examine the effect of oil expulsion efficiency and kerogen type on gas generation potential in the postmature shales. Their findings revealed that retained oil, rather than kerogen composition, played a dominant role in the late-stage gas generation in shales with $EqVR_o$ greater than 1.22 %. As thermal maturity increases, this retained oil transforms into SB, and SB subsequently contributes to gas generation (Mastalerz et al., 2018; Luo et al., 2021). Although SB is usually ignored, it constitutes the major insoluble OM in the mature-postmature marine shales (Petersen et al., 2013; Haeri-Ardakani et al., 2015; Hackley and Cardott, 2016; Liu et al., 2017; Luo et al., 2018; Mastalerz et al., 2018; Wang et al., 2019; Luo et al., 2020; Luo et al., 2021). Its significant contribution to gas generation highlights the role of retained oil during the gas generation stage (Gai et al., 2015; Gai et al., 2019). Mastalerz et al. (2018) isolated SB from the Duvernay shale (~1.0 % VR_o) and analyzed its Fourier-transform infrared (FTIR) spectrum, discovering that its A-factor was 0.54, similar to that of oil-prone type II kerogen at a thermal maturity of 0.55 % (A = 0.58), and higher than coal with thermal maturity of 0.55 % and 1.00 % (A = 0.28 and A = 0.41, respectively). Liu et al. (2019a) reported an A-factor value of 0.65 for SB in the Devonian New Albany mature shale with VR_o of 0.98 %. In a graptolite-bearing shale from the Baltic basin with a thermal maturity of 0.80 %, SB had A-factor value ranging from 0.36 to 0.46 (Wang et al., 2022b). Yang et al. (2017) conducted hydrous pyrolysis (300–360 °C) on an organic-rich New Albany shale, analyzing the A- and C-factors of SB as BR_o increased. They observed a significant decrease in A-factor of SB, as it dropped from 0.90 to 1.12 % because of the expulsion of H-containing compounds, demonstrating considerable hydrocarbon generation potential of SB (Yang et al., 2017). Artificial maturation experiments indicate that SB shrinks and becomes more dispersed due to secondary cracking (Luo et al., 2018; Luo et al., 2021). In the postmature shales, SB develops abundant secondary pores through secondary cracking (Mastalerz et al., 2018; Misch et al., 2019; Hu et al., 2020; Luo et al., 2020). These results indirectly indicate that SB possesses a relatively high hydrocarbon generation potential. However, further research is needed to explore its oil- or gas-prone properties of SB through artificial maturation studies (Mastalerz et al., 2018). Liang et al. (2021) conducted artificial heating experiments on low-maturity SB ($EqVR_o$ = 0.74 %) and analyzed its pyrolysate characteristics over a temperature range of 380 °C to 560 °C (Easy%R_o: 0.77 to 3.21 %). Their results showed that gas hydrocarbons and SB residues increased with elevated temperatures, and soluble oil peaked early in pyrolysis at 97.1 % but diminished in later stages (Fig. 11) (Liang et al., 2021). As temperatures rose, gaseous hydrocarbons evolved into dry gas, predominantly methane, with the aromatic structure of the residues gradually becoming more condensed (Fig. 11), consistent with OM aromatization (Stach et al., 1982; Tissot and Welte, 1984). Thermal

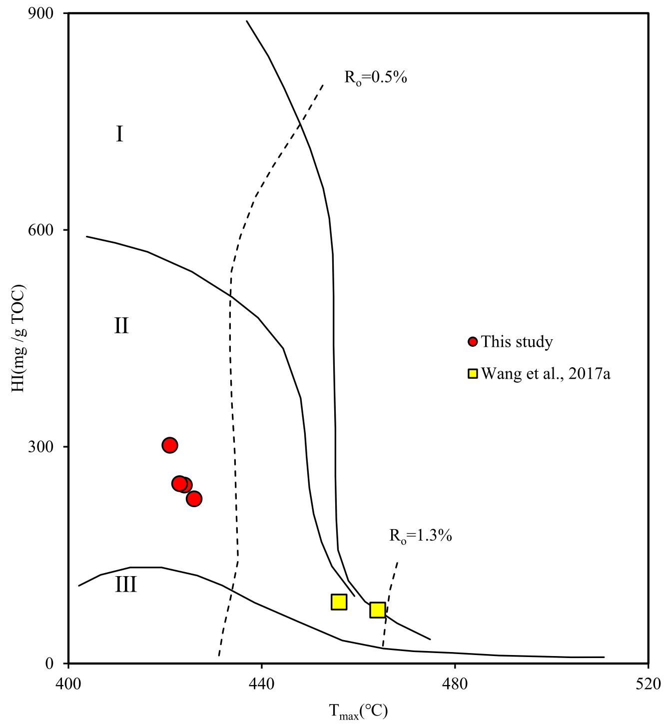

Fig. 10. The plot of HI vs. T_{max} for graptolites.

cracking and condensation reactions are the primary reactions during SB pyrolysis (Liang et al., 2021). Initially, SB cracks into asphaltene, making up 92.6 % of the pyrolysate (Fig. 11) (Liang et al., 2021). Gaseous hydrocarbons are generated by the thermal cracking of the saturated, aromatic, resin, and light hydrocarbons. In addition, condensation reactions play a significant role in the late stages of thermal cracking of SB and are the primary reactions responsible for the residues (Liang et al., 2021). Methyl functional groups in the aromatic structure of the residues are released to produce methane through the condensation reactions, resulting in a higher percentage of methane in the gaseous hydrocarbons (Liao et al., 2015).

9. Conclusions and future work

This paper comprehensively reviews the composition, origin, evolution, and hydrocarbon generation potential of OM in the pre-Devonian marine shales, and discusses relevant thermal maturity indicators for these shales. VLM, which exhibits optical properties similar to classical vitrinite in the post-Devonian sediments, is frequently observed in the pre-Devonian marine shales, though it typically constitutes less than 10 % of total OM. It is proposed that VLM formation was related to the anaerobic biodegradation of algae-derived liptinite macerals during early diagenesis in the Precambrian shales. SB, which is observed filling pores and cracks or finely dispersed within clay minerals, is regarded as a thermally evolved product of soluble OM and algae-derived liptinite macerals. Graptolite periderm, which composes the housing or tubarium of these extinct marine hemichordates, significantly contributes to OM in the shales in specific geological periods and environments, and exhibits considerable hydrocarbon generation potential. Pyrolysis experiments indicate that the reflectance of graptolite, VLM, and SB increases with temperature, responding to thermal evolution similarly to vitrinite, thus providing valuable thermal maturity indicators in the pre-Devonian marine shales. In the low-maturity pre-Devonian marine shales, OM is primarily composed of lamalginite and bituminite, while SB becomes the predominant maceral in the postmature shales, often exceeding 90 % of total OM. SB possesses a significant hydrocarbon generation capacity and plays a crucial role in shale gas generation, as confirmed by previous

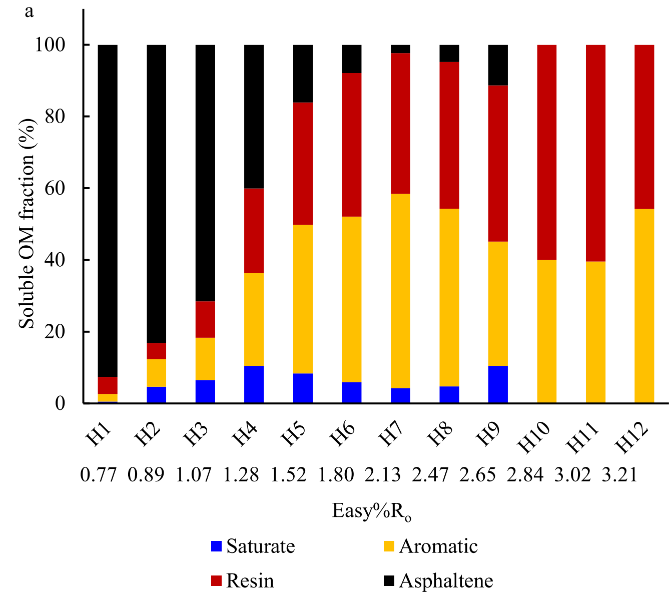

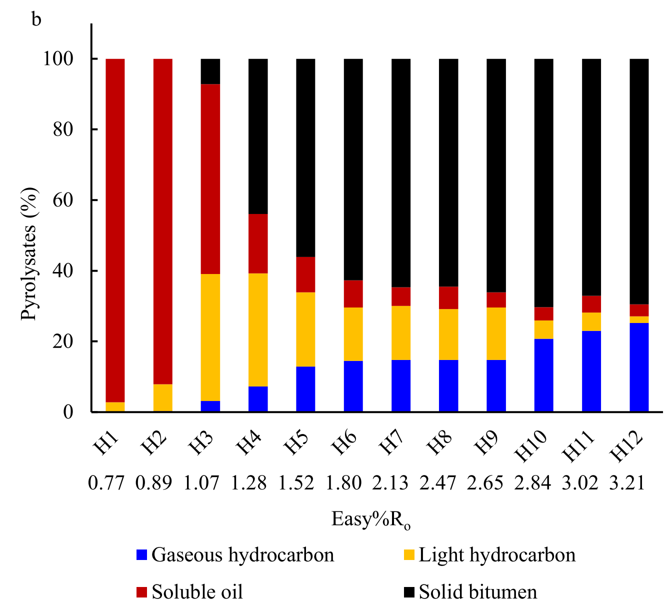

Fig. 11. a, the relative proportions of saturate, aromatic, resin, and asphaltene generated from pyrolysis of low-maturity SB, normalized to 100 %. b, the relative proportions of gaseous hydrocarbons (C_1–C_5), light hydrocarbons (C_6–C_{14}), soluble oil (C_{14+}), and residues (SB) generated from pyrolysis of low-maturity SB, normalized to 100 % (data from Liang et al. (2021)). Easy%R_o values are calculated based on methods of Sweeney and Burnham (1990).

artificial-maturation experiments, which shows that low-maturity algae-derived OM gradually converts to SB as thermal maturity increases. These findings offer valuable insights for evaluating the original OM composition and hydrocarbon generation potential of these marine shales, emphasizing the role of SB in the late stages of thermal evolution and its contribution to the gas generation process.

Reservoir SB displays significantly stronger anisotropy, higher reflectance, and larger particle sizes when compared to in-source SB. Although the exact reasons for their distinct optical characteristics remain uncertain, several factors may contribute to these differences, including growth space and surrounding mineral composition, as well as the varying chemical makeup of their precursor, namely expelled oil in reservoirs versus retained oil in shales. The disparity in BR_o between shales and reservoirs at similar depths within the same well, combined with their differing optical features, suggests that different types of SB follow unique evolutionary paths as thermal maturity progresses. Given these differences, it is valuable to investigate the divergent evolutionary pathways of SB in shales and reservoirs. Future studies should focus on pyrolysis experiments using a range of starting materials and under varying conditions, including fluids, pressure, temperature, and redox environments. These experiments, coupled with advanced analytical techniques such as spectroscopic, petrographic, and bulk geochemical methods, could provide deeper insights into the origins and evolution of VLM. Such research would also help to further distinguish VLM's characteristics from those of other macerals, thereby clarifying its role in hydrocarbon generation and thermal maturity assessment in pre-Devonian marine shales.

Declaration of competing interest

The authors declare the following financial interests/personal relationships which may be considered as potential competing interests:

Qingyong Luo reports financial support was provided by National Natural Science Foundation of China, National Key Research and Development Program of China and Opening Fund of Key Laboratory of Shale Gas Exploration, Ministry of Natural Resources. Vaclav Suchy reports financial support was provided by the program OP RDE, MEYS Czech Republic. If there are other authors, they declare that they have no known competing financial interests or personal relationships that could have appeared to influence the work reported in this paper.

Acknowledgments

The authors wish to thank Dr. Paul Hackley (U.S. Geological Survey) and two anonymous reviewers for providing constructive comments and suggestions that substantially improved the quality of the original manuscript. The authors wish to thank Mr. Julito Reyes of Geological Survey of Canada for his thorough review and suggestions on the initial draft of the manuscript. This work was supported by the National Natural Science Foundation of China (No. 42122016, 42472176, 41773031, and 41503028), National Key Research and Development Program of China (No. 2021YFA0719000) and the Opening Fund of Key Laboratory of Shale Gas Exploration, Ministry of Natural Resources (KLSGE-202201). Václav Suchý wishes to acknowledge the support provided through the program OP RDE, MEYS Czech Republic (Reg. No. CZ.02.1.01/0.0/0.0/16_019/0000728), which enabled him to contribute to the study. We acknowledge Patricia Fraino (University of Calgary) and J.D. Brooker (JK Consulting s.r.o.) for the English polishing.

Data availability

Data will be made available on request.

References

Abouelresh, M.O., 2017. An integrated characterization of the porosity in Qusaiba Shale, Saudi Arabia. J. Pet. Sci. Eng. 149, 75–87.

Abouelresh, M., Babalola, L., Bokhari, A., Omer, M., Koithan, T., Boyde, D., 2020. Sedimentology, geochemistry and reservoir potential of the organic-rich Qusaiba Shale, Tabuk Basin, NW Saudi Arabia. Mar. Pet. Geol. 111, 240–260.

Abraham, H., 1918. Asphalts and Allied Substances: Their Occurrence, Modes of Production, Uses in the Arts and Methods of Testing. Van Nostrand Company, Inc, New York.

Abraham, H., 1960. Asphalts and Allied Substances: Historical Review and Natural Raw Materials. Van Nostrand Company, Inc, New York.

Ahmad, W., Alam, S., 2007. Organic Geochemistry and Source Rock Characteristics of Salt Range Formation, Potwar Basin, Pakistan. Pakistan J. Hydrocarbon Res. 17, 1–35.

Akar, C., Drobniak, A., Mastalerz, M., Schimmelmann, A., 2015. Comparison of hydrocarbon potentials of New Albany Shale and Maquoketa Group in Indiana, USA. Jacobs J. Petrol. Nat. Gas 1 (1), 1–15.

AlGhamdi, F., AlQuraishi, A., Amao, A., Laboun, A.B., Abdel Fattah, K., Kahal, A., Lashin, A., 2023. Depositional setting, mineralogical and diagenetic implication on petrophysical properties of unconventional gas reservoir of the silurian qusaiba formation, northwestern arabian peninsula. Geoenergy Sci. Eng. 223, 211563.

Alpern, B., 1980. Petrographie du kerogene. In: Durand, B. (Ed.), Kerogene, Insoluble Organic Matter from Sedimentary Rocks. Technip, Paris, pp. 339–384.

AlQuraishi, A.A., AlLaboun, A., AlGhamdi, F., AlHussinan, S., 2020. Silurian qusaiba shale: Petrophysical, mineralogical and geochemical analysis. J. Pet. Sci. Eng. 192, 107209.

Ardakani, O.H., Sanei, H., Ghanizadeh, A., Lavoie, D., Chen, Z., Clarkson, C.R., 2018. Do all fractions of organic matter contribute equally in shale porosity? A case study from Upper Ordovician Utica Shale, southern Quebec, Canada. Mar. Pet. Geol. 92, 794–808.

Arysanto, A., Burnaz, L., Zheng, T., Littke, R., 2024. Geochemical and petrographic evaluation of hydrous pyrolysis experiments on core plugs of Lower Toarcian Posidonia Shale: Comparison of artificial and natural thermal maturity series. Int. J. Coal Geol. 284, 104459.

Berry, W.B., Marshall, F.C., 1971. Late Ordovician graptolites from the Maquoketa Formation in eastern Missouri. J. Paleontol. 253–257.

Bertrand, R., 1990. Correlations among the reflectances of vitrinite, chitinozoans, graptolites and scolecodonts. Org. Geochem. 15 (6), 565–574.

Bertrand, R., 1993. Standardization of solid bitumen reflectance to vitrinite in some Paleozoic sequences of Canada. Energy Sources 15 (2), 269–287.

Bertrand, R., Heroux, Y., 1987. Chitinozoan, graptolite, and scolecodont reflectance as an alternative to vitrinite and pyrobitumen reflectance in Ordovician and Silurian strata, Anticosti Island, Quebec, Canada. AAPG Bull. 71 (8), 951–957.

Bertrand, R., Malo, M., 2001. Source rock analysis, thermal maturation and hydrocarbon generation in Siluro-Devonian rocks of the Gaspé Belt basin, Canada. Bull. Can. Petrol. Geol. 49 (2), 238–261.

Bertrand, R., Malo, M., 2012. Dispersed organic matter reflectance and thermal maturation in four hydrocarbon exploration wells in the Hudson Bay Basin: regional implications. Geol. Surv. Canada Open File 7066.

Bertrand, R., Lavoie, D., Fowler, M., 2003. Cambrian-Ordovician shales in the Humber zone: thermal maturation and source rock potential. Bull. Can. Petrol. Geol. 51 (3), 213–233.

Braune, W., 1980. Structural aspects of akinete germination in the cyanobacterium *Anabaena variabilis*. Arch. Microbiol. 126 (3), 257–261.

Buchardt, B., Lewan, M.D., 1990. Reflectance of vitrinite-like macerals as a thermal maturity index for Cambrian-Ordovician Alum shale, southern Scandinavia. AAPG Bull. 74 (4), 394–406.

Bustin, R.M., Guo, Y., 1999. Abrupt changes (jumps) in reflectance values and chemical compositions of artificial charcoals and inertinite in coals. Int. J. Coal Geol. 38 (3), 237–260.

Bustin, R., Link, C., Goodarzi, F., 1989. Optical properties and chemistry of graptolite periderm following laboratory simulated maturation. Org. Geochem. 14 (4), 355–364.

Cai, C., Zhang, C., Worden, R.H., Wang, T., Li, H., Jiang, L., Huang, S., Zhang, B., 2015. Application of sulfur and carbon isotopes to oil–source rock correlation: A case study from the Tazhong area, Tarim Basin, China. Org. Geochem. 83–84, 140–152.

Camp, W.K., 2019. Diagenetic evolution of organic matter cements: Implications for unconventional shale reservoir quality prediction. In: Camp, W., Milliken, K., Taylor, K., Fishman, N., Hackley, P., Macquaker, J. (Eds.), Mudstone Diagenesis: Research Perspectives for Shale Hydrocarbon Reservoirs, Seals, and Source Rocks. AAPG Memoir, pp. 209–224.

Cardott, B.J., 1991. Organic petrology of epi-impsonite at Page, Oklahoma, USA. Org. Geochem. 17 (2), 185–191.

Cardott, B.J., Landis, C.R., Curtis, M.E., 2015. Post-oil solid bitumen network in the Woodford Shale, USA—A potential primary migration pathway. Int. J. Coal Geol. 139, 106–113.

Carr, A.D., Williamson, J.E., 1990. The relationship between aromaticity, vitrinite reflectance and maceral composition of coals: Implications for the use of vitrinite reflectance as a maturation parameter. Org. Geochem. 16 (1), 313–323.

Chen, X., Rong, J., Charles, M., David, H., Fan, J., Zhan, R., Zhang, Y., Li, R., Wang, Y., 2000. Late Ordovician to earliest Silurian graptolite and brachiopod biozonation from the Yangtze region, South China, with a global correlation. Geol. Mag. 137 (6), 623–650.

Chen, X., Rong, J., Li, Y., Boucot, A., 2004. Facies patterns and geography of the Yangtze region, South China, through the Ordovician and Silurian transition. Palaeogeogr. Palaeoclimatol. Palaeoecol. 204 (3), 353–372.

Chen, X., Rong, J., Michael, M., David, S., Charles, M., Fan, J., 2005. Patterns and processes of latest Ordovician graptolite extinction and recovery based on data from South China. J. Paleontol. 79 (5), 824–861.

Chen, Z., Lavoie, D., Malo, M., 2014. Geological Characteristics and Petroleum Resource Assessment of Utica Shale, Quebec, Canada. Natural Resources Canada Open File, p. 7606.

Chen, Z., Liu, X., Osadetz, K.G., 2019. Petroleum generation kinetic models for late ordovician kukersite yeoman Formation source rocks, williston basin (southern saskatchewan), Canada. Fuel 241, 234–246.

Cheng, L., Wang, Y., Chen, H., Wang, Y., Zhong, Y., 2013. Sedimentary and burial environment of black shales of Sinian to Early Palaeozoic in Upper Yangtze region. Acta Petrol. Sin. 29 (8), 2906–2912 (in Chinese with English abstract).

Cheng, M., Li, C., Zhou, L., Algeo, T.J., Zhang, F., Romaniello, S., Jin, C.-S., Lei, L.-D., Feng, L.-J., Jiang, S.-Y., 2016. Marine Mo biogeochemistry in the context of dynamically euxinic mid-depth waters: A case study of the lower Cambrian Niutitang shales, South China. Geochim. Cosmochim. Acta 183, 79–93.

Cheng, M., Li, C., Chen, X., Zhou, L., Algeo, T.J., Ling, H.-F., Feng, L.-J., Jin, C.-S., 2018. Delayed Neoproterozoic oceanic oxygenation: Evidence from Mo isotopes of the Cryogenian Datangpo Formation. Precambrian Res. 319, 187–197.

Cheshire, S., Craddock, P.R., Xu, G., Sauerer, B., Pomerantz, A.E., McCormick, D., Abdallah, W., 2017. Assessing thermal maturity beyond the reaches of vitrinite reflectance and Rock-Eval pyrolysis: A case study from the Silurian Qusaiba formation. Int. J. Coal Geol. 180, 29–45.

Clausen, C., Teichmüller, M., 1982. Die Bedeutung der Graptolithenfragmente im Paläozoikum von Soest-Erwitte für Stratigraphie und Inkohlung. Fortschritte Geol. Rheinland Westfalen 30, 145–167.

Close, D.I., Côté, A.J., Baruch, E.T., Altmann, C.M., Mohinudeen, F.M., Richards, B., Ilett, R., 2017. Proterozoic shale gas plays in the Beetaloo Basin and the Amungee NW-1H discovery. Annu. Geosci. Explor. Semin. 91–97.

Cohen, P.A., Knoll, A.H., Kodner, R.B., 2009. Large spinose microfossils in Ediacaran rocks as resting stages of early animals. Proc. Natl. Acad. Sci. 106 (16), 6519–6524.

Cole, G.A., 1994. Graptolite-chitinozoan reflectance and its relationship to other geochemical maturity indicators in the Silurian Qusaiba Shale, Saudi Arabia. Energy Fuel 8 (6), 1443–1459.

Cole, G.A., Abu-Ali, M.A., Aoudeh, S.M., Carrigan, W.J., Tobey, M.H., 1994. Organic Geochemistry of the Paleozoic Petroleum System of Saudi Arabia. Energy Fuel 8 (6), 1425–1442.

Colţoi, O., Nicolas, G., Safa, P., 2016. The assessment of the hydrocarbon potential and maturity of Silurian intervals from eastern part of Moesian Platform – Romanian sector. Mar. Pet. Geol. 77, 653–667.

Cox, G.M., Collins, A.S., Jarrett, A.J., Blades, M.L., Shannon, A.V., Yang, B., Farkas, J., Hall, P.A., O'Hara, B., Close, D., 2022. A very unconventional hydrocarbon play: The Mesoproterozoic Velkerri Formation of northern Australia. AAPG Bull. 106 (6), 1213–1237.

Craig, J., Hakhoo, N., Bhat, G., Hafiz, M., Khan, M., Misra, R., Pandita, S., Raina, B., Thurow, J., Thusu, B., 2018. Petroleum systems and hydrocarbon potential of the North-West Himalaya of India and Pakistan. Earth Sci. Rev. 187, 109–185.

Crick, I., 1992. Petrological and maturation characteristics of organic matter from the Middle Proterozoic McArthur Basin, Australia. Aust. J. Earth Sci. 39 (4), 501–519.

Crick, I., Boreham, C., Cook, A., Powell, T., 1988. Petroleum geology and geochemistry of Middle Proterozoic McArthur Basin, northern Australia II: Assessment of source rock potential. AAPG Bull. 72 (12), 1495–1514.

Crowther, P.R., 1981. The Fine Structure of Graptolite Periderm. In: Special papers in palaeontology, no. 26. Palaeontological Association, London.

Curiale, J.A., 1986. Origin of solid bitumens, with emphasis on biological marker results. Org. Geochem. 10 (1), 559–580.

Curtis, M.E., Cardott, B.J., Sondergeld, C.H., Rai, C.S., 2012. Development of organic porosity in the Woodford Shale with increasing thermal maturity. Int. J. Coal Geol. 103, 26–31.

Czarnecka, E., Gillott, J., 1980. Formation and characterization of clay complexes with bitumen from Athabasca oil sand. Clay Clay Miner. 28 (3), 197–203.

Dai, J., Zou, C., Liao, S., Dong, D., Ni, Y., Huang, J., Wu, W., Gong, D., Huang, S., Hu, G., 2014. Geochemistry of the extremely high thermal maturity Longmaxi shale gas, southern Sichuan Basin. Org. Geochem. 74, 3–12.

Dai, J., Zou, C., Dong, D., Ni, Y., Wu, W., Gong, D., Wang, Y., Huang, S., Huang, J., Fang, C., Liu, D., 2016. Geochemical characteristics of marine and terrestrial shale gas in China. Mar. Pet. Geol. 76, 444–463.

De Freitas, T., Trettin, H., Dixon, O., Mallamo, M., 1999. Silurian system of the Canadian arctic archipelago. Bull. Can. Petrol. Geol. 47 (2), 136–193.

Dean, K.R., McAtee, J.L., 1986. Asphaltene adsorption on clay. Appl. Clay Sci. 1 (4), 313–319.

Demoulin, C.F., Lara, Y.J., Cornet, L., François, C., Baurain, D., Wilmotte, A., Javaux, E. J., 2019. Cyanobacteria evolution: Insight from the fossil record. Free Radic. Biol. Med. 140, 206–223.

Dewing, K., Obermajer, M., 2009. Lower Paleozoic thermal maturity and hydrocarbon potential of the Canadian Arctic Archipelago. Bull. Can. Petrol. Geol. 57 (2), 141–166.

Diessel, C., Offler, R., 1975. Change in physical properties of coalified and graphitized phytoclasts with grade of metamorphism. Neues Jahrb. Mineral. Monatshefte 3, 1–7.

Diessel, C., Brothers, R., Black, P., 1978. Coalification and graphitization in high-pressure schists in New Caledonia. Contrib. Mineral. Petrol. 68 (1), 63–78.

Dubey, S., Waxman, M., 1991. Asphaltene adsorption and desorption from mineral surfaces. SPE Reserv. Eng. 6 (3), 389–395.

Durand, B., 1980. Kerogen: Insoluble Organic Matter from Sedimentary Rocks. Editions technip.

Ellsworth, H.V., 1928. I. Thucholite, a remarkable primary carbon mineral from the vicinity of parry sound, ontario II. Cyrtolite intergrowth associated with the parry sound thucholite. J. Mineral. Soc. Am. 13, 419–441.

England, G.L., Rasmussen, B., Krapež, B., Groves, D.I., 2001. The origin of uraninite, bitumen nodules, and carbon seams in Witwatersrand gold-uranium-pyrite ore deposits, based on a Permo-Triassic analogue. Econ. Geol. 96 (8), 1907–1920.

Ertug, K., Vecoli, M., İnan, S., 2019. Palynofacies, paleoenvironment and thermal maturity of early Silurian shales in Saudi Arabia (Qusaiba Member of Qalibah Formation). Rev. Palaeobot. Palynol. 270, 8–18.

Espitalié, J., Laporte, J.L., Madec, M., Marquis, F., Leplat, P., Paulet, J., 1977. Méthode rapide de caractérisation des rochès, de leur potential pétrolier et de leur degree d'évolution. Rev. Inst. Fr. Pétrol. 32, 23–43.

Faiz, M., Altmann, C., Baruch, E., Côté, A., Gong, S., Schinteie, R., Ranasinghe, P., 2022. Organic matter composition and thermal maturity evaluation of Mesoproterozoic source rocks in the Beetaloo Sub-Basin, Australia. Org. Geochem. 174, 104513.

Fakhraee, M., Tarhan, L.G., Reinhard, C.T., Crowe, S.A., Lyons, T.W., Planavsky, N., 2023. Earth's surface oxygenation and the rise of eukaryotic life: Relationships to the Lomagundi positive carbon isotope excursion revisited. Earth Sci. Rev. 240, 104398.

Fay, P., 1983. The Blue-Greens. Institute of Biology's Studies in Biology 160. Camelot Press, Southampton, 88 pp.

Feng, G., Chen, S., 1988. Relationship between the reflectance of bitumen and vitrinite in rock. Nat. Gas Ind. 8 (3), 20–25 (in Chinese with English abstract).

Feng, L., Li, C., Huang, J., Chang, H., Chu, X., 2014. A sulfate control on marine mid-depth euxinia on the early Cambrian (ca. 529–521Ma) Yangtze platform, South China. Precambrian Res. 246, 123–133.

Fu, S.T., Fu, J.H., Xi, S.L., Huang, Z.L., 2021a. Geological characteristics of Ordovician marine shale gas in the Ordos Basin and its prospects. China Petrol. Explor. 26 (2), 33–44 (in Chinese with English abstract).

Fu, S.T., Wang, W.X., Li, X.W., Xi, S.L., Hu, X.F., Zhang, Y.M., 2021b. Volume fracturing and drainage technologies for low-pressure marine shale gas reservoirs in the Ordos Basin. Nat. Gas Ind. 41 (3), 72–79 (in Chinese with English abstract).

Gai, H., Xiao, X., Cheng, P., Tian, H., Fu, J., 2015. Gas generation of shale organic matter with different contents of residual oil based on a pyrolysis experiment. Org. Geochem. 78, 69–78.

Gai, H., Tian, H., Xiao, X., 2018. Late gas generation potential for different types of shale source rocks: Implications from pyrolysis experiments. Int. J. Coal Geol. 193, 16–29.

Gai, H., Tian, H., Cheng, P., Zhou, Q., Li, T., Wang, X., Xiao, X., 2019. Influence of retained bitumen in oil-prone shales on the chemical and carbon isotopic compositions of natural gases: Implications from pyrolysis experiments. Mar. Pet. Geol. 101, 148–161.

Gao, P., Liu, G., Lash, G.G., Li, B., Yan, D., Chen, C., 2018. Occurrences and origin of reservoir solid bitumen in Sinian Dengying Formation dolomites of the Sichuan Basin, SW China. Int. J. Coal Geol. 200, 135–152.

Gautier, D., Charpentier, R., Gaswirth, S., Klett, T., Pitman, J., Schenk, C., Tennyson, M., Whidden, K., 2013. Undiscovered Gas Resources in the Alum Shale, Denmark. US Geological Survey Fact Sheet, 3103: Fact Sheet 2013–3103.

Gentzis, T., Goodarzi, F., 1993. Regional thermal maturity in the Franklinian Mobile Belt, Melville Island, Arctic Canada. Mar. Pet. Geol. 10 (3), 215–230.

Gentzis, T., de Freitas, T., Goodarzi, F., Melchin, M., Lenz, A., 1996. Thermal maturity of Lower Paleozoic sedimentary successions in Arctic Canada. AAPG Bull. 80 (7), 1065–1083.

George, S., Llorca, S., Hamilton, P., 1994. An integrated analytical approach for determining the origin of solid bitumens in the McArthur Basin, northern Australia. Org. Geochem. 21 (3), 235–248.

Golubev, Y.A., Kovaleva, O.V., Yushkin, N.P., 2008. Observations and morphological analysis of supermolecular structure of natural bitumens by atomic force microscopy. Fuel 87 (1), 32–38.

Gonçalves, P.A., Kus, J., Hackley, P.C., Borrego, A.G., Hámor-Vidó, M., Kalkreuth, W., Mendonça Filho, J.G., Petersen, H.I., Pickel, W., Reinhardt, M.J., Suárez-Ruiz, I., 2024. The petrology of dispersed organic matter in sedimentary rocks: Review and update. Int. J. Coal Geol. 294, 104604.

Goodarzi, F., 1984. Organic petrography of graptolite fragments from Turkey. Mar. Pet. Geol. 1 (3), 202–210.

Goodarzi, F., 1985a. Dispersion of optical properties of graptolite epiderms with increased maturity in early Paleozoic organic sediments. Fuel 64 (12), 1735–1740.

Goodarzi, F., 1985b. Reflected light microscopy of chitinozoan fragments. Mar. Pet. Geol. 2 (1), 72–78.

Goodarzi, F., Higgins, A., 1987. Optical properties of scolecodonts and their use as indicators of thermal maturity. Mar. Pet. Geol. 4 (4), 353–359.

Goodarzi, F., Norford, B., 1985. Graptolites as indicators of the temperature histories of rocks. J. Geol. Soc. 142 (6), 1089–1099.

Goodarzi, F., Norford, B., 1987. Optical properties of graptolite epiderm—A review. Bull. Geol. Soc. Denmark 35, 141–147.

Goodarzi, F., Norford, B., 1989. Variation of graptolite reflectance with depth of burial. Int. J. Coal Geol. 11 (2), 127–141.

Goodarzi, F., Eckstrand, O.R., Snowdon, L., Williamson, B., Stasiuk, L.D., 1992a. Thermal metamorphism of bitumen in Archean rocks by ultramafic volcanic flows. Int. J. Coal Geol. 20 (1–2), 165–178.

Goodarzi, F., Fowler, M., Bustin, M., McKirdy, D., 1992b. Thermal maturity of Early Paleozoic sediments as determined by the optical properties of marine-derived organic matter—A review. In: Early Organic Evolution. Springer, Berlin, pp. 279–295.

Goodarzi, F., Gentzis, T., Harrison, C., Thorsteinsson, R., 1992c. The significance of graptolite reflectance in regional thermal maturity studies, Queen Elizabeth Islands, Arctic Canada. Org. Geochem. 18 (3), 347–357.

Goodarzi, F., Gentzis, T., Jackson, G., Macqueen, R.W., 1993. Optical characteristics of heat-affected bitumens from the Nanisivik Mine, NW Baffin Island, Arctic Canada. Energy Sources 15 (2), 359–376.

Goodarzi, F., Hosseininejad, S., Pedersen, P.K., Gentzis, T., Sanei, H., 2022. Characterization of immature oil shales from the Cretaceous Second White Specks Formation in Saskatchewan and Manitoba, Canada. Mar. Pet. Geol. 143, 105774.

Guthrie, J.M., 1996. Molecular and carbon isotopic analysis of individual biological markers: evidence for sources of organic matter and paleoenvironmental conditions in the Upper Ordovician Maquoketa Group, Illinois Basin, USA. Org. Geochem. 25 (8), 439–460.

Guthrie, J.M., Pratt, L.M., 1994. Geochemical indicators of depositional environment and source-rock potential for the Upper Ordovician Maquoketa Group, Illinois Basin. AAPG Bull. 78 (5), 744–757.

Hackley, P.C., Cardott, B.J., 2016. Application of organic petrography in North American shale petroleum systems: A review. Int. J. Coal Geol. 163, 8–51.

Hackley, P.C., Lewan, M., 2018. Understanding and distinguishing reflectance measurements of solid bitumen and vitrinite using hydrous pyrolysis: Implications to petroleum assessment. AAPG Bull. 102 (6), 1119–1140.
Hackley, P.C., SanFilipo, J.R., 2016. Organic petrology and geochemistry of Eocene Suzak bituminous marl, north-central Afghanistan: Depositional environment and source rock potential. Mar. Pet. Geol. 73, 572–589.
Hackley, P.C., Walters, C.C., Kelemen, S.R., Mastalerz, M., Lowers, H.A., 2017a. Organic petrology and micro-spectroscopy of Tasmanites microfossils: applications to kerogen transformations in the early oil window. Org. Geochem. 114, 23–44.
Hackley, P.C., Zhang, L., Zhang, T., 2017b. Organic petrology of peak oil maturity Triassic Yanchang Formation lacustrine mudrocks, Ordos Basin, China. Interpretation 5 (2), SF211–SF223.
Hackley, P.C., Valentine, B.J., Hatcherian, J.J., 2018. On the petrographic distinction of bituminite from solid bitumen in immature to early mature source rocks. Int. J. Coal Geol. 196, 232–245.
Hackley, P.C., Araujo, C.V., Borrego, A.G., Bouzinos, A., Cardott, B.J., Carvajal-Ortiz, H., López Cely, M.R., Chabalala, V., Crosdale, P.J., Demchuk, T.D., Eble, C.F., Flores, D., Furmann, A., Gentzis, T., Gonçalves, P.A., Guvad, C., Hámor-Vidó, M., Jelonek, I., Johnston, M.N., Juliao-Lemus, T., Kalaitzidis, S., Knowles, W.R., Kus, J., Li, Z., Macleod, G., Mastalerz, M., Menezes, T.R., Ocubalidet, S., Orban, R., Pickel, W., Ranasinghe, P., Ribeiro, J., Gómez Rojas, O.P., Ruiz-Monroy, R., Schmidt, J.S., Seyedolali, A., Siavalas, G., Suarez-Ruiz, I., Vargas, C.V., Valentine, B.J., Wagner, N., Wrolson, B., Jaramillo Zapata, J.E., 2020a. Testing reproducibility of vitrinite and solid bitumen reflectance measurements in North American unconventional source-rock reservoir petroleum systems. Mar. Pet. Geol. 114, 104172.
Hackley, P.C., Zhang, T., Jubb, A.M., Valentine, B.J., Dulong, F.T., Hatcherian, J.J., 2020b. Organic petrography of Leonardian (Wolfcamp A) mudrocks and carbonates, Midland Basin, Texas: The fate of oil-prone sedimentary organic matter in the oil window. Mar. Pet. Geol. 112, 104086.
Hackley, P.C., Jubb, A.M., Smith, P.L., McAleer, R.J., Valentine, B.J., Hatcherian, J.J., Botterell, P.J., Birdwell, J.E., 2022. Evaluating aromatization of solid bitumen generated in the presence and absence of water: Implications for solid bitumen reflectance as a thermal proxy. Int. J. Coal Geol. 258, 104016.
Hackley, P.C., Scott, C., Birdwell, J.E., Nedzweckas, J.L., Valentine, B.J., Zhang, T., Nesheim, T.O., 2024. Insights on Using Solid Bitumen Reflectance as a Thermal Maturity Proxy in the Bakken Formation, Williston Basin, USA. ACS Omega 9 (31), 33983–33997.
Haeri-Ardakani, O., Sanei, H., Lavoie, D., Chen, Z., Jiang, C., 2015. Geochemical and petrographic characterization of the Upper Ordovician Utica Shale, southern Quebec, Canada. Int. J. Coal Geol. 138, 83–94.
Hao, S.S., Gao, Y.B., Zhang, Y.C., Lu, X.S., Lu, B.Z., Wen, X.D., S, D.J., 1990. Neoproterozoic-Mesoproterozoic Petroleum Geology in North China. Petroleum University Press, Dongying (in Chinese).
Hao, J., Zhong, N., Luo, Q., Liu, D., Wu, J., Liu, A., 2019. Raman spectroscopy of graptolite periderm and its potential as an organic maturity indicator for the Lower Paleozoic in southwestern China. Int. J. Coal Geol. 213, 103278.
Hayton, S., Jaeger, H., 2017. Organic Matter Variability in the Early Silurian Qusaiba Source Rocks, Saudi Arabia, Abu Dhabi International Petroleum Exhibition & Conference pp. D021S053R007.
Hayton, S., Rees, A.J., Vecoli, M., 2017. A punctuated Late Ordovician and early Silurian deglaciation and transgression: Evidence from the subsurface of northern Saudi Arabia. AAPG Bull. 101 (6), 863–886.
He, Z.X., 2003. Tectonic Evolution and Oil and Gas Resources in Ordos Basin. Petroleum Industry Press, Beijing, pp. 3–152 (in Chinese with English abstract).
Herdman, M., 1988. Cellular differentiation: Akinetes. Methods Enzymol. 167, 222–232.
Hoffknecht, A., 1991. Mikropetrographische, organisch-geochemische, mikrothermometrische und mineralogische Untersuchungen zur Bestimmung der organischen Reife von Graptolithen-Periderm. Göttinger Arbeiten Geol. Paläontol. 48, 1–98.
Hu, A., Li, M., Wong, J., Reyes, J., Achal, S., Milovic, M., Robinson, R., Shou, J., Yang, C., Dai, J., Ma, Y., Guo, T., 2010. Chemical and petrographic evidence for thermal cracking and thermochemical sulfate reduction of paleo-oil accumulations in the NE Sichuan Basin, China. Org. Geochem. 41 (9), 924–929.
Hu, G., Pang, Q., Jiao, K., Hu, C., Liao, Z., 2020. Development of organic pores in the Longmaxi Formation overmature shales: Combined effects of thermal maturity and organic matter composition. Mar. Pet. Geol. 116, 104314.
Huang, H., Zhang, S., Su, J., 2016. Palaeozoic oil–source correlation in the Tarim Basin, NW China: A review. Org. Geochem. 94, 32–46.
Hunt, J.M., Stewart, F., Dickey, P.A., 1954. Origin of hydrocarbons of Uinta basin, Utah. AAPG Bull. 38 (8), 1671–1698.
Hwang, R., Teerman, S., Carlson, R., 1998. Geochemical comparison of reservoir solid bitumens with diverse origins. Org. Geochem. 29 (1), 505–517.
İnan, S., Goodarzi, F., Mumm, A.S., Arouri, K., Qathami, S., Ardakani, O.H., İnan, T., Tuwailib, A.A., 2016. The Silurian Qusaiba Hot Shales of Saudi Arabia: An integrated assessment of thermal maturity. Int. J. Coal Geol. 159, 107–119.
ISO, 2009. Methods for the Petrographic Analysis of Coals – Part 2: Methods of Preparing Coal Samples, p. 7404-2. www.iso.org/standard/42798.html.
Jacob, H., 1989. Classification, structure, genesis and practical importance of natural solid oil bitumen ("migrabitumen"). Int. J. Coal Geol. 11 (1), 65–79.
Jamil, A., Sheikh, R.A., 2012. An overview of Neoproterozoic reservoirs in Pakistan. Geol. Soc. Lond., Spec. Publ. 366 (1), 111–121.
Jarrett, A.J., MacFarlane, S., Palu, T., Boreham, C., Hall, L., Edwards, D., Cox, G., Munson, T.J., Brocks, J., Carr, L., 2019. Source rock geochemistry and petroleum systems of the greater McArthur Basin and links to other northern Australian Proterozoic basins. In: Australian Geoscience Exploration Seminar (AGES) Proceedings, Alice Springs, pp. 19–20.
Jin, S., Liu, Y., Ma, C., Zhang, Q., Chen, A., 2024. Orbital cycles recorded in Early Cambrian shales with implications for organic matter accumulation. J. Asian Earth Sci. 263, 106033.
Johnson, M., Armstrong, D., Sanford, B., Telford, P., Rutka, M., 1992. Paleozoic and Mesozoic geology of Ontario. Geol. Ontario Ontario Geol. Surv. Spec. 4 (Part 2), 907–1008.
Jubb, A.M., Hackley, P.C., Hatcherian, J.J., Qu, J., Nesheim, T.O., 2019. Nanoscale molecular fractionation of organic matter within unconventional petroleum source beds. Energy Fuel 33 (10), 9759–9766.
Khan, I., Zhong, N., Luo, Q., Ai, J., Yao, L., Luo, P., 2020. Maceral composition and origin of organic matter input in Neoproterozoic–Lower Cambrian organic-rich shales of Salt Range Formation, upper Indus Basin, Pakistan. Int. J. Coal Geol. 217, 103319.
Killops, S.D., Killops, V.J., 2013. Introduction to Organic Geochemistry. John Wiley & Sons.
Kirschbaum, M.A., Schenk, C.J., Cook, T.A., Ryder, R.T., Charpentier, R.R., Klett, T.R., Gaswirth, S.B., Tennyson, M.E., Whidden, K.J., 2012. Assessment of undiscovered oil and gas resources of the Ordovician Utica Shale of the Appalachian Basin Province. US Geological Survey, pp. 2327–6932.
Kisch, H., 1980. Incipient metamorphism of Cambro-Silurian clastic rocks from the Jamtland Supergroup, Central Scandinavian Caledonides, Western Sweden: illite crystallinity and 'vitrinite' reflectance. J. Geol. Soc. Lond. 137, 271–288.
Landis, C.R., Castaño, J.R., 1995. Maturation and bulk chemical properties of a suite of solid hydrocarbons. Org. Geochem. 22 (1), 137–149.
Lavoie, D., 1994. Diachronous tectonic collapse of the Ordovician continental margin, eastern Canada: comparison between the Quebec Reentrant and St. Lawrence Promontory. Can. J. Earth Sci. 31 (8), 1309–1319.
Lavoie, D., 2008. Appalachian foreland basin of Canada. In: Sedimentary Basins of the World, 5, pp. 65–103.
Lavoie, D., Pinet, N., Bordeleau, G., Ardakani, O.H., Ladevèze, P., Duchesne, M.J., Rivard, C., Mort, A., Brake, V., Sanei, H., 2016. The Upper Ordovician black shales of southern Quebec (Canada) and their significance for naturally occurring hydrocarbons in shallow groundwater. Int. J. Coal Geol. 158, 44–64.
Li, Z., Lu, Y., Wang, J., Duan, T., Gao, Y., 2004. Sedimentary characteristics and lithofacies palaeogeography of the Late Sinian and Early Cambrian in middle Yangtze region. J. Palaeogeogr. 6 (2), 151–162 (in Chinese with English abstract).
Li, C., Love, G.D., Lyons, T.W., Fike, D.A., Sessions, A.L., Chu, X., 2010. A stratified redox model for the Ediacaran ocean. Science 328 (5974), 80–83.
Li, C., Love, G.D., Lyons, T.W., Scott, C.T., Feng, L., Huang, J., Chang, H., Zhang, Q., Chu, X., 2012. Evidence for a redox stratified Cryogenian marine basin, Datangpo Formation, South China. Earth Planet. Sci. Lett. 331–332, 246–256.
Li, C., Jin, C., Planavsky, N.J., Algeo, T.J., Cheng, M., Yang, X., Zhao, Y., Xie, S., 2017. Coupled oceanic oxygenation and metazoan diversification during the early–middle Cambrian? Geology 45 (8), 743–746.
Li, H., Chen, K., Bao, S., Zhang, Y., Song, T., Wang, P., 2019. Evaluation of shale gas resources of the Sinian Doushantuo Formation in the southern Huangling anticline, western Hubei Province. Pet. Geol. Exp. 41 (1), 31–37 (in Chinese with English abstract).
Li, F., Huang, Z., Wang, X., Liu, X., Liu, W., Cai, Z., Luo, H., Wang, Q., Zhang, D., 2022. Geochemical Characteristics of Graptolite Shale in the Pingliang Formation of the Ordos Basin, China: Implications for Organic Matter, Thermal Evolution, and Hydrocarbon Reservoir. Energies 15 (21), 8238.
Li, Z., Sun, Z., Bao, Y., Xu, E., Zhou, Y., Zhang, Y., 2023. Discussion on prospecting shale oil potential of Mesoproterozoic Hongshuizhuang Formation in the Jibei Depression. Pet. Geol. Exp. 45 (1), 29–40 (in Chinese with English abstract).
Liang, T., Zhan, Z., Mejia, J., Zou, Y., 2021. Hydrocarbon generation characteristics of solid bitumen and molecular simulation based on the density functional theory. Mar. Pet. Geol. 134, 105369.
Liao, Y., Zheng, Y., Pan, Y., Sun, Y., Geng, A., 2015. A method to quantify C1–C5 hydrocarbon gases by kerogen primary cracking using pyrolysis gas chromatography. Org. Geochem. 79, 49–55.
Link, C., Bustin, R., Goodarzi, F., 1990. Petrology of graptolites and their utility as indices of thermal maturity in Lower Paleozoic strata in northern Yukon, Canada. Int. J. Coal Geol. 15 (2), 113–135.
Liu, D., Shi, J., 1994. Discussion on unconventional evaluation method of high evolution carbonate source rock. Pet. Explor. Dev. 21 (3), 113–115 (in Chinese with English abstract).
Liu, B., Schieber, J., Mastalerz, M., 2017. Combined SEM and reflected light petrography of organic matter in the New Albany Shale (Devonian-Mississippian) in the Illinois Basin: A perspective on organic pore development with thermal maturation. Int. J. Coal Geol. 184, 57–72.
Liu, B., Schieber, J., Mastalerz, M., 2019a. Petrographic and micro-FTIR study of organic matter in the Upper Devonian New Albany Shale during thermal maturation: Implications for kerogen transformation. In: Camp, W., Milliken, K., Taylor, K., Fishman, N., Hackley, P., Macquaker, J. (Eds.), Mudstone Diagenesis: Research Perspectives for Shale Hydrocarbon Reservoirs, Seals, and Source Rocks. AAPG Memoir, pp. 165–188.
Liu, J., Zhou, Z., Liu, X., Ren, S., Wang, J., Wang, H., Zhou, C., Liu, Y., 2019b. Geological conditions of the Mesoproterozoic shale gas accumulation in Yanshan area, North China. Acta Pet. Sin. 40 (3), 268–278 (in Chinese with English abstract).
Liu, B., Mastalerz, M., Schieber, J., Teng, J., 2020. Association of uranium with macerals in marine black shales: Insights from the Upper Devonian New Albany Shale, Illinois Basin. Int. J. Coal Geol. 217, 103351.
Liu, B., Mastalerz, M., Schieber, J., 2022. SEM petrography of dispersed organic matter in black shales: A review. Earth Sci. Rev. 224, 103874.

Loucks, R.G., Reed, R.M., Ruppel, S.C., Jarvie, D.M., 2009. Morphology, genesis, and distribution of nanometer-scale pores in siliceous mudstones of the Mississippian Barnett Shale. J. Sediment. Res. 79 (12), 848–861.
Loucks, R.G., Reed, R.M., Ruppel, S.C., Hammes, U., 2012. Spectrum of pore types and networks in mudrocks and a descriptive classification for matrix-related mudrock pores. AAPG Bull. 96 (6), 1071–1098.
Lüning, S., Craig, J., Loydell, D.K., Štorch, P., Fitches, B., 2000. Lower Silurian 'hot shales' in North Africa and Arabia: regional distribution and depositional model. Earth Sci. Rev. 49 (1), 121–200.
Lüning, S., Kolonic, S., Loydell, D.K., Craig, J., 2003. Reconstruction of the original organic richness in weathered Silurian shale outcrops (Murzuq and Kufra basins, southern Libya). GeoArabia 8 (2), 299–308.
Luo, Q., Zhong, N., Zhu, L., Wang, Y., Qin, J., Qi, L., Zhang, Y., Ma, Y., 2013. Correlation of burial organic carbon and paleoproductivity in the Mesoproterozoic Hongshuizhuang Formation, northern North China. Chin. Sci. Bull. 58, 1299–1309.
Luo, Q., Zhong, N., Qin, J., Li, K., Zhang, Y., Wang, Y., Ma, L., 2014. Thucholite in Mesoproterozoic shales from northern China: Occurrence and indication for thermal maturity. Int. J. Coal Geol. 125 (1), 1–9.
Luo, G., Hallmann, C., Xie, S., Ruan, X., Summons, R.E., 2015. Comparative microbial diversity and redox environments of black shale and stromatolite facies in the Mesoproterozoic Xiamaling Formation. Geochim. Cosmochim. Acta 151, 150–167.
Luo, Q., George, S.C., Xu, Y., Zhong, N., 2016a. Organic geochemical characteristics of the Mesoproterozoic Hongshuizhuang Formation from northern China: implications for thermal maturity and biological sources. Org. Geochem. 99, 23–37.
Luo, Q., Zhong, N., Dai, N., Zhang, W., 2016b. Graptolite-derived organic matter in the Wufeng–Longmaxi Formations (Upper Ordovician–Lower Silurian) of southeastern Chongqing, China: Implications for gas shale evaluation. Int. J. Coal Geol. 153, 87–98.
Luo, Q., Hao, J., Li, K., Dai, N., Luan, J., Cheng, L., Zhang, Z., Hu, K., Zhong, N., 2017a. The optical characteristics of the graptolites in the Wufeng-Longmaxi formations and its application for the thermal maturity evaluation. Nat. Gas Ind. 28 (12), 1855–1863 (in Chinese with English abstract).
Luo, Q., Hao, J., Skovsted, C.B., Luo, P., Khan, I., Wu, J., Zhong, N., 2017b. The organic petrology of graptolites and maturity assessment of the Wufeng–Longmaxi Formations from Chongqing, China: Insights from reflectance cross-plot analysis. Int. J. Coal Geol. 183, 161–173.
Luo, Q., Hao, J., Skovsted, C.B., Xu, Y., Liu, Y., Wu, J., Zhang, S., Wang, W., 2018. Optical characteristics of graptolite-bearing sediments and its implication for thermal maturity assessment. Int. J. Coal Geol. 195, 386–401.
Luo, Q., Hao, J., Li, K., Xu, Y., Wang, X., Wang, h., Luan, J., Hu, K., Li, T. and Zhong, N., 2019. A new parameter for the thermal maturity assessment in the Paleozoic sediments: a restudy of the optical characteristics of the graptolite. Acta Geol. Sin. 93 (9), 2362–2371 (in Chinese with English abstract).
Luo, Q., Goodarzi, F., Zhong, N., Wang, Y., Qiu, N., Skovsted, C.B., Suchý, V., Hemmingsen Schovsbo, N., Morga, R., Xu, Y., Hao, J., Liu, A., Wu, J., Cao, W., Min, X., Wu, J., 2020. Graptolites as fossil geo-thermometers and source material of hydrocarbons: An overview of four decades of progress. Earth Sci. Rev. 200, 103000.
Luo, Q., Zhang, L., Zhong, N., Wu, J., Goodarzi, F., Sanei, H., Skovsted, C.B., Suchý, V., Li, M., Ye, X., Cao, W., Liu, A., Min, X., Pan, Y., Yao, L., Wu, J., 2021. Thermal evolution behavior of the organic matter and a ray of light on the origin of vitrinite-like maceral in the Mesoproterozoic and Lower Cambrian black shales: Insights from artificial maturation. Int. J. Coal Geol. 244, 103813.
Luo, Q., Zhong, N., Li, M., Wu, J., Imran, K., Zhang, Y., Chen, Q., Ye, X., Li, W., Ji, W., Liu, A., Hao, J., Yao, L., Wu, J., 2023. Classification, origins, and evolution of macerals in the Precambrian-Eopaleozoic sedimentary rocks. Oil Gas Geol. 44 (5), 1084–1101 (in Chinese with English abstract).
Lyons, T.W., Reinhard, C.T., Planavsky, N.J., 2014. The rise of oxygen in Earth's early ocean and atmosphere. Nature 506 (7488), 307–315.
Ma, Y., Zhong, N., Cheng, L., Pan, Z., Dai, N., Zhang, Y., Yang, L., 2016. Pore structure of the graptolite-derived OM in the Longmaxi Shale, southeastern Upper Yangtze Region, China. Mar. Pet. Geol. 72, 1–11.
Ma, K., Hu, S., Wang, T., Zhang, B., Qin, S., Shi, S., Wang, K., Huang, Q., 2017. Sedimentary environments and mechanisms of organic matter enrichment in the Mesoproterozoic Hongshuizhuang Formation of northern China. Palaeogeogr. Palaeoclimatol. Palaeoecol. 475, 176–187.
Ma, Z., Liu, X., Yu, W., Du, Y., Du, Q., 2019. Redox conditions and manganese metallogenesis in the Cryogenian Nanhua Basin: Insight from the basal Datangpo Formation of South China. Palaeogeogr. Palaeoclimatol. Palaeoecol. 529, 39–52.
Machel, H., 2001. Bacterial and thermochemical sulfate reduction in diagenetic settings—old and new insights. Sediment. Geol. 140 (1), 143–175.
Machel, H.G., Krouse, H.R., Sassen, R., 1995. Products and distinguishing criteria of bacterial and thermochemical sulfate reduction. Appl. Geochem. 10 (4), 373–389.
Mahmoud, M., Vaslet, D., Husseini, M., 1992. The lower silurian Qalibah formation of Saudi Arabia: an important hydrocarbon source rock (1). AAPG Bull. 76 (10), 1491–1506.
Malán, O., 1980. Petrological investigation of dispersed organic matter (MOD) in the deep bore Tobolka 1. Folia Mus. Rer. Natur. Bohemia Occident. Geol. 15, 1–52.
Malinconico, M.A.L., 1992. Graptolite reflectance in the prehnite-pumpellyite zone of Northern Maine, USA. Org. Geochem. 18 (3), 263–271.
Malinconico, M.A.L., 1993. Reflectance cross-plot analysis of graptolites from the anchi-metamorphic region of northern Maine, USA. Org. Geochem. 20 (2), 197–207.
Mandal, A., Saha, D., Kumar, A., 2022. Structural analysis and seismic stratigraphy for delineation of Neoproterozoic-Cambrian petroleum system in central and eastern part of Bikaner–Nagaur basin, India. J. Pet. Explor. Prod. Technol. 12 (6), 1709–1725.
Mastalerz, M., Drobniak, A., Stankiewicz, A.B., 2018. Origin, properties, and implications of solid bitumen in source-rock reservoirs: A review. Int. J. Coal Geol. 195, 14–36.
McKerrow, W.S., Scotese, C.R., Brasier, M.D., 1992. Early Cambrian continental reconstructions. J. Geol. Soc. 149 (4), 599–606.
Medina, C.R., Mastalerz, M., Lahann, R.W., Rupp, J.A., 2020. A novel multi-technique approach used in the petrophysical characterization of the Maquoketa Group (Ordovician) in the southeastern portion of the Illinois Basin: Implications for seal efficiency for the geologic sequestration of CO2. Int. J. Greenh. Gas Contr. 93, 102883.
Meng, F., Zhang, Z., Bukowski, K., Zhuo, Q., Ahsan, N., Ur-Rehman, S., Ni, P., 2021. A strongly positive sulphur isotopic shift in late Ediacaran-early Cambrian seawater: evidence from evaporites in the Salt Range Formation, northern Pakistan. Geol. Quart. 65 (2), 1–13.
Misch, D., Gross, D., Hawranek, G., Horsfield, B., Klaver, J., Mendez-Martin, F., Urai, J. L., Vranjes-Wessely, S., Sachsenhofer, R.F., Schmatz, J., Li, J., Zou, C., 2019. Solid bitumen in shales: Petrographic characteristics and implications for reservoir characterization. Int. J. Coal Geol. 205, 14–31.
Morga, R., Kamińska, M., 2018. The chemical composition of graptolite periderm in the gas shales from the Baltic Basin of Poland. Int. J. Coal Geol. 199, 10–18.
Mu, C., Zhou, K., Liang, W., Ge, X., 2011. Early Paleozoic sedimentary environment of hydrocarbon source rocks in the Middle-Upper Yangtze Region and petroleum and gas exploration. Acta Geol. Sin. 85 (4), 526–532 (in Chinese with English abstract).
Munson, T., 2014. Petroleum Geology and Potential of the Onshore Northern Territory. Northern Territory Geological Survey. Report 22.
Munson, T., Denyszyn, S., Simmons, J., Kunzmann, M., 2020. A 1642 Ma age for the fraynes formation, birrindudu basin, confirms correlation with the economically significant barney creek formation, mcarthur basin, northern territory. Aust. J. Earth Sci. 67 (3), 321–330.
Nichols, J.M., Adams, D.G., Carr, N.G., 1980. Effect of canavanine and other amino acid analogues on akinete formation in the cyanobacterium *Anabaena cylindrica*. Arch. Microbiol. 127 (1), 67–75.
Nielsen, A.T., Schovsbo, N.H., 2006. Cambrian to basal Ordovician lithostratigraphy in southern Scandinavia. Bull. Geol. Soc. Den. 53, 47–92.
Norford, B., Haidl, F., Bezys, R., Cecile, M., McCabe, H., Paterson, D., Mossop, G., Shetson, I., 1994. Middle Ordovician to lower Devonian strata of the western Canada sedimentary basin, Geological atlas of the Western Canada sedimentary basin. In: Canadian Society of Petroleum Geologists and Alberta Research Council, pp. 109–127.
Obermajer, M., Fowler, M., Goodarzi, F., Snowdon, L., 1996. Assessing thermal maturity of Palaeozoic rocks from reflectance of chitinozoa as constrained by geochemical indicators: an example from southern Ontario, Canada. Mar. Pet. Geol. 13 (8), 907–919.
Obermajer, M., Fowler, M., Snowdon, L., 1999. Depositional environment and oil generation in Ordovician source rocks from southwestern Ontario, Canada: organic geochemical and petrological approach. AAPG Bull. 83 (9), 1426–1453.
Osadetz, K.G., Brooks, P.W., Snowdon, L.R., 1992. Oil families and their sources in Canadian Williston Basin,(southeastern Saskatchewan and southwestern Manitoba). Bull. Can. Petrol. Geol. 40 (3), 254–273.
Peng, B., Liu, Y., Qi, F., Dong, Y., Wang, Z., 2017. Study on the Accumulation Conditions of Shale Gas in Doushantuo Formation in Western Hubei. Geol. Rev. 63 (5), 1293–1306 (in Chinese with English abstract).
Perez, R., Maldener, I., Salerno, G., Forchhammer, K., 2016. Clear differences in metabolic and morphological adaptations of akinetes of two Nostocales living in different habitats. Microbiology 162, 214–223.
Perez, R., Wörmer, L., Sass, P., Maldener, I., 2018. A highly asynchronous developmental program triggered during germination of dormant akinetes of filamentous diazotrophic cyanobacteria. FEMS Microbiol. Ecol. 94 (1) fix131.
Pernyeszi, T., Patzko, A., Berkesi, O., Dékány, I., 1998. Asphaltene adsorption on clays and crude oil reservoir rocks. Colloids Surf. A Physicochem. Eng. Asp. 137 (1), 373–384.
Peters, K., Clark, M., Das Gupta, U., McCaffrey, M., Lee, C., 1995. Recognition of an Infracambrian source rock based on biomarkers in the Baghewala-1 oil, India. AAPG Bull. 79 (10), 1481–1493.
Peters, K.E., Walters, C.C., Moldowan, J.M., 2005. The Biomarker Guide. Cambridge University Press, Cambridge.
Petersen, H.I., Schovsbo, N.H., Nielsen, A.T., 2013. Reflectance measurements of zooclasts and solid bitumen in Lower Palaeozoic shales, southern Scandinavia: Correlation to vitrinite reflectance. Int. J. Coal Geol. 114, 1–18.
Pickel, W., Kus, J., Flores, D., Kalaitzidis, S., Christanis, K., Cardott, B.J., Misz-Kennan, M., Rodrigues, S., Hentschel, A., Hamor-Vido, M., Crosdale, P., Wagner, N., 2017. Classification of liptinite–ICCP System 1994. Int. J. Coal Geol. 169, 40–61.
Planavsky, N.J., Mills, D.B., 2021. Global aerobics before Earth's oxygenation. Nat. Ecol. Evol. 5 (4), 407–408.
Planavsky, N.J., McGoldrick, P., Scott, C.T., Li, C., Reinhard, C.T., Kelly, A.E., Chu, X., Bekker, A., Love, G.D., Lyons, T.W., 2011. Widespread iron-rich conditions in the mid-Proterozoic ocean. Nature 477 (7365), 448–451.
Planavsky, N.J., Asael, D., Hofmann, A., Reinhard, C.T., Lalonde, S.V., Knudsen, A., Wang, X., Ossa Ossa, F., Pecoits, E., Smith, A.J., 2014a. Evidence for oxygenic photosynthesis half a billion years before the Great Oxidation Event. Nat. Geosci. 7 (4), 283–286.
Planavsky, N.J., Reinhard, C.T., Wang, X., Thomson, D., McGoldrick, P., Rainbird, R.H., Johnson, T., Fischer, W.W., Lyons, T.W., 2014b. Low Mid-Proterozoic atmospheric oxygen levels and the delayed rise of animals. Science 346 (6209), 635–638.

Planavsky, N.J., Crowe, S.A., Fakhraee, M., Beaty, B., Reinhard, C.T., Mills, B.J., Holstege, C., Konhauser, K.O., 2021. Evolution of the structure and impact of Earth's biosphere. Nat. Rev. Earth Environ. 2 (2), 123–139.

Pool, W., Geluk, M., Abels, J., Tiley, G., Idiz, E., Leenaarts, E., 2012. Assessment of an unusual European shale gas play: the Cambro-Ordovician alum shale, southern Sweden. In: SPE/EAGE European Unconventional Resources Conference and Exhibition. SPE pp. SPE-152339-MS.

Pope, M.C., Steffen, J.B., 2003. Widespread, prolonged late Middle to Late Ordovician upwelling in North America: A proxy record of glaciation? Geology 31 (1), 63–66.

Ranasinghe, S., Crosdale, P., 2022. Source Rock Type, Maturation Levels and Hydrocarbon Potential of a Suite of Samples from NDI Carrara 1 Well, Northern Territory. Geoscience Australia, Canberra.

Rasmussen, B., Glover, J., Alexander, R., 1989. Hydrocarbon rims on monazite in Permian-Triassic arenites, northern Perth Basin, Western Australia: Pointers to the former presence of oil. Geology 17 (2), 115–118.

Rasmussen, B., Glover, J., Foster, C., 1993. Polymerisation of hydrocarbons by radioactive minerals in sedimentary rocks: Diagenetic and Economic Significance. In: Parnell, J. (Ed.), Bitumens in Ore Deposits. Springer, Berlin, pp. 490–509.

Reinhard, C.T., Planavsky, N.J., Gill, B.C., Ozaki, K., Robbins, L.J., Lyons, T.W., Fischer, W.W., Wang, C., Cole, D.B., Konhauser, K.O., 2017. Evolution of the global phosphorus cycle. Nature 541 (7637), 386–389.

Revie, D., MacDonald, G., 2017. Volumetric resource assessment of the lower Kyalla and middle Velkerri formations of the McArthur Basin. In: Annual Geoscience Exploration Seminar (AGES) Proceedings, Northern Territory, Darwin.

Reyes, J., Jiang, C., Lavoie, D., Armstrong, D.K., Milovic, M., Robinson, R., 2018. Organic petrographic analysis of artificially matured chitinozoan- and graptolite-rich Upper Ordovician shale from Hudson Bay Basin, Canada. Int. J. Coal Geol. 199, 138–151.

Riaz, A., McCann, J., Saqi, M., 2003. Distribution of Infracambrian reservoir in Punjab Platform. In: Annual Technical Conference (ATC), Islamabad, Pakistan.

Riediger, C., 1993. Solid bitumen reflectance and Rock-Eval Tmax as maturation indices: an example from the "Nordegg Member", Western Canada Sedimentary Basin. Int. J. Coal Geol. 22 (3), 295–315.

Riediger, C., Goodarzi, F., Macqueen, R., 1989. Graptolites as indicators of regional maturity in lower Paleozoic sediments, Selwyn Basin, Yukon and Northwest Territories, Canada. Can. J. Earth Sci. 26 (10), 2003–2015.

Rogers, M., McAlary, J., Bailey, N., 1974. Significance of reservoir bitumens to thermal-maturation studies, Western Canada Basin. AAPG Bull. 58 (9), 1806–1824.

Rozkošný, I., Machovič, V., Pavlíková, H., Hemelíková, B., 1994. Chemical structure of migrabitumens from Silurian Crinoidea, Prague Basin, Barrandian (Bohemia). Org. Geochem. 21 (10), 1131–1140.

Sanei, H., 2020. Genesis of solid bitumen. Sci. Rep. 10 (1), 1–10.

Sanei, H., Petersen, H.I., Schovsbo, N.H., Jiang, C., Goodsite, M.E., 2014. Petrographic and geochemical composition of kerogen in the Furongian (U. Cambrian) Alum Shale, central Sweden: Reflections on the petroleum generation potential. Int. J. Coal Geol. 132, 158–169.

Sanei, H., Haeri-Ardakani, O., Wood, J.M., Curtis, M.E., 2015. Effects of nanoporosity and surface imperfections on solid bitumen reflectance (BRo) measurements in unconventional reservoirs. Int. J. Coal Geol. 138, 95–102.

Schieber, J., 2010. Common themes in the formation and preservation of intrinsic porosity in shales and mudstones–illustrated with examples across the Phanerozoic. In: SPE Unconventional Gas Conference. OnePetro.

Schmidt, J.S., Araujo, C.V., Souza, I.V., Chagas, R.B., 2015. Hydrous pyrolysis maturation of vitrinite-like and humic vitrinite macerals: Implications for thermal maturity analysis. Int. J. Coal Geol. 144, 5–14.

Schmidt, J.S., Menezes, T.R., Souza, I.V.A.F., Spigolon, A.L.D., Pestilho, A.L.S., Coutinho, L.F.C., 2019. Comments on empirical conversion of solid bitumen reflectance for thermal maturity evaluation. Int. J. Coal Geol. 201, 44–50.

Schoenherr, J., Littke, R., Urai, J.L., Kukla, P.A., Rawahi, Z., 2007. Polyphase thermal evolution in the Infra-Cambrian Ara Group (South Oman Salt Basin) as deduced by maturity of solid reservoir bitumen. Org. Geochem. 38 (8), 1293–1318.

Schovsbo, N.H., Nielsen, A.T., Gautier, D.L., 2014. The Lower Palaeozoic shale gas play in Denmark. GEUS Bull. 31, 19–22.

Schovsbo, N.H., Nielsen, A.T., Erlström, M., 2016. Middle–Upper Ordovician and Silurian stratigraphy and basin development in southernmost Scandinavia. GEUS Bull. 35, 39–42.

Shalaby, M.R., Hakimi, M.H., Abdullah, W.H., 2012. Geochemical characterization of solid bitumen (migrabitumen) in the Jurassic sandstone reservoir of the Tut Field, Shushan Basin, northern Western Desert of Egypt. Int. J. Coal Geol. 100, 26–39.

Song, J., Hackley, P.C., Sanders, M.M., Jubb, A.M., Luo, Q., 2023. Thermal evolution of graptolite and solid bitumen properties at high maturity under natural and artificial conditions. Int. J. Coal Geol. 273, 104269.

Stach, E., Mackowski, M.T., Teichmüller, M., Taylor, G.H., Chandra, D., Teichmüller, R., 1982. Stach's Textbook of Coal Petrology. Gebruder Borntraeger, Berlin.

Stasiuk, L.D., 1993. Algal bloom episodes and the formation of bituminite and micrinite in hydrocarbon source rocks: evidence from the Devonian and Mississippian, northern Williston Basin, Canada. Int. J. Coal Geol. 24 (1), 195–210.

Stasiuk, L.D., 1997. The origin of pyrobitumens in Upper Devonian Leduc Formation gas reservoirs, Alberta, Canada: an optical and EDS study of oil to gas transformation. Mar. Pet. Geol. 14 (7–8), 915–929.

Stasiuk, L., Fowler, M., 1994. Paleozoic hydrocarbon source rocks, Truro Island, Arctic Canada: organic petrology, organic geochemistry and thermal maturity. Bull. Can. Petrol. Geol. 42 (4), 419–431.

Stasiuk, L.D., Osadetz, K.G., 1993. Thermal maturity, alginite-bitumen transformation, and hydrocarbon generation in Upper Ordovician source rocks, Saskatchewan, Canada. Energy Sources 15 (2), 205–237.

Stasiuk, L., El-Ezhary, A., Asgar-Deen, M., Dieckmann, V., Robinson, R., Green, G., 2014. Assessment of organic petrology methodology and characterization of primary and secondary dispersed organic matter in liquid-rich shales: using optical microscopy methodologies. Search Discov. Article 80367.

Stewart, S.A., Reid, C.T., Hooker, N.P., Kharouf, O.W., 2016. Mesozoic siliciclastic reservoirs and petroleum system in the Rub' Al-Khali basin, Saudi Arabia. AAPG Bull. 100 (5), 819–841.

Strapoc, D., Mastalerz, M., Schimmelmann, A., Drobniak, A., Hasenmueller, N.R., 2010. Geochemical constraints on the origin and volume of gas in the New Albany Shale (Devonian–Mississippian), eastern Illinois Basin. AAPG Bull. 94 (11), 1713–1740.

Suárez-Ruiz, I., Flores, D., Mendonça Filho, J.G., Hackley, P.C., 2012. Review and update of the applications of organic petrology: Part 1, geological applications. Int. J. Coal Geol. 99, 54–112.

Suchý, V., Rozkošný, I., 1996. Diagenesis of Clay Minerals and Organic Matter in the Přídolí Formation (Upper Siluian), the Barrandian Basin, Czech Republic: First Systematic Survey. Acta Univ. Carolinae Geol. 38, 401–409.

Suchý, V., Sýkorová, I., Stejskal, M., Šafanda, J., Machovič, V.r. and Novotná, M., 2002. Dispersed organic matter from Silurian shales of the Barrandian Basin, Czech Republic: optical properties, chemical composition and thermal maturity. Int. J. Coal Geol. 53 (1), 1–25.

Suchý, V., Sýkorová, I., Melka, K., Filip, J., Machovič, V., 2007. Illite 'crystallinity', maturation of organic matter and microstructural development associated with lowest-grade metamorphism of Neoproterozoic sediments in the Tepla-Barrandian unit, Czech Republic. Clay Miner. 42 (4), 503–526.

Suchý, V., Sandler, A., Slobodník, M., Sýkorová, I., Filip, J., Melka, K., Zeman, A., 2015. Diagenesis to very low-grade metamorphism in lower Palaeozoic sediments: A case study from deep borehole Tobolka 1, the Barrandian Basin, Czech Republic. Int. J. Coal Geol. 140, 41–62.

Summons, R.E., Taylor, D., Boreham, C.J., 1994. Geochemical tools for evaluating petroleum generation in Middle Proterozoic sediments of the McArthur Basin, Northern Territory, Australia. APPEA J. 34 (1), 692–706.

Sweeney, J.J., Burnham, A.K., 1990. Evaluation of a simple model of vitrinite reflectance based on chemical kinetics1. AAPG Bull. 74 (10), 1559–1570.

Synnott, D.P., Dewing, K., Ardakani, O.H., Obermajer, M., 2018. Correlation of zooclast reflectance with Rock-Eval Tmax values within Upper Ordovician Cape Phillips Formation, a potential petroleum source rock from the Canadian Arctic Islands. Fuel 227, 165–176.

Taylor, G.H., Teichmqller, M., Davis, A., Diessel, C.F.K., Littke, R., Robert, P., 1998. Organic Petrology. Gebrqder Borntrager, Berlin.

Teichmüller, M., 1978. Nachweis von graptolithen-periderm in geschieferten gesteinen mit hilfe kohlenpetrologischer methoden. Neues Jb. Geol. Paläontol. Monat. 7, 430–447.

Teng, J., Mastalerz, M., Liu, B., Gognat, T., Hauser, E., McLaughlin, P., 2020. Variations of organic matter transformation in response to hydrothermal fluids: Example from the Indiana part of the Illinois Basin. Int. J. Coal Geol. 219, 103410.

Teng, J., Mastalerz, M., Liu, B., 2021. Petrographic and chemical structure characteristics of amorphous organic matter in marine black shales: Insights from Pennsylvanian and Devonian black shales in the Illinois Basin. Int. J. Coal Geol. 235, 103676.

Teng, J., Liu, B., Mastalerz, M., Schieber, J., 2022. Origin of organic matter and organic pores in the overmature Ordovician-Silurian Wufeng-Longmaxi Shale of the Sichuan Basin, China. Int. J. Coal Geol. 253, 103970.

Thomsen, E., Lindgreen, H., Wrang, P., 1983. Investigation on the source rock potential of Denmark. In: Kaasschieter, J., Reijers, T. (Eds.), Petroleum Geology of the Southeastern North Sea and the Adjacent Onshore Areas. Geologie en Mijnbouw, The Hague, pp. 221–239.

Tissot, B., Welte, D., 1984. Petroleum Formation and Occurrence. Springer-Verlag, New York.

Tissot, B., Durand, B., Espitalie, J., Combaz, A., 1974. Influence of nature and diagenesis of organic matter in formation of petroleum. AAPG Bull. 58 (3), 499–506.

Valentine, B.J., Hackley, P.C., Hatcherian, J.J., 2021. Hydrous pyrolysis of New Albany Shale: A study examining maturation changes and porosity development. Mar. Pet. Geol. 134, 105368.

Van Gijzel, P., 1981. Applications of the geomicrophotometry of kerogen, solid hydrocarbons and crude oils to petroleum exploration. In: Brooks, J. (Ed.), Organic Maturation Studies and Fossil Fuel Exploration. Academic Press, London, pp. 351–377.

Volk, H., 2000. Source Rocks, Bitumens and Petroleum Inclusions from the Prague Basin (Barrandian, Czech Republic): Constraints for Petroleum Generation and Migration from Petrology, Organic Geochemistry and Basin Modelling. Aachen, Techn, Hochsch., Diss., Aachen, pp. 1–337.

Volk, H., Mann, U., Burde, O., Horsfield, B., Suchý, V., 2000. Petroleum inclusions and residual oils: constraints for deciphering petroleum migration. J. Geochem. Explor. 71 (3), 307–311.

Wang, Q., Qian, M., Jiang, Q., Yang, Y., Tenger, B., 2017a. A study on hydrocarbon generation capacity of graptolite in marine hydrocarbon source rocks in Southern China. Rock Miner. Anal. 36 (3), 258–264 (in Chinese with English abstract).

Wang, X., Zhang, S., Wang, H., Bjerrum, C.J., Hammarlund, E.U., Haxen, E.R., Su, J., Wang, Y., Canfield, D.E., 2017b. Oxygen, climate and the chemical evolution of a 1400 million year old tropical marine setting. Am. J. Sci. 317 (8), 861–900.

Wang, Y., Zhai, G., Bao, S., Zhou, Z., Song, T., Li, H., 2017c. Evaluation of Sinian Doushantuo formation shale gas content and fracturing property of Eyangye1 well in Hubei Province. China Min. Mag. 26 (6), 166–172 (in Chinese with English abstract).

Wang, X., Zhao, W., Zhang, S., Wang, H., Su, J., Canfield, D.E., Hammarlund, E.U., 2018. The aerobic diagenesis of Mesoproterozoic organic matter. Sci. Rep. 8 (1), 1–10.

Wang, Y., Qiu, N., Borjigin, T., Shen, B., Xie, X., Ma, Z., Lu, C., Yang, Y., Yang, L., Cheng, L., Fang, G., Cui, Y., 2019. Integrated assessment of thermal maturity of the

Upper Ordovician–Lower Silurian Wufeng–Longmaxi shale in Sichuan Basin, China. Mar. Pet. Geol. 100, 447–465.
Wang, Y., Qiu, N., Ma, Z., Ning, C., Zheng, L., Zhou, Y., Fang, G., Rui, X., Rao, D., 2020. Evaluation of equivalent relationship between vitrinite reflectance and solid bitumen reflectance. J. China Univ. Min. Technol. 49 (3), 563–575 (In Chinese with English abstract).
Wang, C., Lechte, M.A., Reinhard, C.T., Asael, D., Cole, D.B., Halverson, G.P., Porter, S. M., Galili, N., Halevy, I., Rainbird, R.H., 2022a. Strong evidence for a weakly oxygenated ocean–atmosphere system during the Proterozoic. Proc. Natl. Acad. Sci. 119 (6), e2116101119.
Wang, K., Ma, L., Taylor, K.G., 2022b. Nanoscale geochemical heterogeneity of organic matter in thermally-mature shales: An AFM-IR study. Fuel 310, 122278.
Wei, L., Wang, Y., Mastalerz, M., 2016. Comparative optical properties of macerals and statistical evaluation of mis-identification of vitrinite and solid bitumen from early mature Middle Devonian–Lower Mississippian New Albany Shale: Implications for thermal maturity assessment. Int. J. Coal Geol. 168, 222–236.
Wu, D.X., Wu, X.N., Li, C.S., Yu, Z., Li, W.L., Cai, J., Li, G.J., 2021a. Sedimentary model and hydrocarbon-generation potential of source rock of the Ordovician Ulalik Formation in western Ordos Basin. Marine Oil Gas Geol. 26 (2), 123–130 (in Chinese with English abstract).
Wu, L., Zhu, G., Yan, L., Feng, X., Zhang, Z., 2021b. Late Ediacaran to Early Cambrian tectonic–sedimentary controls on Lower Cambrian black shales in the Tarim Basin, Northwest China. Glob. Planet. Chang. 205, 103612.
Wu, J., Li, H., Goodarzi, F., Min, X., Cao, W., Huang, L., Pan, Y., Luo, Q., 2022. Geochemistry and depositional environment of the Mesoproterozoic Xiamaling shales, northern North China. J. Pet. Sci. Eng. 215, 110730.
Wu, J., Luo, Q., Zhang, Y., Zhong, N., Goodarzi, F., Suchý, V., Li, M., Li, D., Wang, W., Tian, X., Song, Z., 2023a. The organic petrology of vitrinite-like maceral in the Lower Paleozoic shales: Implications for the thermal maturity evaluation. Int. J. Coal Geol. 274, 104282.
Wu, J., Luo, Q., Zhong, N., Goodarzi, F., Suchý, V., Sanei, H., Skovsted, C.B., Li, M., Zhang, Y., Li, D., Wu, J., Song, D., 2023b. Chemical structure and thermal maturation of the vitrinite-like maceral in the Lower Paleozoic shales: Insights from Raman spectroscopy of artificial pyrolysis residues. J. Anal. Appl. Pyrolysis 172, 106024.
Xi, S.L., Mo, W.L., Liu, X.S., Zhang, L., Li, J., Huang, Z.L., Wang, M., Zhang, C.L., Zhu, Q. Y., Yan, Y., Zhou, N.W., 2021. Shale gas exploration potential of Ordovician Wulalike Formation in the western margin of Ordos Basin:Case study of Well Zhongping 1. Nat. Gas Geosci. 32 (8), 1235–1246 (in Chinese with English abstract).
Xi, S.L., Liu, X.S., Huang, Z.L., Zhao, H.T., Zhang, C.L., Liu, Y., 2023. Enrichment characteristics and exploration direction of shale oil and gas in Wulalike Formation of Middle Ordovician in the Ordos Basin. Nat. Gas Ind. 43 (3), 12–22 (in Chinese with English abstract).
Xiao, X., Liu, D., Fu, J., 1996. Multiple phases of hydrocarbon generation and migration in the Tazhong petroleum system of the Tarim Basin, People's Republic of China. Org. Geochem. 25 (3), 191–197.
Xiao, X., Liu, D., Fu, J., Wilkins, R.W., 1997. Marine vitrinite-an important hydrocarbon source matter in marine source rocks. Acta Pet. Sin. 18 (1), 44–48 (in Chinese with English abstract).
Xiao, S., Zhang, Y., Knoll, A.H., 1998. Three-dimensional preservation of algae and animal embryos in a Neoproterozoic phosphorite. Nature 391 (6667), 553–558.
Xiao, X., Wilkins, R., Liu, D., Liu, Z., Fu, J., 2000. Investigation of thermal maturity of lower Palaeozoic hydrocarbon source rocks by means of vitrinite-like maceral reflectance–a Tarim Basin case study. Org. Geochem. 31 (10), 1041–1052.
Xiao, S., Knoll, A.H., Yuan, X., Pueschel, C.M., 2004. Phosphatized multicellular algae in the Neoproterozoic Doushantuo Formation, China, and the early evolution of florideophyte red algae. Am. J. Bot. 91 (2), 214–227.
Xu, Z., Guo, S., 2015. Research on Pore Structures of Sinian Doushantuo Formation Shale in Middle Yangtze Area. Geoscience 29 (1), 206–212 (in Chinese with English abstract).
Xu, X., Sun, W., Wang, S., 2019. Maturity evaluation of marine shale in the Lower Paleozoic in South China. Earth Sci. 44 (11), 3717–3724 (in Chinese with English abstract).
Yang, S., Horsfield, B., 2020. Critical review of the uncertainty of Tmax in revealing the thermal maturity of organic matter in sedimentary rocks. Int. J. Coal Geol. 225, 103500.
Yang, J., Hatcherian, J., Hackley, P.C., Pomerantz, A.E., 2017. Nanoscale geochemical and geomechanical characterization of organic matter in shale. Nat. Commun. 8, 2179.
Yao, L., Zhong, N., Khan, I., Chen, J., Luo, Q., Zhang, Y., Ai, J., Sun, W., 2021. Comparison of in-source solid bitumen with migrated solid bitumen from Ediacaran-Cambrian rocks in the Upper Yangtze region, China. Int. J. Coal Geol. 240, 103748.
Yasin, Q., Baklouti, S., Sohail, G.M., Asif, M., Xufei, G., 2022. Evaluation of Neoproterozoic source rock potential in SE Pakistan and adjacent Bikaner–Nagaur Basin India. Sci. Rep. 12 (1), 11102.
Ye, Y., Wang, H., Zhai, L., Wang, X., Wu, C., Zhang, S., 2018. Contrasting Mo–U enrichments of the basal Datangpo Formation in South China: Implications for the Cryogenian interglacial ocean redox. Precambrian Res. 315, 66–74.
Yin, L., Zhu, M., Knoll, A.H., Yuan, X., Zhang, J., Hu, J., 2007. Doushantuo embryos preserved inside diapause egg cysts. Nature 446 (7136), 661–663.
Yong, Z., Zhang, X., Deng, H., Liu, S., Ran, B., Sun, W., Yang, D., Luo, C., Wang, S., Ye, Y., 2012. Differences about organic matter enrichment in the shale section of Ediacaran Doushantuo Formation in West Hubei of China. J. Chengdu Univ. Technol. Sci. Technol. Ed. 39 (6), 567–574 (in Chinese with English abstract).
Yu, W., Algeo, T.J., Du, Y., Maynard, B., Guo, H., Zhou, Q., Peng, T., Wang, P., Yuan, L., 2016. Genesis of Cryogenian Datangpo manganese deposit: Hydrothermal influence and episodic post-glacial ventilation of Nanhua Basin, South China. Palaeogeogr. Palaeoclimatol. Palaeoecol. 459, 321–337.
Zhang, T., Shen, Y., Zhan, R., Shen, S., Chen, X., 2009. Large perturbations of the carbon and sulfur cycle associated with the Late Ordovician mass extinction in South China. Geology 37 (4), 299–302.
Zhang, Y.Q., Guo, Y.R., Hou, W., Zhao, Z.Y., Gao, J.R., 2013. Geochemical Characteristics and Exploration Potential of the Middle-Upper Ordovician Source Rocks on the Western and Southern Margin of Ordos Basin. Nat. Gas Geosci. 24 (5), 894–904 (in Chinese with English abstract).
Zhang, S., Wang, X., Hammarlund, E.U., Wang, H., Costa, M.M., Bjerrum, C.J., Connelly, J.N., Zhang, B., Bian, L., Canfield, D.E., 2015. Orbital forcing of climate 1.4 billion years ago. Proc. Natl. Acad. Sci. 112 (12), E1406–E1413.
Zhang, S., Wang, X., Wang, H., Bjerrum, C.J., Hammarlund, E.U., Costa, M.M., Connelly, J.N., Zhang, B., Su, J., Canfield, D.E., 2016. Sufficient oxygen for animal respiration 1,400 million years ago. Proc. Natl. Acad. Sci. 113 (7), 1731–1736.
Zhang, P., Liu, G., Cai, C., Li, M., Chen, R., Gao, P., Xu, C., Wan, W., Zhang, Y., Jiang, M., 2019a. Alteration of solid bitumen by hydrothermal heating and thermochemical sulfate reduction in the Ediacaran and Cambrian dolomite reservoirs in the Central Sichuan Basin, SW China. Precambrian Res. 321, 277–302.
Zhang, S., Wang, X., Wang, H., Bjerrum, C.J., Hammarlund, E.U., Haxen, E.R., Wen, H., Ye, Y., Canfield, D.E., 2019b. Paleoenvironmental proxies and what the Xiamaling Formation tells us about the mid-Proterozoic ocean. Geobiology 17 (3), 225–246.
Zhang, J., Shi, M., Wang, D., Tong, Z., Hou, X., Niu, J., Li, X., Li, Z., Zhang, P., Huang, Y., 2022. Fields and directions for shale gas exploration in China. Nat. Gas Indus. 9 (1), 20–32 (in Chinese with English abstract).
Zhang, Y., Li, R., Xi, S., Gao, J., Chen, L., Huang, H., Zhao, B., Khaled, A., 2023. Quartz Origins and Paleoenvironmental Controls on Organic Matter Accumulation of Marine Shale in the Ordovician Wulalike Formation, Northwestern Ordos Basin, China: Significance for Shale Gas Exploration. Energies 16 (14), 5278.
Zheng, X., Sanei, H., Schovsbo, N.H., Luo, Q., Wu, J., Zhong, N., Galloway, J.M., Goodarzi, F., 2021a. Role of zooclasts in the kerogen type and hydrocarbon potential of the lower Paleozoic Alum Shale. Int. J. Coal Geol. 248, 103865.
Zheng, X., Schovsbo, N.H., Bian, L., Luo, Q., Zhong, N., Rudra, A., Goodarzi, F., Sanei, H., 2021b. Alteration of organic macerals by uranium irradiation in lower Paleozoic marine shales. Int. J. Coal Geol. 239, 103713.
Zheng, X., Schovsbo, N.H., Luo, Q., Wu, J., Zhong, N., Goodarzi, F., Sanei, H., 2022. Graptolite reflectance anomaly. Int. J. Coal Geol. 261, 104072.
Zheng, T., Grohmann, S., Arysanto, A., Baniasad, A., Zhang, Q., Littke, R., 2023a. Petrographical and geochemical investigation on maturation and primary migration in intact source rock micro-plugs: Insight from hydrous pyrolysis on Woodford Shale. Int. J. Coal Geol. 266, 104170.
Zheng, X., Schovsbo, N.H., Bian, L., Rudra, A., Sanei, H., 2023b. Organic geochemical and petrographic characteristics of the Cambrian-Ordovician organic-rich marine shales in Scandinavia. Pet. Sci. 20 (5), 2637–2647.
Zhong, N., Qin, Y., 1995. Organic Petrology of Carbonate Rocks: Characteristics, Origin and Evolution of Macerals with Respects to Hydrocarbon Generation. Science Press. Beijing (in Chinese).
Zhu, G., Chen, F., Chen, Z., Zhang, Y., Xing, X., Tao, X., Ma, D., 2016. Discovery and basic characteristics of high-quality source rocks found in the Yuertusi Formation of the Cambrian in Tarim Basin, China. J. Nat. Gas Geosci. 1 (1), 21–33.
Zhu, G., Chen, F., Wang, M., Zhang, Z., Ren, R., Wu, L., 2018. Discovery of the lower Cambrian high-quality source rocks and deep oil and gas exploration potential in the Tarim Basin, China. AAPG Bull. 102 (10), 2123–2151.
Zhu, G., Li, T., Zhang, Z., Zhao, K., Zhang, K., Chen, W., Yan, H., Wang, P., 2020. Distribution and geodynamic setting of the Late Neoproterozoic–Early Cambrian hydrocarbon source rocks in the South China and Tarim Blocks. J. Asian Earth Sci. 201, 104504.
Zhu, G., Li, T., Zhao, K., Li, C., Cheng, M., Chen, W., Yan, H., Zhang, Z., Algeo, T.J., 2021. Mo isotope records from Lower Cambrian black shales, northwestern Tarim Basin (China): Implications for the early Cambrian ocean. GSA Bull. 134 (1–2), 3–14.
Zou, C., Dong, D., Wang, S., Li, J., Li, X., Wang, Y., Li, D., Cheng, K., 2010. Geological characteristics and resource potential of shale gas in China. Pet. Explor. Dev. 37 (6), 641–653.
Zou, C., Dong, D., Yang, H., Wang, Y., Huang, J., Wang, S., Fu, C., 2011. Conditions of shale gas accumulation and exploration practices in China. Nat. Gas Ind. 31 (12), 26–39 (in Chinese with English abstract).
Zou, C., Yang, Z., Tao, S., Li, W., Wu, S., Hou, L., Zhu, R., Yuan, X., Wang, L., Gao, X., Jia, J., Guo, Q., Bai, B., 2012. Nano-hydrocarbon and the accumulation in coexisting source and reservoir. Pet. Explor. Dev. 39 (1), 13–26 (in Chinese with English abstract).
Zou, C., Dong, D., Wang, Y., Li, X., Huang, J., Wang, S., Guan, Q., Zhang, C., Wang, H., Liu, H., Bai, W., Liang, F., Lin, W., Zhao, Q., Liu, D., Yang, Z., Liang, P., Sun, S., Qiu, Z., 2015. Shale gas in China: Characteristics, challenges and prospects (I). Pet. Explor. Dev. 42 (6), 753–767.
Zou, C., Dong, D., Wang, Y., Li, X., Huang, J., Wang, S., Guan, Q., Zhang, C., Wang, H., Liu, H., Bai, W., Liang, F., Lin, W., Zhao, Q., Liu, D., Yang, Z., Liang, P., Sun, S., Qiu, Z., 2016. Shale gas in China: Characteristics, challenges and prospects (II). Pet. Explor. Dev. 43 (2), 182–196.
Zou, C., Zhao, Z., Pan, S., Yin, J., Lu, G., Fu, F., Yuan, M., Liu, H., Zhang, G., Luo, C., Wang, W., Jing, Z., 2024. Unveiling the Oldest Industrial Shale Gas Reservoir: Insights for the Enrichment Pattern and Exploration Direction of Lower Cambrian Shale Gas in the Sichuan Basin. Engineering 42, 278–294.